

## **Electromagnetic trapping of cold atoms**

V I Balykin, V G Minogin and V S Letokhov

Institute of Spectroscopy, Russian Academy of Sciences, 142190 Troitsk, Moscow Region, Russia

Received 8 March 2000

### **Abstract**

This review describes the methods of trapping cold atoms in electromagnetic fields and in the combined electromagnetic and gravity fields. We discuss first the basic types of the dipole radiation forces used for cooling and trapping atoms in the laser fields. We outline next the fundamentals of the laser cooling of atoms and classify the temperature limits for basic laser cooling processes. The main body of the review is devoted to discussion of atom traps based on the dipole radiation forces, dipole magnetic forces, combined dipole radiation–magnetic forces, and the forces combined of the dipole radiation–magnetic and gravity forces. Physical fundamentals of atom traps operating as waveguides and cavities for cold atoms are also considered. The review ends with the applications of cold and trapped atoms in atomic, molecular and optical physics.

**Contents**

	Page
1. Introduction	1431
2. Dynamics of an atom in a laser field	1438
2.1. Dipole radiation force	1438
2.2. Dipole radiation force on a two-level atom	1440
2.3. Dipole radiation force on a multilevel atom	1451
2.4. Kinetic description of atomic motion	1453
3. Laser cooling of atoms	1456
3.1. Doppler cooling	1456
3.2. Sub-Doppler cooling	1460
3.3. Subrecoil cooling	1461
4. Optical trapping	1466
4.1. Trapping in laser beams	1466
4.2. Trapping in standing laser waves. Optical lattices	1469
4.3. Trapping in optical waveguide modes. Atom waveguides	1473
4.4. Atom cavities	1477
5. Magnetic trapping	1479
5.1. Static magnetic traps	1479
5.2. Quadrupole magnetic trap with time-orbiting potential	1481
5.3. Magnetic trap with an optical plug	1483
5.4. Magnetic mirrors and cavities	1483
5.5. Magnetic trapping of molecules	1486
6. Magneto-optical trapping	1486
6.1. Simplified scheme and basic configuration	1486
6.2. (1 + 3)-level atom model	1488
6.3. (3 + 5)-level atom model	1489
6.4. 3D MOT	1491
6.5. Density effects	1491
6.6. Experimental results	1492
7. Gravito-optical traps and cavities	1493
8. Applications	1497
8.1. Laser trapping spectroscopy	1497
8.2. Bose–Einstein condensation	1497
8.3. Atom laser	1497
8.4. Intense atomic beams	1498
8.5. Nuclear physics	1498
8.6. Ultrasensitive isotope trace analysis	1499
8.7. Ultracold atom collisions	1499
8.8. Formation of cold molecules	1501
8.9. Cavity QED, single atoms etc	1503
Acknowledgment	1503
References	1503

## 1. Introduction

The trapping of atoms in a restricted space volume is a fundamental physical problem of considerable interest from the standpoint of both the performance of physical investigations with small amounts of atoms and the development of new technologies based on the localization of the spatial motion of atoms. Important physical applications of the methods of trapping atoms in 3D spatial regions include studies into the spectral properties of small amounts of atoms, including counted numbers of radioactive atomic isotopes, improvement of the accuracy and sensitivity of spectral measurements, and studies of quantum statistical effects in atomic ensembles at low temperatures, such as the Bose–Einstein condensation (BEC). No less important physical and technological applications may be associated with the trapping atoms in one or two dimensions, allowing atomic waveguides and cavities to be developed. Important technological applications are expected to ensue from the use of trapped atoms in the atomic frequency and time standards.

In the course of the many decades that this problem has been discussed, numerous physical ideas were put forward that could be used either for trapping atoms in 3D regions of space or for trapping atoms in one or two dimensions. In essence, the practically developed methods appeared to be based on the use of the forces of electric dipole interaction of atoms with quasiresonance laser fields and (or) magnetic dipole interaction of atoms with static magnetic fields. In a sense, the main methods of trapping neutral atoms proved to be similar to those for trapping charged particles (electrons, protons, atom ions). To trap the latter, use is made of electromagnetic traps formed by inhomogeneous radio-frequency fields (Paul traps) or inhomogeneous stationary electric and magnetic fields (Penning traps) (Dehmelt 1967, 1969, Paul 1990).

From the physical standpoint, all the known techniques for trapping neutral atoms can be classed with but a few basic methods. These basic methods are: *optical trapping* using the forces of electric dipole interaction between atoms and laser fields, *magnetic trapping* based on the use of the forces of magnetic dipole interaction, mixed *magneto-optical trapping* using simultaneous interaction between atoms and magnetic and laser fields, and also mixed *gravito-optical* and *gravito-magnetic trapping*.

Historically, the first to be discussed were the methods of magnetic trapping. The very first suggestions on the possibility of electromagnetic trapping of atoms were already made when the first experiments were conducted on the deflection of atomic beams by a nonuniform magnetic field (Stern and Gerlach 1921). The development of the idea of the magnetic deflection of atoms and molecules led to the appearance in the 1950s of the hexapole magnetic lenses and hexapole magnetic traps for particles with a permanent magnetic moment (Friedburg and Paul 1951, Lemonick *et al* 1955). These traps were successfully used to trap ultracold neutrons (Kugler *et al* 1978, 1985, Golub and Pendlebury 1979). Many types of traps for particles with a permanent magnetic moment, starting with the most simple quadrupole trap and ending with the fairly complex Ioffe trap, were discussed in the works on plasma physics (Gott *et al* 1962, Artsimovich 1964, Krall and Trivelpiece 1973). Concrete magnetic trap arrangements for trapping atoms started to be discussed in the 1960s (Vladimirskii 1960, Heer 1963, Letokhov and Minogin 1980, Pritchard 1983, Metcalf 1984, Bergeman *et al* 1987).

The possibility of trapping atoms in magnetic traps could not be experimentally verified for a long time, mainly because of the absence of methods to obtain cold atoms. The potential well depth  $U_m = \mu|\Delta B|$  produced by an inhomogeneous magnetic field varying in the interval  $\Delta B$  at typical atomic magnetic moment values of the order of the Bohr magneton,  $\mu \approx \mu_B$ , and moderate value of the laboratory magnetic field is usually very small compared with the thermal energy of atoms at room temperature. Accordingly, inhomogeneous magnetic fields

can only be used to trap very cold atoms whose temperature  $T$  does not exceed the potential well depth,

$$T < \mu|\Delta B|/k_B, \quad (1.1)$$

where  $k_B$  is the Boltzmann constant. To illustrate, when the magnetic field varies by an amount of  $|\Delta B| = 100$  G, the trap can hold atoms with a temperature no higher than 10 mK.

In the late 1960s the first suggestion was made on the possibility of optical trapping of atoms in the nodes or loops of an off-resonance standing laser wave (Letokhov 1968). The first idea of the optical trapping of atoms was based on the use of the electric dipole interaction between the atoms and a standing laser wave to form a periodic lattice of potential wells whose minima coincided with the nodes or antinodes of the standing laser wave. A free atom is known to have no electric dipole moment by virtue of its symmetry with respect to the inversion operation. An electric dipole moment can, however, be induced by a laser field if an atom is in an incoherent mixture of states or a coherent superposition of states of opposite parity. Exactly such mixed states are produced when an atom interacts with a resonance or off-resonance light field. The theory of atomic trapping by an off-resonance standing laser wave was discussed in a number of works (Kazantsev 1972, Letokhov and Pavlik 1976).

Recalling the history of this idea, one of the authors of this review (Letokhov) must say that it has its roots in the experiments by Ramsey and co-workers (Goldenberg *et al* 1960). In these experiments, hydrogen atoms were trapped in a closed vessel whose inside surface was coated with a special paraffin layer. Colliding with this coating, the atoms remained with a high probability in their initial hyperfine-structure state. The vessel was placed inside a microwave cavity. The size of the vessel,  $a$ , and the cavity was chosen to be close to the wavelength  $\lambda = 21$  cm of the microwave transition between the hyperfine-structure levels of the hydrogen atom (see figure 1). Thanks to the fact that the free-flight length  $L$  of the atoms satisfied the condition

$$L \leq \lambda, \quad (1.2)$$

the motion of the atoms was localized within a small volume  $V \leq \lambda^3$ . As a result of the localization of atoms there took place the elimination of the Doppler broadening of spectral lines in the so-called Lamb–Dicke limit (Dicke 1953). It seemed very tempting to find a way to localize atoms in a micron-size region of space and extend thus the approach to the optical spectral region. Since it was practically impossible to make such small cavities, the natural idea was conceived of localizing atoms in the nodes or antinodes of a standing laser wave, i.e. in regions the size of the optical wavelength (Letokhov 1968). To localize atoms in the inhomogeneities of a standing laser wave, use could be made of the gradient dipole force (Gaponov and Miller 1958, Askarian 1962). Of course, the kinetic energy of a thermal atom far exceeds the height of the potential barrier produced by the gradient force. For this reason, it was only the trapping of thermal atoms moving almost parallel to the wavefront of the standing laser wave, i.e. the 1D trapping of atoms, that was discussed in the first proposal (see figure 2). Naturally the fraction of such atoms in a collimated thermal atomic beam is always small, which presented certain difficulties for an experiment.

In the early 1970s an attempt was made to observe the 1D trapping of molecules in a standing wave produced by an intense CW CO<sub>2</sub> laser. But it proved abortive because of the difficulties involved in detecting the trapped molecules (see Letokhov 1992). An earlier work (Letokhov and Pavlik 1976) discussed possible methods to implement a 3D trapping of atoms by way of predominant photodeflection of slow atoms into a region where a 3D laser wave could trap slow atoms without the destructive collisional influence of the much larger number of thermal atoms (figure 4). Periodic lattices of trapped atoms proposed in the early works later became known as optical lattices.

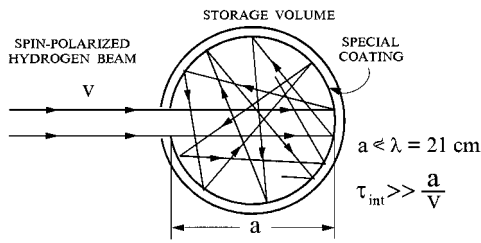


**Figure 1.** Scheme of geometrical trapping hydrogen atoms in a storage vessel placed inside the microwave cavity (Goldenberg *et al* 1960).

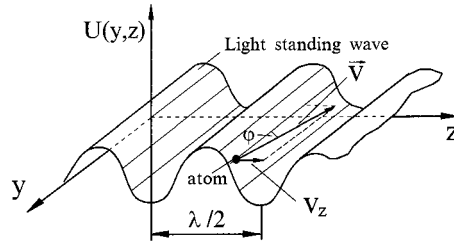


**Figure 2.** Scheme of the 1D trapping of atoms in the periodic potential  $U(y, z)$  produced by a standing laser wave (Letokhov 1968).

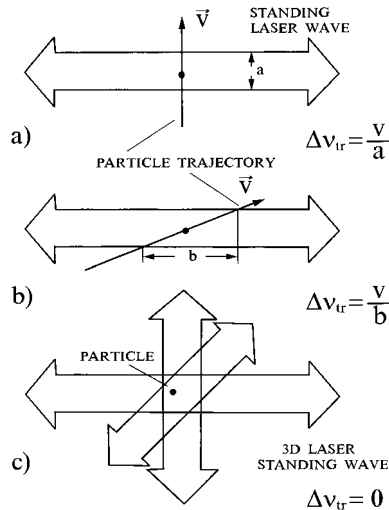


**Figure 3.** Three methods of the Doppler-free optical spectroscopy differ in the contribution of the transit-time broadening,  $\Delta v_{\text{tr}}$ : (a) saturation spectroscopy in a standing wave; (b) two-photon spectroscopy in a standing wave; (c) particle trapping in a 3D standing wave (Letokhov 1975).

At the time of these first suggestions, Ashkin (1970, 1980) published interesting proposals on the laser trapping and levitation of dielectric microparticles, which later led to the development of ‘optical tweezers’. These are now an important tool in biological investigations (Ashkin 1988).

In the same years it was appreciated that the trapping of atoms by laser light might give birth to so-called particle trapping spectroscopy (Letokhov 1975). This would be an important supplement to the Doppler-free laser spectroscopy techniques developed earlier (see table 1): the standing-wave absorption saturation spectroscopy (Lamb 1964, Lee and Skolnick 1967, Letokhov 1967, Lisitsyn and Chebotayev 1968, Barger and Hall 1969) and standing-wave two-photon spectroscopy suggested by Chebotayev and co-workers (Vasilenko *et al* 1970). In contrast to these nonlinear spectroscopy techniques, particle trapping spectroscopy is completely free from the so-called transit broadening effect resulting from the finite particle–field interaction time (figure 3).

Despite the promising applications that trapped atoms could have in spectroscopy, the trapping of atoms by an off-resonance laser field was not at once developed experimentally because the methods for obtaining sufficiently cold atoms were lacking at the time. The potential wells produced by the dipole interaction of an atom with an off-resonance standing light wave,  $E = 2E_0 \cos kz \cos \omega t$ , have a shallow depth  $U_e = \alpha E_0^2$  because of the low off-resonance atomic polarizability  $\alpha$ . Accordingly, the off-resonance optical trapping can be

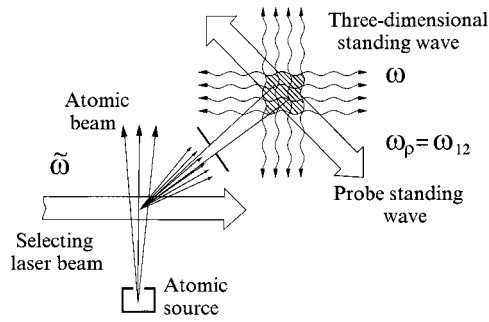


**Figure 4.** The first proposal on trapping slow atoms in a 3D standing laser wave (first idea of the optical lattice) (Letokhov and Pavlik 1976).

**Table 1.** Methods of Doppler-free laser spectroscopy.

Method	Physical phenomena	Author
1. Saturation spectroscopy	Change of the atomic (molecular velocity distribution at the quantum levels of the optically saturated transition).	Lamb (1964)
2. Two-photon spectroscopy	Compensation of the Doppler shift due to simultaneous absorption of photons from counter-propagating laser waves.	Vasilenko <i>et al</i> (1970)
3. Spectroscopy of trapped atoms and molecules	Oscillatory motion of slow atoms or molecules in a standing laser wave (trapping of atoms or molecules).	Letokhov (1968)

implemented only for sufficiently cold atoms whose temperature is limited by the condition (Letokhov 1968)

$$T < \alpha E_0^2 / k_B. \quad (1.3)$$

For example, at an intensity of the counter-propagating travelling laser waves producing the standing laser wave, of the order of  $I = (c/8\pi)E_0^2 \approx 1 \text{ kW cm}^{-2}$ , and typical atomic polarizability  $\alpha \approx 3 \times 10^{-23} \text{ cm}^3$ , condition (1.3) is satisfied for atoms with quite a low temperature  $T < 1 \mu\text{K}$ .

In the mid-1970s a principal change occurred in the view of the problem of trapping atoms in electromagnetic fields. The first suggestion was put forward at the time on the possibility of deep cooling of atoms by a resonance optical radiation red-detuned with respect to the atomic transition (Hänsch and Shawlow 1975), and concrete schemes were proposed for cooling atoms by standing laser waves (Letokhov *et al* 1976, 1977). From the quantum mechanical point of view, the idea of optical cooling of atoms consisted in the reduction of atomic velocities by the photon recoil associated with the absorption by the moving atoms of counter-propagating laser photons. Recall that, due to the Doppler effect, when the laser field is a red-detuned with respect to the atomic transition, an atom predominantly absorbs counter-propagating photons. From the semiclassical point of view, the mechanism of the optical cooling of atoms consisted in the retardation of atoms by the radiation pressure force which for a red-detuned laser light is directed opposite to the atomic velocity.

The discovery of the optical cooling of atoms has shown that the problem of trapping neutral atoms can be solved by both magnetic and optical methods, provided that the atoms are preliminarily cooled by laser radiation. At the same period there were developed various

experimental methods for the laser cooling of atoms. Basically, there proved to be two principal schemes. One is the scheme of simultaneous deceleration and longitudinal cooling of an atomic beam by a counter-propagating red-detuned laser beam (Balykin *et al* 1979, 1980, 1984b, Andreev *et al* 1981, 1982, Phillips and Metcalf 1982, Prodan *et al* 1982). The other principal scheme is that of cooling atoms in counter-propagating red-detuned laser beams (Letokhov *et al* 1976, 1977). This second scheme provides for the cooling of atoms at a zero average velocity. In the case of transverse irradiation of an atomic beam by counter-propagating laser beams, this scheme provides for the transverse cooling and collimation of the beam (Balykin *et al* 1984a, c, 1985b, Aspect *et al* 1986). When irradiating an atomic gas by three pairs of counter-propagating laser waves, the scheme makes it possible to effect the 3D cooling of atoms (Chu *et al* 1985, Lett *et al* 1988).

Theoretical analysis of a most simple model of interaction of a two-level atom with counter-propagating laser beams has shown that laser cooling makes it possible to reach extremely low temperatures, five to six orders of magnitude lower than room temperature. It was shown that in a two-level atom model the cooling mechanism is based on single-photon absorption (emission) processes and found that the minimum temperature of atoms is reached at a red detuning equal to the natural half-width of the atomic transition line,  $\delta = -\gamma$ , and is determined by the atomic transition natural half-width (Letokhov *et al* 1977):

$$T_D = \hbar\gamma/k_B. \quad (1.4)$$

The value of temperature (1.4) found by Letokhov, Minogin, and Pavlik is nowadays referred to as the Doppler temperature or the Doppler cooling limit. To avoid misunderstanding, one should stress that temperature (1.4) is defined by the natural linewidth and not by the Doppler width. At typical value of the natural linewidth  $\Gamma = 2\gamma 2\pi \times 10$  MHz the temperature  $T_D$  is of the order of 100  $\mu$ K.

Subsequent experimental investigations have shown that real multilevel atoms can be cooled in counter-propagating laser waves down to temperatures an order or two below minimum temperature (1.4) predicted by the two-level atom model (Lett *et al* 1988, Weiss *et al* 1989). The deeper cooling of multilevel atoms in comparison with the idealized two-level atoms proves possible owing to the contribution from the two-photon friction mechanism specific to multilevel atoms (Dalibard and Cohen-Tannoudji 1989, Ungar *et al* 1989, Chang *et al* 1990a, b, 1999a, b, Cohen-Tannoudji 1997, Jun *et al* 1999a, b). In multilevel dipole interaction schemes, the laser field excites the atoms from many magnetic sublevels of the ground electronic state. Accordingly, in multilevel cooling schemes the two-photon and higher-order multiphoton processes produce an additional friction that lowers the atomic temperature below the value  $T_D$ .

The fundamental lower temperature limit for any laser cooling process based on the photon recoil was shown to be determined by the quantum fluctuations of the atomic momentum and accordingly cannot be lower than the value defined by the recoil energy,

$$T_r = \hbar^2 k^2 / 2Mk_B, \quad (1.5)$$

where  $k = \omega_0/c$  is the wavevector corresponding to the frequency  $\omega_0$  of the atomic transition excited by the laser light. Temperature (1.5) is customarily called the recoil temperature. For atoms of moderate mass whose resonance transitions are in the visible region, typical values of the recoil temperature  $T_r$  amount to a few microKelvin. In practical schemes, the multilevel atoms are frequently cooled by counter-propagating laser beams down to temperatures of the order of 10  $\mu$ K (Letokhov and Minogin 1981, Balykin *et al* 1985a, Phillips 1998, Adams and Riis 1997).

Finally, it should be noted that in addition to the laser cooling methods based on the photon recoil, there has also been developed the laser methods for the optical pumping of the velocity-

selective translational atomic states described by the effective temperatures below the recoil temperature  $T_r$  (Aspect *et al* 1988, Kasevich and Chu 1992, Lawall *et al* 1995, Lee *et al* 1996). One of these methods is based on the velocity-selective coherent trapping of atomic population in the superpositional state composed of the ground-state substates (Aspect *et al* 1988, Lawall *et al* 1995). Another method is based on the use of the narrow two-photon Raman transitions between two hyperfine levels in the ground state to select a narrow velocity group of atoms and push it toward zero velocity (Kasevich and Chu 1992).

After the development of laser cooling techniques, the first successful experiment was performed on the trapping of cold atoms in a quadrupole magnetic trap (Migdal *et al* 1985). This experiment has initiated numerous experiments on magnetic trapping neutral atoms (Petrich *et al* 1995, Davis *et al* 1995, Ketterle and Van Druten 1996, Hinds and Hughes 1999).

At this period many new schemes for the optical trapping of cold atoms were proposed. It was suggested that cold atoms could be trapped in the periodic potential produced by the dipole interaction of an atom with a resonance standing laser wave (Kazantsev 1974, Botin *et al* 1976, Letokhov *et al* 1976, 1977, Kazantsev *et al* 1990). Possibilities were considered of trapping atoms by dipole forces in the intersection regions of counter-propagating laser beams (Letokhov and Minogin 1978, Ashkin 1978) or in the focus of a single laser beam (Ashkin 1978). All proposals as to the development of purely optical traps for atoms ran into the principal difficulty caused by the finite lifetime of atoms in traps due to the momentum diffusion in laser fields (Cook 1980a, b, Gordon and Ashkin 1980). To get over this difficulty, it was suggested that use should be made of two laser fields separated in time, one for cooling the atoms and the other for trapping them (Dalibard *et al* 1983, 1984). Similar approaches to atom trapping by means of time-varying fields were considered by Lovelace *et al* (1985), Cornell *et al* (1991) and Morinaga and Shimizu (1994).

When optical atom traps were first discussed, it seemed very promising to create a purely optical trap based only on the resonance radiation pressure force. It was presumed that a central-symmetric light field composed of several divergent laser beams could be used to produce a potential well for cold atoms due to the coordinate-dependent radiation pressure force (Minogin and Javanainen 1982). The attraction of the idea was the fact that for red-detuned laser beams this trap could simultaneously cool and trap the atoms. Later on, however, it was shown that such laser field configurations were incapable of producing stable potential wells for atoms (Ashkin and Gordon 1983). The limitations formulated by Ashkin and Gordon on the structures of the trapping laser fields came to be known as the optical Earnshaw theorems by analogy with the well known electrostatics theorem.

However, the optical Earnshaw theorems cease to hold true when the atoms are placed in the external force fields (Pritchard *et al* 1986). Using this circumstance, Dalibard suggested a magneto-optical trap (MOT) (Dalibard 1987) which was soon realized experimentally (Raab *et al* 1987) and subsequently gained wide recognition. In the MOT, a nonuniform magnetic field produces the Zeeman shifts of atomic magnetic sublevels, so that the counter-propagating laser beams not only cool the atoms, but also trap them in the central region of the trap.

The cooling of atoms in counter-propagating laser beams which may interfere to produce the periodic optical potential renewed interest in the first idea of the optical trapping of atoms in the nodes or antinodes of standing laser waves (Letokhov 1968). With cold atoms, numerous experiments became possible on the creation of periodic lattices of cold atoms that are often called the optical lattices (Jessen and Deutsch 1996).

In 1982, the original idea of an atom mirror was introduced, which greatly influenced the development of the methods of trapping cold atoms. The idea was to use an evanescent laser wave propagating along a dielectric–vacuum interface as a reflecting mirror for atoms (Cook and Hill 1982). Since the evanescent light wave penetrates into the vacuum to a distance of

the order of the optical wavelength, the high gradient of the evanescent wave field produces a substantial dipole gradient force on the atom. At a large detuning of the evanescent wave with respect to the atomic transition, the radiation pressure force proves very weak, and the atomic dynamics in the evanescent wave is essentially governed by the dipole gradient force alone. In the case of a large blue detuning, the gradient force produces in the vacuum region a repulsive barrier which reflects atoms. This barrier is not very high, but it is quite sufficient to reflect cold atoms. The first experiments on the reflection of a thermal beam of sodium atoms at a grazing angle (Balykin *et al* 1987, 1988b) and on the reflection of normally incident cold atoms (Kasevich *et al* 1990, Aminoff *et al* 1993) confirmed that an evanescent wave can effectively reflect atoms. It was also shown that the reflection coefficient of the atom mirror may be high even at low intensity of the laser wave. It was found that introducing metal coatings of additional dielectric layers in the vicinity of the dielectric–vacuum interface substantially enhanced the evanescent wave field as a result of excitation of surface plasmons (Esslinger *et al* 1993) or on account of the formation of a dielectric waveguide (Kaiser *et al* 1994).

The development of an atom mirror gave impetus to the development of methods for the gravito-optical trapping of cold atoms. It was theoretically demonstrated that a horizontally arranged concave atom mirror could be used to create gravito-optical traps for cold atoms (Wallis *et al* 1992). Ten reflections of cold atoms from a concave atomic mirror were experimentally observed (Aminoff *et al* 1993). In recent years, there have been suggested and experimentally realized half-open gravito-optical traps (Ovchinnikov *et al* 1995, Soding *et al* 1995).

Another important atom mirror application suggested was the development of cavities for the de Broglie atom waves, similar to the Fabry–Perot optical cavities (Balykin and Letokhov 1989). There were also suggested and analysed 3D atomic cavities based on evanescent waves (Dowling and Gea-Banacloche 1995). The evanescent-wave atom mirror idea was subsequently transformed to the proposal to develop atom waveguides similar to optical waveguides (Ol'shania *et al* 1993, Savage *et al* 1993, Marksteiner *et al* 1994). The first experiments verified the serviceability of atom waveguides (Renn *et al* 1995, 1996, Ito *et al* 1996).

Some promising schemes for trapping cold atoms still await their analysis and experimental implementation. Classed with such still imperfectly understood schemes can be electrostatic traps (Wing 1980) and gravito-magnetic traps based on magnetic mirrors (Sidorov *et al* 1996, Hughes *et al* 1997).

Summarizing the brief history of ideas in the field of trapping neutral atoms, one can note that while the impetuous developments in this field take their course there still remain the two principal objectives already formulated in the first works on the laser cooling and trapping atoms (Letokhov and Minogin 1981, Minogin and Letokhov 1987). One of these objectives is the use of trapped cold atoms to perform precision experiments in atomic and nuclear physics and spectroscopy and to develop new generations of quantum frequency and time standards. The other important objective is to use traps for cold atoms to materially enhance the phase density of atomic ensembles, i.e. to increase the number of atoms in narrow spatial and velocity intervals in order to achieve a regime of quantum degeneracy wherein the classical atomic gas becomes a quantum one. In the case of Bose atoms, the overlapping of atom wavepackets under quantum degeneracy conditions leads to the BEC of the atomic gas, when the density of atoms and the de Broglie wavelength  $\lambda_{dB} = h/p$  are related by the well known relation

$$n\lambda_{dB}^3 \geq 2.62. \quad (1.6)$$

The above two important objectives will no doubt for many years to come inspire investigators to develop new types of atom traps. Recently, owing to the development of the evaporative

cooling technique (Hess 1986, Ketterle and Van Druten 1996), the first observations of the BEC in ultracold atom ensembles trapped in magnetic traps have already been made along these lines (Anderson *et al* 1995, Davis *et al* 1995, Bradley *et al* 1995).

This paper is aimed at discussing the main physical ideas underlying the methods of trapping cold atoms in electromagnetic fields, as well as in electromagnetic–gravity field combinations. Along with the analysis of the physical fundamentals of traps for cold atoms, the paper discusses physical ideas of developing cavities and waveguides for de Broglie atom waves. The key experiments are described, as well as the most striking experimental achievements.

## 2. Dynamics of an atom in a laser field

The most important methods for cooling and trapping atoms are based on the use of the forces acting on atoms in the laser fields or in the fields composed of the laser fields and the magnetic or gravity fields. The dynamics of atoms in the laser field is thus a key for understanding the techniques of atom cooling and trapping. In this section we review the forces on atoms in the laser fields and discuss the equations of atomic motion. In the discussion below, the atomic medium is considered to be very rarefied, so that atomic collisions can be disregarded.

### 2.1. Dipole radiation force

The dynamics of the centre of mass of an atom in the laser field with a wavelength much larger than the characteristic atomic size is determined by the electric dipole interaction. Under the dipole interaction with the electric field  $\mathbf{E} = \mathbf{E}(\mathbf{r}, t)$  described by the dipole interaction operator

$$V = -\mathbf{D}\mathbf{E}, \quad (2.1)$$

the atom acquires an induced dipole moment  $\langle \mathbf{D} \rangle$ . The value of the induced atomic dipole moment is determined as usual by the quantum mechanical mean,

$$\langle \mathbf{D} \rangle = \text{Tr}(\rho \mathbf{D}), \quad (2.2)$$

where  $\rho$  is the atomic density matrix. Finally, the interaction of the induced atomic dipole moment  $\langle \mathbf{D} \rangle$  with the spatially varying laser field  $\mathbf{E} = \mathbf{E}(\mathbf{r}, t)$  causes a dipole radiation force on the atom.

From a quantum mechanical point of view, the induced atomic dipole moment  $\langle \mathbf{D} \rangle$  originates from the dipole transitions between the quantized atomic states describing the stationary motion of the electrons in the atom and stationary translational motion of the atom. For this reason, the induced dipole moment generally includes both the average value and the quantum fluctuations. As is well known, the concept of a force on a particle is always a classical concept. According to general physical rules a notion of the force can be applied to a particle which can be considered as a structureless particle moving classically or quasiclassically. In the case of an atom interacting with a laser field the concept of the dipole radiation force can accordingly be used when the quantum fluctuations of the atomic dipole moment are small compared with its average value and the atom moves classically or quasiclassically. This means that the notion of the dipole radiation force on an atom can be applied under two basic conditions. One of them is the condition of small fluctuations in the induced atomic dipole moment. Under this condition the atom can be considered as a structureless classical particle well characterized by the average value of the induced dipole moment. Another condition on the use of the dipole radiation force is the usual condition for the quasiclassical character

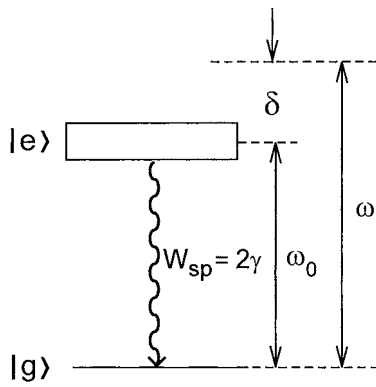


**Figure 5.** Two-level atom interacting with a monochromatic laser field.

of the translational motion of the atom, requiring that the quantum fluctuations of the atomic momentum should be small compared with the atomic momentum itself.

Physically, both the above conditions are satisfied when the time of the dipole interaction between the atom and the laser field,  $t$ , is substantially longer than the characteristic relaxation times  $\tau_{\text{intern}}$  of the internal atomic states involved in the dipole interaction and the quantum fluctuations  $\delta p_{\text{qu}}$  of the atomic momentum are small compared with the variations  $\delta p$  of the mean atomic momentum,

$$\begin{aligned} \tau_{\text{intern}} &\ll t \\ \delta p_{\text{qu}} &\ll \delta p. \end{aligned} \quad (2.3)$$

When the first condition in equation (2.3) is satisfied, the internal atomic states quickly decay to quasistationary values corresponding to small fluctuations in the induced atomic dipole moment. In turn, under the second condition (2.3) the quantum fluctuations in the atomic momentum are small compared with both the variations of the classical momentum and the classical atom momentum itself.

In the simplest case of a two-level atom shown in figure 5 the only internal relaxation time is the spontaneous decay time  $\tau_{\text{intern}} = \tau_{\text{sp}} = 1/W_{\text{sp}}$ , where  $W_{\text{sp}} = A = 2\gamma$  is the spontaneous decay probability (or the Einstein coefficient  $A$ ). In this case the concept of the dipole radiation force becomes valid when the atom interacts with a laser field for a time period longer than the spontaneous decay time. The second condition of (2.3) is automatically satisfied for a two-level atom since in this case the quantum fluctuations of atomic momentum are defined by the photon momentum,  $\delta p_{\text{qu}} = \hbar k$ , where  $k = \omega/c$  is the wavevector of the laser light, and the smallest value of the classical atomic momentum is defined from the condition of resonance between classically moving atom and the laser field,  $\delta p \approx M\gamma/k$  (Minogin and Letokhov 1987). As one can see, the condition  $\hbar k \ll M\gamma/k$  is equivalent to the condition that the recoil frequency  $\omega_r = \hbar k^2/2M$  defined by the recoil energy  $R = \hbar\omega_r$  is small compared with the natural half-width of the dipole transition:

$$\omega_r \ll \gamma. \quad (2.4)$$

This last inequality is always satisfied for dipole atomic transitions. For the multilevel dipole interaction schemes general conditions (2.3) may introduce more rigid constraints on atomic parameters since the atomic states may possess two or more different relaxation times (see section 2.3).

When conditions (2.3) are satisfied, the induced atomic dipole moment is determined by the quasiclassical atomic density matrix  $\rho = \rho(\mathbf{r}, \mathbf{v}, t)$  which is a function of the coordinate

$\mathbf{r}$  and velocity  $\mathbf{v}$  of a classically moving atom,

$$\langle \mathbf{D} \rangle = \rho_{\alpha\beta} \mathbf{D}_{\beta\alpha}. \quad (2.5)$$

Here  $\mathbf{D}_{\alpha\beta}$  are the matrix elements of the atomic dipole moment operator that are defined with respect to the time-dependent atomic eigenfunctions,

$$\mathbf{D}_{\alpha\beta} = \mathbf{d}_{\alpha\beta} \exp[i(E_\alpha - E_\beta)t/\hbar], \quad (2.6)$$

where  $\mathbf{d}_{\alpha\beta} = \langle \alpha | \mathbf{d} | \beta \rangle$  are the dipole moment matrix elements defined with respect to the time-independent eigenfunctions, and  $E_\alpha, E_\beta$  are the energies of the internal atomic states connected by the dipole transitions.

According to relation (2.1), the energy of the dipole interaction of an atom with the laser field is

$$U = \langle V \rangle = -\langle \mathbf{D} \rangle \mathbf{E}. \quad (2.7)$$

Relation (2.7) formally coincides with the classical expression for the interaction energy of a permanent dipole with the electric field  $\mathbf{E}$ . Accordingly, equation (2.7) can be directly used to calculate the force  $\mathbf{F}$  on an atom in the laser field  $\mathbf{E}$ . Applying the well known classical formula for the force on a particle with a permanent dipole moment  $\langle \mathbf{D} \rangle$  one can find the dipole radiation force as

$$\mathbf{F} = \nabla U = \nabla(\langle \mathbf{D} \rangle \mathbf{E}) = \langle D_i \rangle \nabla E_i, \quad (2.8)$$

where the subscript  $i = x, y, z$  determines the rectangular coordinates of the vectors. In the above expression the atomic dipole moment is treated as a permanent quantity which must not be differentiated with respect to the coordinate.

Equation (2.8) gives the most general expression for the dipole radiation force on the atom moving classically or quasiclassically in a laser field. From a quantum mechanical point of view, radiation force (2.8) arises as a result of the quantum mechanical momentum exchange between the atom and the laser field in the presence of the spontaneous relaxation. The change in the atomic momentum comes from the elementary processes of photon absorption and emission: stimulated absorption, stimulated emission and spontaneous emission. Radiation force (2.8) is, generally speaking, a function of the coordinate and velocity of the atom's centre of mass. The dependence of the force on the coordinate may originate from the dependence of the laser field  $\mathbf{E}$  and the atomic density matrix  $\rho$  on the coordinate  $\mathbf{r}$ . The velocity dependence of the force may come from the dependence of the atomic density matrix on velocity. The specific dependence of the force on the coordinate and velocity is governed by the structure of the atomic energy levels participating in the dipole interaction and the spatial-temporal structure of the laser field.

The basic types of radiation force (2.8) can be understood on simple models of the quasiresonance interaction of a two-level atom with the monochromatic field of a laser beam, a standing laser wave, and an evanescent wave of laser radiation, as well as on some simple models describing the interaction of multilevel atoms with laser fields. Some examples of the force on a two-level atom are described in section 2.2 and on multilevel atoms in section 2.3.

## 2.2. Dipole radiation force on a two-level atom

**2.2.1. Radiation force in a laser beam. Potential of the gradient force.** In the case of the dipole interaction of a two-level atom with a spatially inhomogeneous field  $\mathbf{E}$  of a monochromatic laser beam defined by a unit polarization vector  $\mathbf{e}$ , amplitude  $E_0(\mathbf{r})$ , wavevector  $\mathbf{k}$  and frequency  $\omega = kc$ ,

$$\mathbf{E} = \mathbf{e} E_0(\mathbf{r}) \cos(\mathbf{k}\mathbf{r} - \omega t) \quad (2.9)$$

the atom acquires the induced dipole moment

$$\langle \mathbf{D} \rangle = \text{Tr}(\rho \mathbf{D}) = \rho_{12} \mathbf{d}_{21} \exp(i\omega_0 t) + \rho_{21} \mathbf{d}_{12} \exp(-i\omega_0 t), \quad (2.10)$$

where  $\omega_0 = (E_2 - E_1)/\hbar$  is the atomic transition frequency (see figure 5). The magnitude of the induced dipole moment (2.10) is determined by the atomic density matrix elements  $\rho_{\alpha\beta}$  describing the internal quantum states of a two-level atom, where  $\alpha, \beta = 1, 2$ , and the matrix elements of the atomic dipole moment operator.

In the standard rotating wave approximation (RWA) and with the dipole moment matrix elements chosen to be real,  $\mathbf{d}_{12} = \mathbf{d}_{21} = \mathbf{d}$ , the atomic density matrix elements obey the well known equations of motion (see, for example, Minogin and Letokhov 1987):

$$\begin{aligned} \left( \frac{\partial}{\partial t} + \mathbf{v} \frac{\partial}{\partial \mathbf{r}} \right) \rho_{22} &= i\Omega(\mathbf{r})(\rho_{12} e^{i(\mathbf{k}\mathbf{r} - \delta t)} - \rho_{21} e^{-i(\mathbf{k}\mathbf{r} - \delta t)}) - 2\gamma \rho_{22}, \\ \left( \frac{\partial}{\partial t} + \mathbf{v} \frac{\partial}{\partial \mathbf{r}} \right) \rho_{21} &= i\Omega(\mathbf{r})(\rho_{11} - \rho_{22}) e^{i(\mathbf{k}\mathbf{r} - \delta t)} - \gamma \rho_{21}, \\ \left( \frac{\partial}{\partial t} + \mathbf{v} \frac{\partial}{\partial \mathbf{r}} \right) \rho_{11} &= i\Omega(\mathbf{r})(\rho_{21} e^{-i(\mathbf{k}\mathbf{r} - \delta t)} - \rho_{12} e^{i(\mathbf{k}\mathbf{r} - \delta t)}) + 2\gamma \rho_{22}, \end{aligned} \quad (2.11)$$

where  $\Omega(\mathbf{r})$  is the Rabi frequency defined as

$$\Omega(\mathbf{r}) = d E_0(\mathbf{r}) / 2\hbar, \quad (2.12)$$

where  $d = \mathbf{d} \cdot \mathbf{e}$  is the projection of the dipole moment matrix element on the laser beam polarization vector  $\mathbf{e}$  and  $\delta$  is the detuning of the laser field frequency  $\omega$  with respect to the atomic transition frequency  $\omega_0$ :

$$\delta = \omega - \omega_0. \quad (2.13)$$

In equations (2.11), the quantity  $2\gamma$  defines the rate of the spontaneous decay of the atom from the upper level  $|2\rangle$  to the lower level  $|1\rangle$ , i.e. the Einstein coefficient  $A$ :

$$W_{\text{sp}} = A = 2\gamma = \frac{4d^2 \omega_0^3}{\hbar c^3} = \frac{4\|d\|^2 \omega_0^3}{3\hbar c^3}, \quad (2.14)$$

where  $\|d\|$  is the reduced dipole matrix element. The total (convective) time derivatives on the left-hand side of equations (2.11) describe the changes of the density matrix elements both in time and due to the spatial motion of the atom.

Moving in equations (2.11) from the off-diagonal elements  $\rho_{12}, \rho_{21} = \rho_{12}^*$  to the new off-diagonal elements  $\sigma_{12}, \sigma_{21} = \sigma_{12}^*$ :

$$\sigma_{12} = \rho_{12} \exp(i(\mathbf{k}\mathbf{r} - \delta t)) \quad (2.15)$$

one may rewrite the induced dipole moment of a two-level atom as

$$\langle \mathbf{D} \rangle = (\sigma_{12} \exp(-i\mathbf{k}z + i\omega t) + \sigma_{21} \exp(i\mathbf{k}z - i\omega t)) \mathbf{d}. \quad (2.16)$$

After substitution (2.15) the equations of motion (2.11) are reduced to equations containing no explicit time dependence:

$$\begin{aligned} \left( \frac{\partial}{\partial t} + \mathbf{v} \frac{\partial}{\partial \mathbf{r}} \right) \rho_{22} &= i\Omega(\mathbf{r})(\sigma_{12} - \sigma_{21}) - 2\gamma \rho_{22}, \\ \left( \frac{\partial}{\partial t} + \mathbf{v} \frac{\partial}{\partial \mathbf{r}} \right) \sigma_{21} &= i\Omega(\mathbf{r})(\rho_{11} - \rho_{22}) - [\gamma + i(\delta - \mathbf{k}\mathbf{v})] \sigma_{21}, \\ \left( \frac{\partial}{\partial t} + \mathbf{v} \frac{\partial}{\partial \mathbf{r}} \right) \rho_{11} &= i\Omega(\mathbf{r})(\sigma_{21} - \sigma_{12}) + 2\gamma \rho_{22}. \end{aligned} \quad (2.17)$$

Applying now the basic formula (2.8) one can see that the radiation force on a two-level atom in the field of a laser beam (2.9) is defined by the steady-state atomic density matrix

elements  $\sigma_{\alpha\beta}$  as a sum of two forces: the radiation pressure force  $\mathbf{F}_{\text{rp}}$  and the dipole gradient force  $\mathbf{F}_{\text{gr}}$ ,

$$\mathbf{F} = \mathbf{F}_{\text{rp}} + \mathbf{F}_{\text{gr}}, \quad (2.18a)$$

$$\mathbf{F}_{\text{rp}} = \mathbf{k} \left( \frac{dE_0(\mathbf{r})}{2} \right) i(\sigma_{12} - \sigma_{21}), \quad (2.18b)$$

$$\mathbf{F}_{\text{gr}} = \left( \frac{d\nabla E_0(\mathbf{r})}{2} \right) (\sigma_{12} + \sigma_{21}). \quad (2.18c)$$

The dipole gradient force  $\mathbf{F}_{\text{gr}}$  is frequently referred to simply as the gradient force.

Within the framework of the considered semiclassical approach, the radiation pressure force  $\mathbf{F}_{\text{rp}}$  is due to the interaction of the induced atomic dipole moment with the light field varying on the scale of the optical wavelength  $\lambda = 2\pi/k$ . The gradient force  $\mathbf{F}_{\text{gr}}$  is due to the interaction of the induced dipole moment of an atom with the light field varying on the scale of the field amplitude  $E_0(\mathbf{r})$ .

The explicit expressions for the two parts of the radiation force can be found by taking into account the fact that, according to conditions (2.3), the radiation force is defined by the steady-state values of the density matrix elements  $\sigma_{21}$  and  $\sigma_{21} = \sigma_{12}^*$ . The steady-state solution to equations (2.17) can be found, putting  $\partial/\partial t = 0$ ,  $\partial/\partial r = 0$  and using the normalization condition  $\rho_{11} + \rho_{22} = 1$ . The steady-state values for the off-diagonal density matrix elements are

$$\sigma_{12} = \sigma_{21}^* = -\frac{\Omega(\mathbf{r})(\delta - \mathbf{k}\mathbf{v} + i\gamma)}{\gamma^2 + 2\Omega^2(\mathbf{r}) + (\delta - \mathbf{k}\mathbf{v})^2}. \quad (2.19)$$

Substituting quantities (2.19) into equations (2.18b) and (2.18c), one can obtain the final expressions for the two parts of the radiation force on a two-level atom,

$$\mathbf{F}_{\text{rp}} = \hbar\mathbf{k}\gamma \frac{G(\mathbf{r})}{1 + G(\mathbf{r}) + (\delta - \mathbf{k}\mathbf{v})^2/\gamma^2}, \quad (2.20a)$$

$$\mathbf{F}_{\text{gr}} = -\frac{1}{2}\hbar(\delta - \mathbf{k}\mathbf{v}) \frac{\nabla G(\mathbf{r})}{1 + G(\mathbf{r}) + (\delta - \mathbf{k}\mathbf{v})^2/\gamma^2}, \quad (2.20b)$$

where  $G(\mathbf{r})$  is the dimensionless saturation parameter,

$$G(\mathbf{r}) = \frac{2\Omega^2(\mathbf{r})}{\gamma^2} = \frac{1}{2} \left( \frac{dE_0(\mathbf{r})}{\hbar\gamma} \right)^2 = \frac{I(\mathbf{r})}{I_S}, \quad (2.21)$$

$I(\mathbf{r}) = (c/8\pi)E_0^2(\mathbf{r})$  is the intensity of the laser beam at point  $\mathbf{r}$  and  $I_S = (c/4\pi)(\hbar\gamma/d)^2$  is the saturation intensity. Figure 6 shows the dependences of the radiation pressure force and the gradient force on the atomic velocity projection  $v_z = v$  on the propagation direction of a Gaussian laser beam.

For the above-considered case of interaction of a two-level atom with a monochromatic laser beam, one can give a simple interpretation of the two parts of the radiation force in terms of the elementary processes of photon absorption and emission. The radiation pressure force (2.20a) can be interpreted as coming from the stimulated absorption of a photon from the laser beam and its subsequent spontaneous emission into one of the vacuum modes. (The stimulated emission of a photon into the same laser mode causes no change in the momentum of the laser field and, hence, in the atomic momentum.) Insofar as the direction of the spontaneous photon emission is arbitrary, the value of the momentum transferred to the atom, averaged over many spontaneous emission events, is equal to the momentum of the absorbed photon. Thus, the radiation pressure force (2.20a) results from the transfer to the atom of the photon momentum in the course of its stimulated absorption and subsequent spontaneous emission.

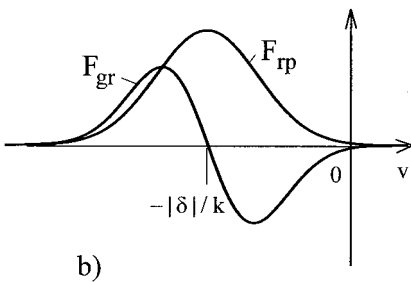
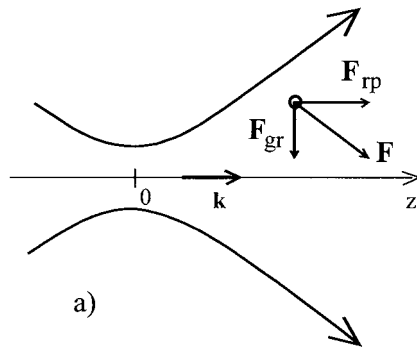


**Figure 6.** (a) Dipole radiation force  $\mathbf{F} = \mathbf{F}_{\text{rp}} + \mathbf{F}_{\text{gr}}$  on a two-level atom in a focused Gaussian laser beam and (b) the velocity dependence of the radiation pressure force  $\mathbf{F}_{\text{rp}}$  and the gradient force  $\mathbf{F}_{\text{gr}}$  at red detuning,  $\delta < 0$ . The atom is at exact resonance with the laser beam at the longitudinal velocity  $v_{\text{res}} = -|\delta|/k$ .

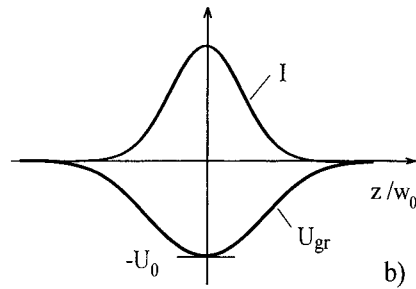
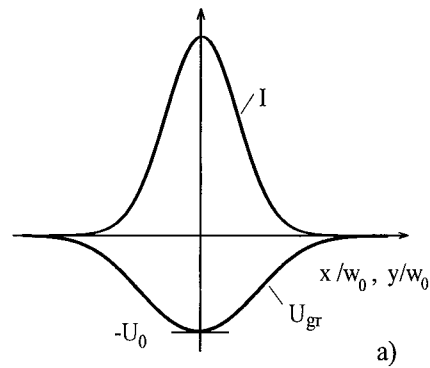


**Figure 7.** Intensity  $I$  of a Gaussian laser beam and potential of the gradient force  $U_{\text{gr}}$  as functions of coordinates  $x, y, z$ : (a) in the transverse direction and (b) along the beam propagation direction.

The radiation pressure force is thus related to the dissipative optical processes. Note next that the field of a spatially inhomogeneous laser beam can be considered as a superposition of many plane waves propagating within the divergence angle of the beam. In the field composed of many plane light waves the atom momentum can be changed by another elementary process, the stimulated absorption by the atom of a photon from one plane wave and its subsequent stimulated emission into another plane wave. Both photons participating in this process have the same energy and differ only by the propagation direction. This process results in the gradient force which is accordingly directed along the intensity gradient of the laser beam as defined by expression (2.20b). The gradient force is thus related to the conservative optical processes.

The effects of the radiation pressure force and the gradient force on the atom are essentially different. The radiation pressure force (2.20a) always accelerates the atom in the direction of the wavevector  $\mathbf{k}$ . The gradient force (2.20b) pulls the atom into the laser beam or pushes it out the beam depending on the sign of the Doppler-shifted detuning  $\delta - \mathbf{k}\mathbf{v}$ .

At a low velocity of the atom along the laser beam,  $|v| \ll |\delta|/k$ , the gradient force depends only on the position of the atom. Accordingly, for atoms slowly moving along the laser beam, the gradient force can in the lowest approximation be treated as a velocity-independent potential force. In that case, one can put in formula (2.20b)  $\mathbf{k}\mathbf{v} = k v = 0$  and introduce the potential

of the gradient force, putting its value equal to zero at infinity (Gordon and Ashkin 1980):

$$U_{\text{gr}}(\mathbf{r}) = \int_r^\infty \mathbf{F}_{\text{gr}}(v=0) d\mathbf{r} = \frac{1}{2} \hbar \delta \ln \left( 1 + \frac{G(\mathbf{r})}{1 + \delta^2/\gamma^2} \right). \quad (2.22)$$

For a conventional laser beam possessing the intensity maximum at the symmetry axis, at negative (red) detuning,  $\delta < 0$ , equation (2.22) defines the potential well for slow moving atoms. An important example of the above situation is a Gaussian laser beam. For a Gaussian beam propagating along  $Oz$  axis and having its focus at the origin of the coordinate frame (figure 6(a)), the beam intensity varies as  $I(\mathbf{r}) = I(0)(w_0/w)^2 \exp(-(x^2 + y^2)/w^2)$ , where  $w$  is the beam radius dependent on the longitudinal coordinate  $z$ ,  $w = w_0 \sqrt{1 + (\lambda z/2\pi w_0)^2}$ ,  $w_0$  is the waist radius of the laser beam, and  $\lambda$  is the laser wavelength. In that case, at red detuning the potential (2.22) is reduced to a 3D potential well (figure 7). The depth of the potential well,  $U_0$ , produced by the Gaussian beam is the same in all directions. For a laser beam possessing the intensity minimum near the axis, for example a beam produced by a  $\text{TEM}_{01}^*$  laser mode, a potential well is formed, on the contrary, at positive (blue) detuning.

At large detuning,  $|\delta| \gg \gamma$ ,  $\Omega$ , the potential of the gradient force (2.22) reduces to a simple expression useful for practical estimations,

$$U_{\text{gr}}(\mathbf{r}) = \hbar \frac{\Omega^2(\mathbf{r})}{\delta}. \quad (2.23)$$

It should be noted that the total potential for slow moving atoms generally differs from the potential of the gradient force (2.22), for it additionally includes the potential produced by the radiation pressure force:

$$U_{\text{rp}} = \int_r^\infty \mathbf{F}_{\text{rp}}(v=0) d\mathbf{r}. \quad (2.24)$$

When potential (2.24) is taken into consideration, the total potential of the atom in the laser beam (2.9) becomes asymmetric in the direction of the  $z$ -axis, because the potential due to the radiation pressure force is shifted in the direction of the wavevector  $\mathbf{k}$ . The magnitude of the asymmetric potential (2.24) can be reduced by increasing the value of the detuning.

**2.2.2. Radiation force in a standing laser wave.** The structure of the dipole radiation force on a two-level atom in a monochromatic standing laser wave with a unit polarization vector  $\mathbf{e}$  and frequency  $\omega = kc$ ,

$$\mathbf{E} = 2eE_0 \cos kz \cos \omega t, \quad (2.25)$$

substantially differs from that in a travelling laser wave. For a spatially periodic field (2.25) the quasistationary elements of the atomic density matrix are the periodic functions of the coordinate  $z$ . Accordingly, the use of formula (2.8) in the case of a standing laser wave leads to an expression for the radiation force which is a periodic function of the coordinate  $z$ . Mathematically, the natural representation of the radiation force on an atom in field (2.25) is the representation in the form of the Fourier series. The Fourier representation of the radiation force on a two-level atom in field (2.25) was found for a case of a weak saturation (Letokhov *et al* 1976, 1977), moderate saturation (Stenholm *et al* 1978) and for arbitrary saturation (Minogin and Serimaa 1979). In addition to the Fourier representation, there has also been found a closed analytic expression for the radiation force, which holds true at arbitrary saturation, but only at a low velocity of the two-level atom (Minogin and Serimaa 1979, Gordon and Ashkin 1980).

At a not very high intensity of the standing laser wave (2.25) the Fourier series for the radiation force on a two-level atom can be truncated at the first oscillating terms. The result of

such an approximation is the following expression for the force (Letokhov *et al* 1976, 1977):

$$F = F_0 + F_{2s} \sin 2kz + F_{2c} \cos 2kz, \quad (2.26a)$$

$$F_0 = \hbar k \gamma \frac{G(L_- - L_+)}{1 + G(L_- + L_+)}, \quad (2.26b)$$

$$F_{2s} = \hbar k G \frac{(\delta - kv)L_- + (\delta + kv)L_+}{1 + G(L_- + L_+)}, \quad (2.26c)$$

$$F_{2c} = -F_0, \quad (2.26d)$$

where  $v = v_z$  is the atomic velocity projection on the wave propagation direction  $Oz$ . In the above relations, the dimensionless saturation parameter  $G$  is defined similar to (2.21),  $G = 2\Omega^2/\gamma^2$ ,  $\Omega = dE_0/2\hbar$  is the Rabi frequency and

$$L_{\pm} = \frac{\gamma^2}{\gamma^2 + (\delta \pm kv)^2} \quad (2.27)$$

are the Lorentzian factors. Note that the magnitude of the radiation force (2.26a) averaged over the spatial period in the first-order approximation in the saturation parameter is close to the difference of two radiation pressure forces of form (2.20a),

$$F_0 \approx \hbar k \gamma G(L_- - L_+), \quad (2.28)$$

which allows one to state that at a weak saturation the average radiation force  $F_0$  has the meaning of the radiation pressure force.

Radiation force (2.26a) corresponds to a weak saturation of the atomic transition and accordingly includes the contributions from the one-photon absorption (emission) processes only. The two-photon and higher-order multiphoton processes contribute to the radiation force at high optical saturation. The even-order multiphoton processes produce narrow velocity structure near zero velocity. The odd-order multiphoton processes produce so-called multiDoppleron structures at the velocities corresponding to the multiphoton resonance conditions (figure 8) (Minogin and Serimaa 1979).

At a low atomic velocity one can put into relations (2.26a)–(2.26d)  $v = 0$  as a first approximation. Accordingly, for a slow atom radiation force (2.26a) is reduced to the oscillating gradient force

$$F = F_{gr} = 2\hbar k \delta \frac{G}{1 + 2G + \delta^2/\gamma^2} \sin 2kz. \quad (2.29)$$

Gradient force (2.29) can be considered as being correspondent to the periodic potential

$$U = U_0 \cos 2kz, \quad U_0 = \hbar \delta \frac{G}{1 + 2G + \delta^2/\gamma^2}. \quad (2.30)$$

At a fixed detuning, the depth of potential (2.30) increases as the saturation parameter is increased. At saturation parameter  $G \gg \frac{1}{2}(1 + \delta^2/\gamma^2)$  or, equivalently, at the Rabi frequency  $\Omega \gg \frac{1}{2}\sqrt{\gamma^2 + \delta^2}$ , the depth of potential (2.30) is close to its asymptotic value  $U_0 = \hbar|\delta|$ .

The oscillation frequencies of the atom near the minima of the periodic potential are directly determined from the shape of the potential well bottom. For a red-detuned laser wave,  $\delta < 0$ , potential (2.30) has the minima in the loops of standing light wave (2.25), i.e. at the points  $kz_m = m\pi$ ,  $m = 0, \pm 1, \pm 2, \dots$ . In the vicinity of any minimum, potential (2.30) is a harmonic:

$$U \simeq \frac{1}{2} M \omega_v^2 (z - z_m)^2, \quad (2.31)$$

where the oscillation frequency is

$$\omega_v = 2\sqrt{2(U_0/\hbar)}\omega_r, \quad (2.32)$$

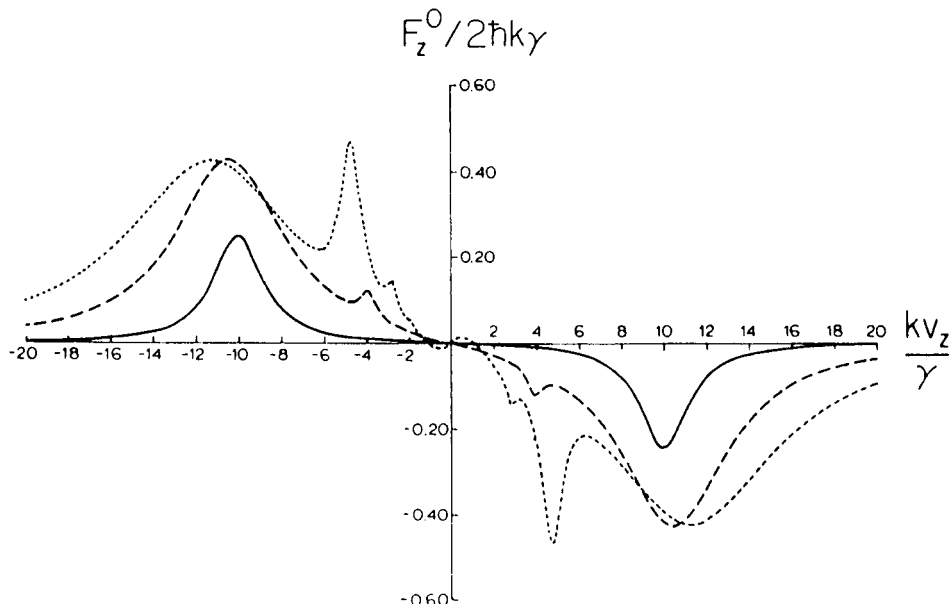


**Figure 8.** Radiation pressure force on a two-level atom in a standing laser wave at red detuning  $\delta = -10\gamma$  for saturation parameter  $G = 1$  (solid curve),  $G = 9$  (dashed curve) and  $G = 25$  (dotted curve). (Minogin and Serimaa 1979.)

and  $\omega_r = \hbar k^2 / 2M$  is the recoil frequency. Accordingly, the spectrum of the atomic quantum states near the minima of the periodic potential is harmonic ( $n = 0, 1, 2, \dots$ ):

$$\varepsilon = \hbar\omega_v(n + \frac{1}{2}). \quad (2.33)$$

At blue detuning,  $\delta > 0$ , relations (2.31)–(2.33) describe small oscillations of an atom in the vicinity of the nodes of the standing laser wave, i.e. at points  $kz_m = \pi/2 + m\pi$ ,  $m = 0, \pm 1, \pm 2, \dots$

When expanded to a first order in velocity, the radiation force (2.26a) also includes, in addition to the gradient force (2.29), the radiation pressure force proportional to the atomic velocity  $v_z = v$ :

$$F = 2\hbar k \delta \frac{G}{1 + 2G + \delta^2/\gamma^2} \sin 2kz + 8\hbar k^2 \frac{\delta}{\gamma} \frac{G \sin^2 kz}{(1 + 2G + \delta^2/\gamma^2)(1 + \delta^2/\gamma^2)} v. \quad (2.34)$$

At red detuning, the radiation pressure force, i.e. the second part of force (2.34), is reduced to a friction force with a friction coefficient  $\beta$  being a periodic function of atomic coordinate  $z$ :

$$F_{\text{fr}} = -M\beta v, \quad \beta = 16\omega_r \frac{|\delta|}{\gamma} \frac{G \sin^2 kz}{\gamma(1 + 2G + \delta^2/\gamma^2)(1 + \delta^2/\gamma^2)}. \quad (2.35)$$

It should be noted that the friction coefficient has a maximum in the neighbourhood of the potential maxima and goes to zero near the minima of the potential. The coordinate dependences of potential (2.30) and of the individual parts of the radiation dipole force are shown in figure 9, along with the coordinate dependence of momentum diffusion coefficient discussed in section 2.4.1.

**2.2.3. Radiation force in an evanescent laser wave.** The radiation force on a two-level atom in an evanescent laser wave propagating along a dielectric–vacuum interface is of the same

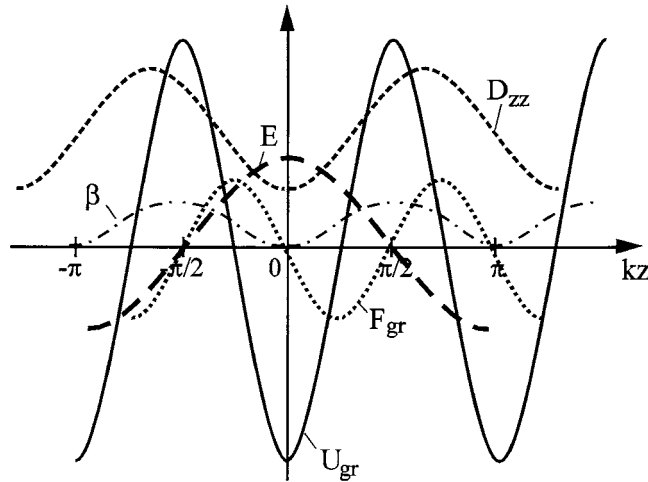


**Figure 9.** Position dependence of the field  $E$  of a standing laser wave (2.25), the gradient force  $F_{\text{gr}}$  (2.29), the potential of the gradient force  $U_{\text{gr}}$  (2.30), the friction coefficient (2.35) and the momentum diffusion coefficient  $D_{zz}$  (2.65) at red detuning.

general structure (2.18a)–(2.18c) as the force in a laser beam. Indeed, the radiation force in the case of evanescent wave includes, as before, the radiation pressure force (2.18b) and the gradient force (2.18c). These two forces depend in their own specific ways on the atomic coordinate because the spatial dependence of the evanescent wave field differs materially from that of the laser beam field. The evanescent light wave propagating along the dielectric–vacuum interface decays very rapidly—at a distance of the order of the optical wavelength—into the vacuum region, producing as a result a substantial gradient force directed across the interface.

In the coordinate frame shown in figure 10, the electric field of the evanescent wave can be written as

$$\mathbf{E} = eE_0 e^{-\alpha z} \cos(ky - \omega t), \quad (2.36)$$

where  $\alpha = k\sqrt{n^2 \sin^2 \theta - 1}$  is the inverse characteristic distance to which the evanescent wave penetrates into the vacuum region, which depends on the refractive index  $n$  of the dielectric and the angle  $\theta$  of incidence of the initial laser wave on the interface, and where  $k = 2\pi/\lambda$  is the wavevector of the laser light with a wavelength  $\lambda$ . It is presumed in the above scheme that the incidence angle of the initial laser wave exceeds the angle of total internal reflection,  $\sin \theta > 1/n$ .

The evanescent wave field (2.36) is a particular case of the field of a spatially inhomogeneous light beam (2.9). Accordingly, the above formulae for the radiation pressure force (2.18b) and the gradient force (2.18c) can be directly used to find the force in field (2.36). Saturation parameter (2.21) describing the interaction between the two-level atom and field (2.36) may conveniently be written as

$$G(\mathbf{r}) = G_0 e^{-2\alpha z}, \quad G_0 = \frac{1}{2} (dE_0 / \hbar \gamma)^2, \quad (2.37)$$

where  $G_0$  is the saturation parameter at the interface. Substituting (2.37) into (2.18b) and (2.18c), one can write the following expressions for the gradient force and the radiation pressure force:

$$F_{\text{gr}} = F_z = \hbar \alpha (\delta - kv_y) \frac{G_0 e^{-2\alpha z}}{1 + G_0 e^{-2\alpha z} + (\delta - kv_y)^2 / \gamma^2}, \quad (2.38)$$

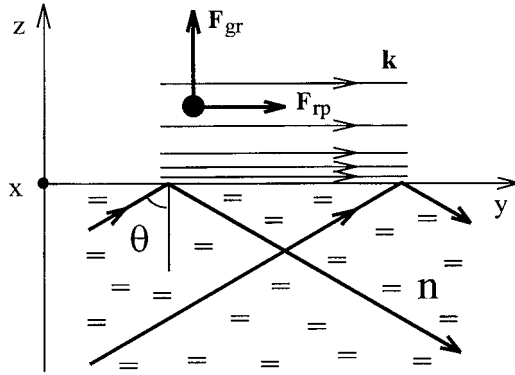


**Figure 10.** Directions of the gradient force  $F_{gr}$  and the radiation pressure force  $F_{rp}$  on a two-level atom in an evanescent laser wave propagating along the dielectric–vacuum interface. The laser wave is chosen to be red detuned with respect to atomic transition.

$$F_{rp} = F_y = \hbar k \gamma \frac{G_0 e^{-2\alpha z}}{1 + G_0 e^{-2\alpha z} + (\delta - kv_y)^2 / \gamma^2}. \quad (2.39)$$

Note that according to the Fresnel laws the saturation parameter  $G_0$  at the interface can be expressed in terms of the saturation parameter  $G_i$  of the incident laser wave in the form (Kaiser *et al* 1994)

$$G_0 = \frac{4n^2 \cos^2 \theta}{(n^2 - 1)[(n^2 + 1) \sin^2 \vartheta - 1]^p} G_i, \quad (2.40)$$

where index  $p = 0,1$  stands for the polarization of the incident wave of TE or TM type respectively.

As can be seen from equation (2.38), at a low atomic velocity along the interface,  $|v_y| \ll |\delta|/k$ , and at blue detuning,  $\delta > 0$ , the gradient force pushes the atom into the region of lower field intensity, i.e. into the vacuum region. This makes it possible to use the evanescent light field as a mirror for atoms (Cook and Hill 1982). For an atom slowly moving along the interface, in particular, at normal incidence of the atom from the vacuum region onto the evanescent wave, the gradient force can be treated as a potential force produced by a potential. In a case of blue detuning, the potential of the gradient force according to (2.22) is

$$U_{gr}(\mathbf{r}) = \frac{1}{2} \hbar \delta \ln \left( 1 + \frac{G_0 e^{-2\alpha z}}{1 + \delta^2 / \gamma^2} \right). \quad (2.41)$$

Where the atomic velocity along the interface remains invariably low throughout the time that the interaction between the atom and the evanescent wave lasts, potential (2.41) provides for the specular reflection of the atom. Actually, the small change of the longitudinal atomic velocity caused by radiation pressure force (2.39) and the weak velocity dependence of the gradient force always make the atom mirror imperfect, leading to a difference between the angles of reflection and incidence. This shortcoming of the atom mirror can be considerably lessened by choosing a large detuning. In this last and practically most important case, when  $|\delta| \gg \gamma, \Omega_0$ , the potential of the gradient force (2.41) reduces to a simple exponential form:

$$U_{gr}(\mathbf{r}) = \frac{\hbar \gamma^2}{2\delta} G_0 e^{-2\alpha z} = \frac{\hbar \Omega_0^2}{\delta} e^{-2\alpha z}, \quad (2.42)$$

where  $\Omega_0 = dE_0/2\hbar$  is the Rabi frequency at the dielectric–vacuum interface.

**2.2.4. Gradient force potential in the dressed state picture.** The above-considered general approach based on formula (2.8) enables one to find the radiation force for any dipole interaction scheme. When the kinetic energy of the atom is small, the atom–field interaction is sometimes

described by the so-called dressed state formalism useful for interpretation of the gradient force and the gradient force potential (Cohen-Tannoudji *et al* 1992). This formalism is a direct extension of the well known quasienergy state concept (Zel'dovich 1973) to a case of the quantized light field.

In the dressed state picture, the 'atom + laser field' system is treated as a closed system possessing the stationary quantum mechanical states. For one to be able to analyse the system 'atom + laser field' quantum mechanically, one treats the classical laser field as a quantized electromagnetic field. Although the dressed state formalism considers the classical laser field as a quantized object without any actual need, it gives a clear picture of the elementary processes responsible for the dipole gradient force.

In the simplest case of interaction of a two-level atom with monochromatic field (2.9), the Hamiltonian of a single-mode quantized electromagnetic field can be represented in the well known form,

$$H_l = \hbar\omega a^\dagger a, \quad (2.43)$$

where  $a^\dagger$  and  $a$  are the photon creation and annihilation operators. In the above equation, it is presumed that the zero-point oscillation energy is extracted from the laser mode energy  $E_l$ ,

$$E_l = n\hbar\omega, \quad (2.44)$$

where  $n$  is the number of photons in the laser mode.

The Hamiltonian  $H_a$  of the two-level atom possessing the ground state  $|g\rangle$  and the excited state  $|e\rangle$  is usually described in the dressed state formalism with the use of the atomic excitation and de-excitation operators  $b^\dagger$ ,  $b$ , defined by the relations

$$\begin{aligned} b|g\rangle &= 0, & b^\dagger|g\rangle &= |e\rangle, \\ b|e\rangle &= |g\rangle, & b^\dagger|e\rangle &= 0. \end{aligned} \quad (2.45)$$

The Hamiltonian of a free atom expressed through the atomic operators  $b$ ,  $b^\dagger$  has the form

$$H_a = \hbar\omega_0 b^\dagger b. \quad (2.46)$$

According to equation (2.45), the eigenvalues of the atomic Hamiltonian are

$$\langle g|H_a|g\rangle = E_g, \quad \langle e|H_a|e\rangle = E_e = E_g + \hbar\omega_0. \quad (2.47)$$

The electric dipole interaction operator in the RWA being expressed through the photon and atomic operators has the form

$$V = -\mathbf{d}(\mathbf{E}b^\dagger a + \mathbf{E}^*ba^\dagger), \quad (2.48)$$

where  $\mathbf{d}$  is the matrix element of the atomic dipole moment operator, and

$$\mathbf{E} = i\mathbf{e}Ee^{ikr} = i\sqrt{\frac{2\pi\hbar\omega}{V}}\mathbf{e}e^{ikr}, \quad (2.49)$$

is the electric field associated with a single photon with the wavevector  $\mathbf{k}$  and the unit polarization vector  $\mathbf{e}$ , and  $V$  is the volume of the laser mode. The matrix elements of the dipole interaction operator  $V$  taken in the RWA are other than zero only for one-photon absorption (emission) processes,

$$\langle e, n|V|g, n+1\rangle = -\mathbf{d}\mathbf{E}\sqrt{n+1}, \quad \langle g, n+1|V|e, n\rangle = -\mathbf{d}\mathbf{E}^*\sqrt{n+1}. \quad (2.50)$$

The Hamiltonian of the closed system 'atom + laser field' includes thus the laser mode Hamiltonian, the atomic Hamiltonian, and the dipole interaction operator  $V$ ,

$$H = H_l + H_a + V = H_a = \hbar\omega a^\dagger a + \hbar\omega_0 b^\dagger b - \mathbf{d}(\mathbf{E}b^\dagger a + \mathbf{E}^*ba^\dagger). \quad (2.51)$$

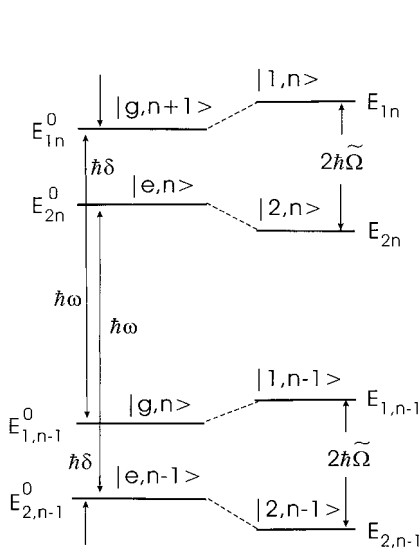


**Figure 11.** Dressed states of a two-level atom in a single-mode quantized electromagnetic wave.

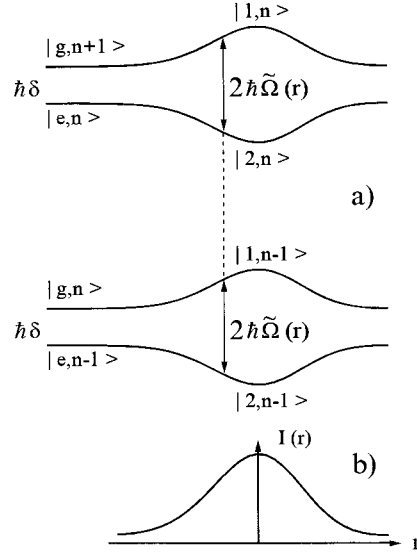


**Figure 12.** Dressed states of a two-level atom in a laser beam as functions of (a) an atom position and (b) the intensity profile of the laser beam.

In the absence of the dipole interaction, when  $V = 0$ , the ‘atom + laser field’ system has the stationary states  $|g, n + 1\rangle = |g\rangle|n + 1\rangle$  and  $|e, n\rangle = |e\rangle|n\rangle$  with the energies (see figure 11)

$$\begin{aligned} E_{1n}^0 &= \langle g, n + 1 | H_l + H_a | g, n + 1 \rangle = E_g + (n + 1)\hbar\omega, \\ E_{2n}^0 &= \langle e, n | H_l + H_a | e, n \rangle = E_g + n\hbar\omega = E_g + (n + 1)\hbar\omega - \hbar\delta, \end{aligned} \quad (2.52)$$

which differ by the amount of the detuning  $\delta = \omega - \omega_0$ . When the dipole interaction term  $V$  is taken into consideration, the system has the new stationary states  $|1n\rangle$  and  $|2n\rangle$  with the energies (figure 11)

$$\begin{aligned} E_{1n} &= \langle 1n | H_l + H_a + V | 1n \rangle = E_g + (n + 1)\hbar\omega - \frac{1}{2}\hbar\delta + \hbar\tilde{\Omega}, \\ E_{2n} &= \langle 2n | H_l + H_a + V | 2n \rangle = E_g + (n + 1)\hbar\omega - \frac{1}{2}\hbar\delta - \hbar\tilde{\Omega}, \end{aligned} \quad (2.53)$$

which depend on the value of the generalized Rabi frequency  $\tilde{\Omega}$ ,

$$\tilde{\Omega} = \sqrt{\Omega^2 + \delta^2/4}, \quad \Omega = \sqrt{n + 1}(dE/\hbar), \quad (2.54)$$

where the new ‘quantum expression’ for the Rabi frequency  $\Omega$  is defined by the ‘amplitude’ of a photon electric field (2.49),  $E = \sqrt{2\pi\hbar\omega/V}$ . The stationary states  $|1n\rangle$  and  $|2n\rangle$ , referred to as the dressed states, are the linear combinations of the initial states  $|g, n + 1\rangle = |g\rangle|n + 1\rangle$  and  $|e, n\rangle = |e\rangle|n\rangle$ ,

$$\begin{aligned} |1n\rangle &= \frac{i\Omega/\tilde{\Omega}}{2\sqrt{2\tilde{\Omega} - \delta}} e^{-ikr/2} |g, n + 1\rangle + \frac{\sqrt{2\tilde{\Omega} - \delta}}{4\tilde{\Omega}} e^{ikr/2} |e, n\rangle, \\ |2n\rangle &= \frac{i\Omega/\tilde{\Omega}}{2\sqrt{2\tilde{\Omega} + \delta}} e^{ikr/2} |g, n + 1\rangle + \frac{\sqrt{2\tilde{\Omega} + \delta}}{4\tilde{\Omega}} e^{-ikr/2} |e, n\rangle. \end{aligned} \quad (2.55)$$

In the field of a spatially inhomogeneous laser beam, the energies of the dressed states depend on the position of the atom,  $E_{1n, 2n} = E_{1n, 2n}(r)$  (see figure 12). In that case, the energies (2.53) can be considered as the potential energies of the atom in the states  $|1n\rangle$  and

$|2n\rangle$ , i.e. in the states with a given number of the laser photons. After subtracting the constant energy term from energies (2.53), the potentials of the motionless atom in the states  $|1n\rangle$  and  $|2n\rangle$  are accordingly  $U_1(\mathbf{r}) = \hbar\tilde{\Omega}(\mathbf{r})$  and  $U_2(\mathbf{r}) = -\hbar\tilde{\Omega}(\mathbf{r})$ .

The dressed state representation allows one to give a simple interpretation of the dependence of the gradient force on a two-level atom on the sign of the detuning  $\delta$  (figure 11). As one can see from equations (2.55), in the case of positive (blue) detuning the state  $|1n\rangle$  contains a greater fraction of the ground atomic state than the state  $|2n\rangle$ . Since the population of the ground atomic state exceeds that of the excited state,  $n_g > n_e$ , the atom spends most of the time in the repulsive potential  $U_1(\mathbf{r}) = \hbar\tilde{\Omega}(\mathbf{r})$ . Accordingly, at  $\delta > 0$  the gradient force pushes the atom out of the laser beam. In the case of negative (red) detuning, the situation is quite the opposite, and the gradient force pulls the atom into the laser beam. At exact resonance,  $\delta = 0$ , the atom is equally distributed between the states  $|1n\rangle$  and  $|2n\rangle$ , and the gradient force vanishes.

The dressed state formalism combined with simple physical arguments can also be used for some quantitative estimations. In particular, at large detuning,  $|\delta| \gg \Omega$ , the greater part of atomic population is in the ground state,  $n_g \approx 1$ ,  $n_e \approx 0$ . Accordingly, the total potential of the atom in the laser field is simply defined by the generalized Rabi frequency,

$$\tilde{\Omega}(\mathbf{r}) \approx \frac{1}{2}\hbar\delta + \hbar\frac{\Omega^2(\mathbf{r})}{\delta}. \quad (2.56)$$

The second term in the right-hand side of this equation defines the position-dependent potential of the atom at large detuning. This potential obviously represents the potential of the gradient force defined by equation (2.23). The gradient force at zero atomic velocity directly follows from potential (2.56):

$$F_{\text{gr}} = -\nabla\tilde{\Omega}(\mathbf{r}) = -2\hbar\Omega(\mathbf{r})\nabla\Omega(\mathbf{r})/\delta. \quad (2.57)$$

The force defined by equation (2.57) coincides with the gradient force defined by equation (2.20b) at zero velocity.

### 2.3. Dipole radiation force on a multilevel atom

As was shown in section 2.2, the dipole interaction of a two-level atom with a weakly saturating laser field is mainly governed by the one-photon optical processes. Accordingly, at a low optical saturation the radiation force on a two-level atom includes mainly the contributions coming from the one-photon absorption (emission) processes. By contrast, in the multilevel dipole interaction schemes, the two-photon and higher-order even multiphoton optical processes can play an important role even at a low saturation. The physical reason for that is that the even-order multiphoton processes connect the ground-state atomic sublevels, possessing high population just under a low saturation.

One of the simplest and practically important multilevel dipole interaction schemes is that described by the model of a (3 + 5)-level atom (figure 13). The atom is assumed to be excited by two counter-propagating circularly polarized laser waves described by the electric field

$$\mathbf{E} = \frac{1}{2}E_0(\mathbf{e}_+e^{i(kz-\omega t)} - \mathbf{e}_-e^{-i(kz-\omega t)}) - \frac{1}{2}E_0(\mathbf{e}_+e^{i(kz+\omega t)} - \mathbf{e}_-e^{-i(kz+\omega t)}), \quad (2.58)$$

where  $\mathbf{e}_{\pm} = \mp\frac{1}{\sqrt{2}}(\mathbf{e}_x \pm i\mathbf{e}_y)$  are the spherical unit vectors,  $k = \omega/c$  is the wavevector, and  $\omega$  is the laser field frequency. With respect to the quantization axis  $Oz$  the first wave in equation (2.58) is a  $\sigma^+$  polarized wave and the second one is a  $\sigma^-$  polarized wave. This interaction scheme is of interest as the simplest model that includes the two-photon optical processes contributing to the radiation force. The scheme is also of practical importance, for it

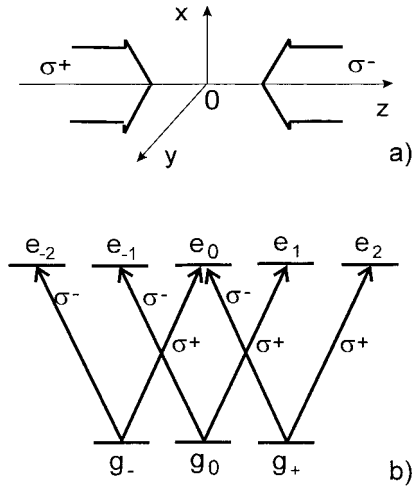


**Figure 13.** A (3 + 5)-level atom excited by two counter-propagating circularly polarized laser waves.

can be applied to a real atom possessing two hyperfine-structure states, the ground state  $F = 1$  with three magnetic sublevels and the excited state  $F = 2$  with five magnetic sublevels.

The above simplest multilevel scheme was first analysed within the framework of the dressed state formalism (Dalibard and Cohen-Tannoudji 1989) as a theoretical model of the sub-Doppler laser cooling of atoms (see section 3.2). The equations for the atomic density matrix for a (3 + 5)-level interaction scheme were discussed by Dalibard and Cohen-Tannoudji (1989) and Chang *et al* (1999b). Below, we describe the radiation force on a (3 + 5)-level atom following the general approach discussed in section 2.1.

According to basic formula (2.8), the radiation force on a (3 + 5)-level atom interacting with a field defined by equation (2.58) can be written as (Chang *et al* 1999a, b)

$$F = 2\hbar k \Omega \text{Im} \left[ (\sigma_{g_-e_{-2}} + \sigma_{e_{+2}g_+}) + \frac{1}{\sqrt{2}}(\sigma_{g_0e_{-1}} + \sigma_{e_{+1}g_0}) + \frac{1}{\sqrt{6}}(\sigma_{g_+e_0} + \sigma_{e_0g_-}) \right], \quad (2.59)$$

where  $\sigma_{\alpha\beta}$  are the quasistationary atomic density matrix elements satisfying the equations which include no explicit time and coordinate dependence, the Rabi frequency is defined as  $\Omega = \|d\| E_0 / 2\sqrt{5}\hbar$ , and  $\|d\|$  is the reduced matrix element of the atomic dipole moment.

At a weak optical saturation and low atomic velocity,  $kv \ll \gamma$ , the above atomic density matrix elements can be found analytically. Under these conditions the radiation force (2.59) is reduced to the form (Dalibard and Cohen-Tannoudji 1989, Chang *et al* 1999a, b)

$$F = \hbar k \gamma \frac{25G}{11(1 + \delta^2/\gamma^2)^2} \frac{(88/85)\mu^2 + k^2v^2}{\mu^2 + k^2v^2} \frac{\delta kv}{\gamma^2} - \hbar k \gamma \frac{5G^2}{44(1 + \delta^2/\gamma^2)^2} \frac{\delta kv}{\mu^2 + k^2v^2}, \quad (2.60)$$

where  $G = 2\Omega^2/\gamma^2$  is the saturation parameter and the quantity  $\mu$  is the half-width of the two-photon resonance originated from the two-photon transitions between the ground-state sublevels  $|g_- \rangle$  and  $|g_+ \rangle$ ,

$$\mu = \frac{1}{4} \sqrt{\frac{17}{33}} G \frac{\gamma^2 \sqrt{5\gamma^2 + \delta^2}}{\gamma^2 + \delta^2}. \quad (2.61)$$

Radiation force (2.60) includes two physically different parts (figure 14). The first part of the force is mainly contributed to by the one-photon resonances localized at resonance velocities  $v_{\text{res}} = \pm\delta/k$ . These resonances have the same physical meaning as the one-photon resonances in the radiation pressure force on a two-level atom in a standing-wave field (2.25). The second part of the force is due to the two-photon resonances which couple the extreme ground-state

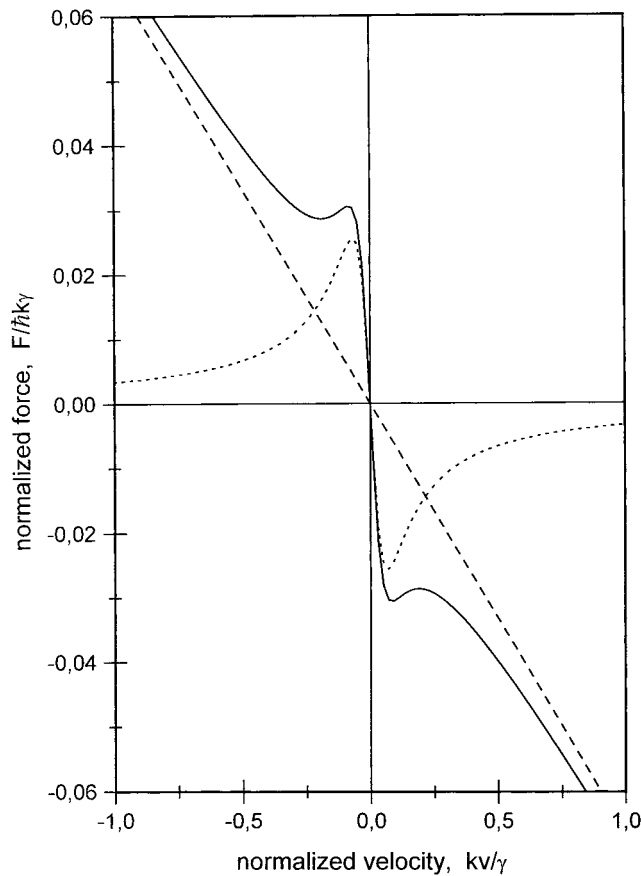


**Figure 14.** Radiation force (solid curve) on a  $(3 + 5)$ -level atom in the field of two counter-propagating  $\sigma^+ - \sigma^-$  polarized laser waves as a function of the velocity projection on the axis  $Oz$  at red detuning  $\delta = -3\gamma$  and saturation parameter  $G = 1$ . The dashed curve shows the one-photon part and the dotted line shows the two-photon part of the total force (Chang *et al* 1999b).

sublevels  $|g_- \rangle, |g_+ \rangle$ . According to the energy conservation law written in the atom rest frame, the two-photon resonances are most effective under the condition  $(\omega \pm kv) - (\omega \mp kv) \approx 0$ , i.e. at zero atomic velocity. The velocity width of the two-photon resonance is defined by the quantity  $\delta v = \mu/k$  which in the case of large detuning may be much smaller than that of the one-photon resonance,  $\delta v \approx (\gamma/k)(\Omega/\delta)^2 \ll \gamma/k$ . For negative (red) detuning both parts of force (2.60) are reduced to the friction forces. The first, one-photon part of the force is responsible for the Doppler cooling of atoms, and the second, two-photon part, for the sub-Doppler cooling of atoms (see section 3).

#### 2.4. Kinetic description of atomic motion

The above-considered radiation forces play the main role in atomic dynamics in the laser fields. At the same time, the radiation force fails to completely describe the motion of the atom in the laser field since the dynamics of the atom in the laser field is a stochastic one. Atomic momentum fluctuates in the laser field because of the fluctuations in the photon emission direction and fluctuations in the number of the emitted photons. For these reasons, a complete

description of atomic dynamics in the laser field is based on the quantum statistical equations for the atomic density matrix, which take into account both the variation of atomic momentum caused by the radiation force and the quantum fluctuations of the atomic momentum (Stenholm 1986, Minogin and Letokhov 1987, Kazantsev *et al* 1990, Cohen-Tannoudji *et al* 1992).

Under the conditions defined by equations (2.3), the quantum statistical description of atomic motion can, as a rule, be reduced to the simpler quasiclassical kinetic description of the time evolution of the atomic distribution function  $w = w(\mathbf{r}, \mathbf{p}, t)$ . For noninteracting atoms the atomic distribution function  $w$  can generally be normalized both to a single atom and to the total number of atoms. Below, we assume, for the sake of definiteness, normalization to a single atom,

$$\int w(\mathbf{r}, \mathbf{p}, t) d^3r d^3p = 1. \quad (2.62)$$

The atomic distribution function satisfies the Fokker–Planck-type kinetic equation,

$$\frac{\partial w}{\partial t} + \mathbf{v} \frac{\partial w}{\partial \mathbf{r}} = - \frac{\partial}{\partial \mathbf{p}} (\mathbf{F}w) + \sum_{i=x,y,z} \frac{\partial^2}{\partial p_i^2} (D_{ii}w), \quad (2.63)$$

which includes the dipole radiation force  $\mathbf{F}$  and the momentum diffusion tensor  $D_{ii}$  describing the broadening of the atomic momentum distribution on account of the quantum fluctuations. Below, we will present the coefficients of the Fokker–Planck equations for the already-considered cases of the dipole interaction between a two-level atom and a monochromatic travelling and standing laser wave and for the interaction between a (3 + 5)-level atom and the field of two counter-propagating circularly polarized laser waves.

**2.4.1. Two-level atoms.** In the case of interaction of a two-level atom with the laser beam (2.9), the radiation force  $\mathbf{F}$  is defined by expressions (2.18a), (2.20a) and (2.20b), and the momentum diffusion tensor is (Minogin 1980)

$$\begin{aligned} D_{ii} &= \frac{1}{2} \hbar^2 k^2 \gamma \frac{G(\mathbf{r})}{1 + G(\mathbf{r}) + (\delta - \mathbf{k}\mathbf{v})^2 / \gamma^2} \chi_{ii}, \\ \chi_{ii} &= \alpha_{ii} + \delta_{iz}(1 + d), \\ d &= \frac{[(\delta - \mathbf{k}\mathbf{v})^2 / \gamma^2 - 3]G(\mathbf{r})}{[1 + G(\mathbf{r}) + (\delta - \mathbf{k}\mathbf{v})^2 / \gamma^2]^2}. \end{aligned} \quad (2.64)$$

In the above formulae, the frequency detuning  $\delta$  and saturation parameter  $G(\mathbf{r})$  are defined, as before, by relations (2.13) and (2.21). The values of the coefficients  $\alpha_{ii}$  depend on the angular anisotropy of spontaneous photon emission. When laser beam (2.9) is circularly polarized and propagates in the direction of the  $z$ -axis, the coefficients  $\alpha_u$  are  $\alpha_{xx} = \alpha_{yy} = \frac{3}{10}$  and  $\alpha_{zz} = \frac{2}{5}$ . When the beam propagates along the same  $z$ -axis but is linearly polarized along the  $x$ -axis, the coefficients  $\alpha_{ii}$  are  $\alpha_{xx} = \frac{1}{5}$ ,  $\alpha_{yy} = \frac{2}{5}$ , and  $\alpha_{zz} = \frac{2}{5}$ . Note that when using the two-level atom model to describe the dynamics of an atom whose two states are degenerate in the total angular momentum projection, one can restrict oneself to approximate values of the coefficients  $\alpha_{ii}$  corresponding to a hypothetical isotropic spontaneous emission:  $\alpha_{ii} = \frac{1}{3}$ .

In the case of interaction of a two-level atom with an evanescent wave defined by expression (2.36), the radiation force  $\mathbf{F}$  consists of components (2.38) and (2.39). The momentum diffusion tensor for evanescent wave (2.36) is defined by formulae (2.64) wherein one should put  $\mathbf{k}\mathbf{v} = kv_y$  and substitute for the saturation parameter its magnitude from expression (2.37).

The quasiclassical motion of a two-level atom in a standing laser wave defined by equation (2.25) is described by a Fokker–Planck equation wherein the dipole radiation force

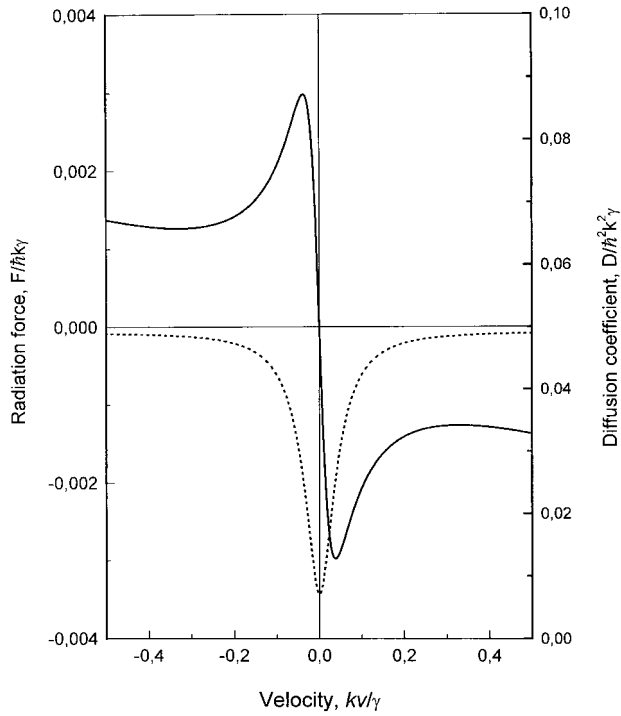


**Figure 15.** Radiation force (solid curve) and momentum diffusion coefficient  $D = D_{zz}$  (dotted curve) for a (3 + 5)-level atom in the field of two counter-propagating  $\sigma^+ - \sigma^-$  polarized laser waves as a function of the velocity projection on the axis  $Oz$  at red detuning  $\delta = -22\gamma$  and saturation parameter  $G = 4.6$  (Chang *et al* 1999b).

and momentum diffusion tensor generally have a very complex form (Minogin and Letokhov 1987). In the case of weak saturation and low atomic velocity, where the force  $F$  is defined by relation (2.34), the momentum diffusion tensor in the zero-velocity approximation is (Minogin and Letokhov 1987)

$$D_{ii} = 2\hbar^2 k^2 \gamma \frac{G}{1 + \delta^2/\gamma^2} (\alpha_{ii} \cos^2 kz + \delta_{zi} \sin^2 kz). \quad (2.65)$$

The longitudinal component of diffusion tensor (2.65) is shown in figure 9.

**2.4.2. Multilevel atoms.** For the multilevel dipole interaction scheme described by a (3 + 5)-level atom model (section 2.3), the coefficients of the Fokker–Planck equation were found for arbitrary interaction parameters (Chang *et al* 1999a, b). The analytical results have shown that in the case of a (3 + 5)-level atom the two-photon optical processes not only increase the friction due to the radiation force, but also sharply reduce the momentum diffusion tensor at a zero atomic velocity (figure 15). At a weak optical saturation and low atomic velocity, the radiation force in a (3 + 5)-level atom model is defined by equation (2.60) and the longitudinal component of the momentum diffusion tensor is

$$D_{zz} = \frac{46}{17} \hbar^2 k^2 \gamma \frac{\Omega^2}{\delta^2}. \quad (2.66)$$

This value of the diffusion coefficient defines jointly with the friction coefficient the effective atomic temperature for the sub-Doppler cooling of atoms (see section 3).

### 3. Laser cooling of atoms

Typically, any scheme of trapping atoms operates not with thermal atoms but atoms preliminary cooled by the laser light. On the other hand, atoms already confined in electromagnetic traps are often subjected to laser cooling since the reduction of the atomic kinetic energy increases the lifetime of atoms in a trap. The laser cooling of atoms is thus a key to successful trapping of atoms. In this section we discuss the basic methods of laser cooling of atoms and the basic temperature limits. Many other important details of laser cooling of atoms can be found in the review literature (Letokhov and Minogin 1981, Balykin *et al* 1985b, Stenholm 1986, Minogin and Letokhov 1987, Phillips *et al* 1988, Kazantsev *et al* 1990, Chu 1991, Metcalf and van der Straten 1994).

#### 3.1. Doppler cooling

The main methods of laser cooling atoms can be illustrated on an idealized model of a two-level atom. As already noted in the introduction, laser cooling in the two-level atom model only proves possible down to minimal temperature (1.4) determined by the natural half-width of the dipole transition line. As the laser cooling mechanism in the case of two-level atom is based on the one-photon absorption by the moving atom of a Doppler-shifted optical radiation, the cooling of atoms down to temperature (1.4) is usually referred to as Doppler cooling.

*3.1.1. Deceleration and longitudinal cooling of an atomic beam.* Figure 16 shows the basic idea of the laser deceleration and longitudinal cooling of a thermal atomic beam by a counter-propagating laser beam. In the scheme of figure 16(a) a red-detuned laser beam produces the radiation pressure force (2.20a) which most effectively decelerates the atoms with longitudinal velocities  $v_z$  close to the resonance velocity  $v_{\text{res}} = |\delta|/k$ . The deceleration of atoms whose velocities are far from the resonance velocity is less effective, for radiation pressure force (2.20a) has a Lorentzian velocity dependence. As a result, the radiation pressure force both decelerates the atoms and narrows the atomic velocity distribution, i.e. produces a cooling of the atomic beam. Figure 17 shows the experimental velocity distribution profile of a beam of sodium atoms decelerated and cooled by a dye laser radiation in the first experiment on the laser cooling of atoms (Andreev *et al* 1981, 1982).

The above simplest method of the longitudinal laser cooling at a fixed detuning is most effective for cooling atoms moving at resonance velocities. The efficiency of deceleration and cooling naturally drops when the atoms fall off resonance with the laser light due to the velocity decrease. To maintain a high deceleration and cooling rate, the experimental techniques make use of chirping of the laser frequency (Balykin *et al* 1979, Ertmer *et al* 1985) or Zeeman tuning of the atomic transition frequency by an inhomogeneous magnetic field whose strength varies along the atomic beam propagation direction (Prodan *et al* 1982). The use of these techniques makes it possible to decelerate an atomic beam having an initial thermal velocity  $v_0$  down to a zero average velocity, the deceleration length being (Zueva *et al* 1981)

$$l = \frac{v_0^2}{2v_r\gamma} \frac{1+G}{G}, \quad (3.1)$$

where  $v_r = \hbar k/M$  is the recoil velocity and  $G$  is the saturation parameter defined by expression (2.21). At thermal velocity  $v_0 \approx 10^5 \text{ cm s}^{-1}$  and a moderate saturation,  $G \approx 1$ , the deceleration length  $l$  ranges between 10 and 100 cm. The longitudinal temperature of an atomic beam under optimal conditions can be reduced down to 100–10 mK. Discussions of the experimental techniques of the longitudinal cooling of atomic beams can be found in Letokhov and Minogin (1981), Balykin *et al* (1985b), Adams and Riis (1997).

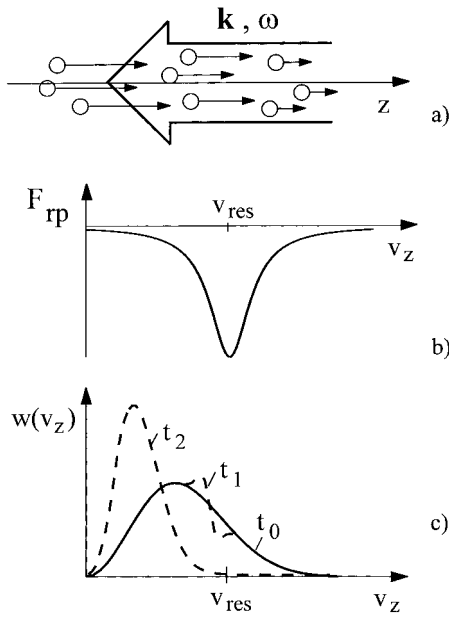


**Figure 16.** (a) Scheme of a longitudinal cooling of a thermal atomic beam by a counter-propagating laser beam. (b) The radiation pressure force as function of the longitudinal atom velocity. (c) The atomic velocity distribution at times  $t_2 > t_1 > t_0$ .

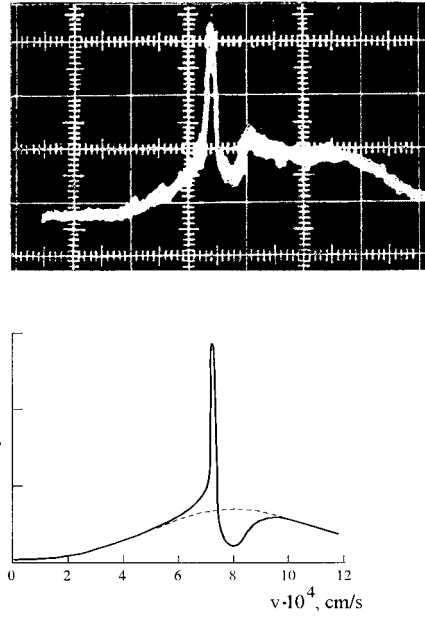


**Figure 17.** Experimental velocity distribution for a beam of sodium atoms decelerated by a dye laser in the first experiment on the laser cooling of atoms and the theoretical prediction for the parameters relevant to the experiment (Andreev *et al* 1981, 1982).

**3.1.2. Transverse cooling (collimation) of an atomic beam.** The second important laser cooling scheme is that for transverse cooling (collimation) of atomic beams by counter-propagating laser waves. This scheme can be used either separately or in combination with the longitudinal cooling scheme to reduce the transverse temperature of the atomic beam in the process of longitudinal cooling.

The method of transverse laser cooling is illustrated in figure 18 for a beam of two-level atoms. In the scheme of figure 18 the counter-propagating laser waves are assumed to be red-detuned with respect to the atomic transition frequency. When the laser waves have the same polarization and frequency the total laser field reduces to a standing light wave (2.25). The standing wave produces on a two-level atom radiation force (2.26a) which is responsible for cooling atoms.

To estimate the cooling effect in the above scheme, one can neglect the small-scale spatial oscillations of the radiation force (2.26a) and take into consideration only the effect of the average force (2.26b), putting  $F \approx F_0$ . If, in addition, one restricts oneself to the case of weak saturation, the average radiation force (radiation pressure force) will have the simple form

$$F = \langle F \rangle \approx \hbar k \gamma G \left( \frac{1}{1 + (\delta - kv_z)^2 / \gamma^2} - \frac{1}{1 + (\delta + kv_z)^2 / \gamma^2} \right). \quad (3.2)$$

At red detuning,  $\delta < 0$ , radiation pressure force (3.2) is directed opposite to the atomic velocity, i.e. it is friction force. In the linear velocity approximation, force (3.2) is

$$F = -M\beta v_z, \quad \beta = 8G\omega_r(|\delta|/\gamma)/(1 + \delta^2/\gamma^2)^2, \quad (3.3)$$

where  $\beta$  is the friction coefficient and  $\omega_r$  is the recoil frequency. Under the same assumptions,

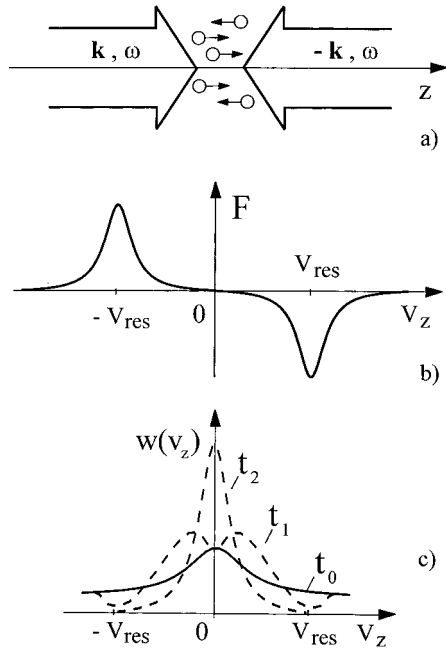


**Figure 18.** (a) 1D scheme of the transverse laser cooling of an atomic beam, (b) the radiation pressure force as a function of velocity and (c) the transverse velocity distribution at  $t_2 > t_1 > t_0$ .

according to expression (2.65) the momentum diffusion coefficient  $D_{zz} = D$  in the zero-velocity approximation is

$$D = \hbar^2 k^2 \gamma \frac{G}{1 + \delta^2 / \gamma^2} (1 + \alpha_{zz}). \quad (3.4)$$

Friction force (3.3) and momentum diffusion coefficient (3.4) fully define the stationary velocity distribution of the cold atoms. This distribution is found as the stationary solution of Fokker–Planck equation (2.63) and is Gaussian:

$$w(v_z) = \frac{1}{\sqrt{\pi}u} \exp\left(-\frac{v_z^2}{u^2}\right). \quad (3.5)$$

The half-width  $u$  of the steady-state velocity distribution is determined by the temperature  $T$ :

$$u = \sqrt{2k_B T / M}, \quad (3.6)$$

$$T = \frac{D}{M\beta k_B}. \quad (3.7)$$

With the friction and momentum diffusion coefficients defined by expressions (3.3) and (3.4), the temperature  $T$  is given by (Letokhov *et al* 1977)

$$T = \frac{1 + \alpha_{zz}}{4} \frac{\hbar \gamma}{k_B} \left( \frac{|\delta|}{\gamma} + \frac{\gamma}{|\delta|} \right). \quad (3.8)$$

The minimum value of temperature (3.8) is  $T_{\min} = (\frac{1}{2})(1 + \alpha_{zz})(\hbar \gamma / k_B)$ , and at a frequency detuning  $\delta = -\gamma$  it coincides with expression (1.3) up to within a numerical factor close to unity. The practical transverse cooling schemes for atomic beams that correspond to the described scheme can be found in the review by Balykin *et al* (1985b). To date, there have been suggested and implemented various transverse cooling schemes which allow the phase density of atomic beams to be substantially increased (Joffe *et al* 1993).

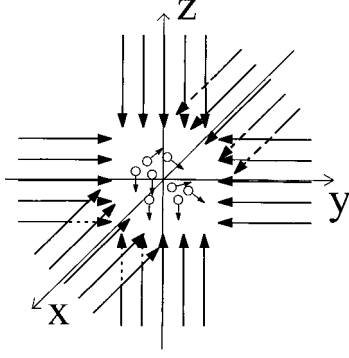


**Figure 19.** Scheme of a 3D cooling of atoms by six laser beams propagating in directions  $\pm x, \pm y, \pm z$ .

**3.1.3. 3D cooling of atoms.** Typical scheme of a 3D laser cooling of an atomic gas is illustrated in figure 19. In this cooling scheme, atoms are irradiated by three pairs of counter-propagating red-detuned laser waves. In a simplest model of a two-level atom and at weak optical saturation the radiation force on the atom averaged over the laser field wavelength in the scheme of figure 19 can be represented as a sum of three forces (3.2),

$$\mathbf{F} = \sum_{i=x,y,z} \hbar \mathbf{k}_i \gamma G \left\{ \frac{1}{1 + (\delta - kv_i)^2 / \gamma^2} - \frac{1}{1 + (\delta + kv_i)^2 / \gamma^2} \right\}, \quad (3.9)$$

where  $\mathbf{k}_i$  are the wavevectors of the laser waves propagating in the positive direction of the axes  $i = x, y, z$  and  $v_i$  is the projection of atomic velocity on the axis  $i$ . At red detuning,  $\delta < 0$ , force (3.9) in a linear approximation in atomic velocity is reduced to the friction force

$$\mathbf{F} = -M\beta\mathbf{v}, \quad (3.10)$$

where the friction coefficient  $\beta$  is defined by equation (3.3). In the same model of a two-level atom and in linear approximation in saturation parameter, the momentum diffusion tensor averaged over the laser wavelength and taken at zero velocity is

$$D_{ii} = D = 2\hbar^2 k^2 \gamma \frac{G}{1 + \delta^2 / \gamma^2}. \quad (3.11)$$

The stationary solution of the Fokker–Planck equation (2.63), which includes friction force (3.10) and momentum diffusion tensor (3.11), is a 3D Gaussian distribution

$$w(\mathbf{v}) = \frac{1}{(\sqrt{\pi}u)^3} \exp\left(-\frac{\mathbf{v}^2}{u^2}\right). \quad (3.12)$$

The half-width of the velocity distribution (3.12),

$$u = \sqrt{2k_B T / M}, \quad (3.13)$$

is defined by an effective temperature (Letokhov *et al* 1977)

$$T = \frac{D}{M\beta k_B} = \frac{\hbar\gamma}{2k_B} \left( \frac{|\delta|}{\gamma} + \frac{\gamma}{|\delta|} \right). \quad (3.14)$$

The above estimation for atomic temperature is in a good agreement with experimental observations in the cases when the dipole interaction between the atoms and the laser field can be described by a two-level model. The first experiment on the 3D Doppler cooling of atoms was done with a sodium vapour (Chu *et al* 1985). A beam of sodium atoms was preliminarily decelerated by a counter-propagating laser beam. Thereafter the slow atomic beam was directed into the intersection region of three mutually orthogonal 1D standing

laser waves producing a 3D standing wave. The minimal temperature of the cold sodium atoms recorded in the experiment amounted to 240  $\mu\text{K}$ , which agreed well with the minimum temperature  $T_{\min} = \hbar\gamma/k_B$  predicted by equation (3.14) for two-level atoms.

It worth noting that laser Doppler cooling of atoms described by a simple two-level model allows one to reach as low a temperature as the recoil temperature (1.5). This lowest temperature limit can be achieved for narrow spectral lines with a half-width about the recoil energy,  $\gamma \approx \omega_r$ . The first experiment on the narrow-line laser cooling of strontium atoms was reported by Katori *et al* (1999). In the experiment,  $^{88}\text{Sr}$  atoms first laser precooled at the broad  $^1\text{S}_0-^1\text{P}_1$  transition at wavelength 461 nm and trapped in the MOT were further laser cooled at the spin-forbidden transition  $^1\text{S}_0-^3\text{P}_1$  at wavelength 689 nm. The laser cooling at a weak transition resulted in an atomic sample with minimum temperature of 400 nK at density over  $10^{12} \text{ cm}^{-3}$ .

### 3.2. Sub-Doppler cooling

As noted in section 2.3, in multilevel dipole interaction schemes, two-photon processes, as well as multiphoton processes of higher order, may contribute to the radiation force, increasing its slope at zero atomic velocity. At the same time, multiphoton processes may reduce the momentum diffusion coefficient at the zero velocity (see section 2.3). Correspondingly, in the case of negative detuning two-photon processes and also multiphoton processes of higher order increase the friction force produced by the radiation force at small momentum diffusion coefficients. As a result the contributions from multiphoton processes allow multilevel atoms to be cooled by laser radiation below the Doppler temperature limit defined by equation (1.4). The deep cooling of multilevel atoms below temperature (1.4) by the radiation force contributed to by multiphoton processes has come to be known as sub-Doppler cooling. In all the sub-Doppler cooling schemes, the minimum cooling temperature is only limited by the magnitude of recoil energy (1.5). The minimum temperature attainable in the sub-Doppler cooling of (3 + 5)-level atoms in the 1D cooling model is estimated below.

In the interaction scheme involving a (3 + 5)-level atom and counter-propagating laser waves (2.58) with a negative frequency detuning, both parts of the radiation force are reduced to friction forces. In the practically important case of large detuning,  $|\delta| \gg \gamma, \Omega$ , the principal contribution to the friction coefficient comes from the second part of the radiation force that is associated with two-photon processes. In that case, the friction coefficient  $\beta \approx (\frac{120}{17})(\gamma/|\delta|)\omega_r$ , and the momentum diffusion coefficient  $D \approx (\frac{46}{17})\hbar^2 k^2 \gamma (\Omega/\gamma)^2$ . As a result, the temperature defined by equation (3.7) is

$$T \approx \frac{23}{30} \frac{\hbar \Omega^2}{|\delta| k_B}. \quad (3.15)$$

The order of magnitude of temperature (3.15) was found by Dalibard and Cohen-Tannoudji (1989), and the value of the coefficient in formula (3.15) was found by Chang and co-workers (1999b). It should be borne in mind that formula (3.15) corresponding to the quasiclassical dynamics of the atom can be used when the temperature  $T$  exceeds the minimum possible temperature defined by recoil energy (1.5) (Castin and Dalibard 1991).

The first experimental observation of the sub-Doppler cooling of atoms was made by the group of NIST lead by W Phillips. The temperature of sodium atoms measured in this experiment in an optical molasses amounted to 43  $\mu\text{K}$  instead of the expected 240  $\mu\text{K}$  corresponding to the cooling limit for two-level atoms. Note as examples two experimental observations of the sub-Doppler cooling of caesium atoms. Salomon and co-workers (1990) reached a temperature of 2.5  $\mu\text{K}$  at the frequency detuning  $-10\gamma$ . Reducing the detuning still more, down to  $-20\gamma$ , Chang and co-workers (1999b) attained apparently the record-low atomic temperature for today, namely, 2  $\mu\text{K}$  (figure 20).

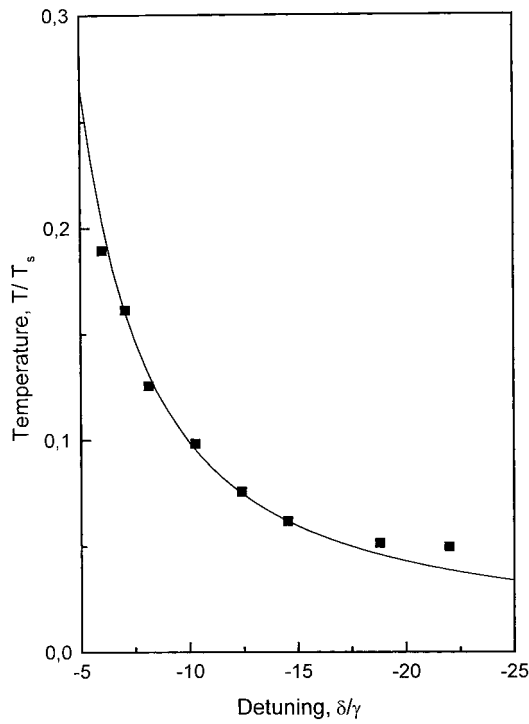


**Figure 20.** Experimental (boxes) and theoretical (solid curve) dependences of the atomic temperature for Cs atoms on the detuning at saturation parameter  $G = 4$ . The atomic sample was laser cooled by a 3D laser field composed of three pairs of  $\sigma^+ - \sigma^-$  laser waves. Atomic temperature is normalized on the Doppler cooling limit  $T_s = T_D = \hbar\gamma/k_B = 127 \mu\text{K}$ ,  $\gamma/2\pi = 2.5 \text{ MHz}$  (Chang *et al* 1999b).

### 3.3. Subrecoil cooling

The methods of cooling atoms below the recoil energy are closely associated with the stochastic nature of the atom–radiation interaction. The possibility of using the stochastic behaviour of atoms in a laser field with a view to their deep cooling was shown by Pritchard and co-workers (1983, 1987). The idea of the method is as follows. In the closed cycle constituted by the stimulated absorption of a photon by the atom and the subsequent spontaneous emission of the photon, there exists a finite probability that the atom will transit to a translational state whose energy  $E_{\text{at}}$  is lower (as desired) than the recoil energy:  $E_{\text{at}} \ll E_r$ . If there exists some *selective* mechanism providing for the repetition of the cycle only for fast atoms ( $E_{\text{at}} > E_r$ ), then on completion of a sufficient number of cycles a substantial fraction of the fast atoms will be cooled down to a temperature below the recoil energy. This method received the name phase-space optical pumping.

To date, two specific phase-space optical pumping schemes have been developed. One uses the two-photon Raman transition and the other is based on the velocity-selective coherent population trapping (VSCPT) effect.

**3.3.1. Raman cooling.** The Raman cooling uses a two-photon transition between two hyperfine-structure levels in the ground state of the atom. The atom is irradiated by two laser pulses of frequencies  $\omega_1$  and  $\omega_2$  (figure 21). If the frequency difference ( $\omega_1 - \omega_2$ ) is equal to the hyperfine splitting of the ground atomic state and the frequencies  $\omega_1$  and  $\omega_2$  are detuned far away enough from the one-photon resonances, the atom makes a transition from the state  $|1\rangle$  to the state  $|2\rangle$  by way of a two-photon Raman process. For an atom having a velocity  $v$ , the two-photon transition is effective under the resonance condition

$$\omega_1 - \omega_2 = (\mathbf{k}_1 - \mathbf{k}_2)v + \delta_{\text{hfs}}. \quad (3.16)$$

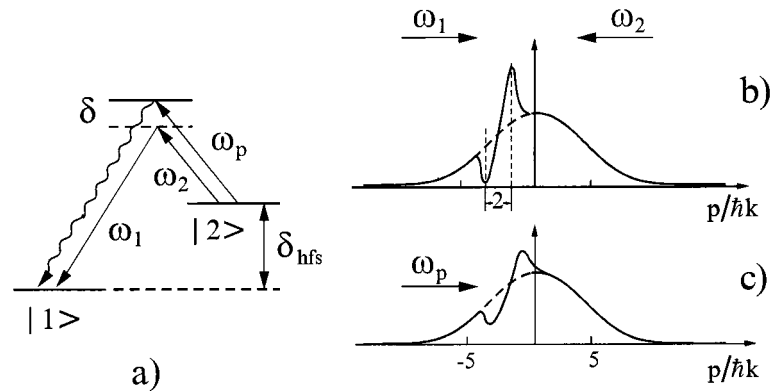


**Figure 21.** Scheme of Raman cooling based on a two-photon transition between two hyperfine-structure components of the ground atomic state. (a) Energy level diagram for the Raman cooling. (b) Deformation of the atomic velocity distribution under the action of a pair of red-detuned Raman laser pulses. (c) Velocity distribution after optical pumping.

As follows from equation (3.16), the Raman transition is insensitive to the Doppler shift in the unidirectional laser beam configuration ( $k_1 \approx k_2$ ). In the counter-propagating laser beam configuration ( $k_1 \approx -k_2$ ), the Doppler shifts add together, and the resonance depends on the atomic velocity. For the ground-state levels the width of the two-photon resonance is extremely narrow and, as a rule, is only governed by the atom–field interaction time. This in turn means that one can selectively excite very narrow velocity groups of atoms.

Figure 21 schematically illustrates the operating principle of the unidirectional Raman cooling of atoms. When the frequency difference ( $\omega_1 - \omega_2$ ) is tuned towards the red side relative to the two-photon resonance frequency (figure 21(a)), an atom moving with a negative velocity  $v$  is at resonance with the field as a result of the Doppler shift and acquires a momentum of  $2\hbar k$  in the zero-velocity direction (figure 21(b)). For an atom moving with a positive velocity, the directions of the laser beams should be reversed. For repeat irradiation with the laser pulses, the atom should be made to move back to the initial state  $|1\rangle$ . This is achieved by means of an additional pump laser of frequency  $\omega_p$  (figure 21(c)) which raises the atom from the sublevel  $|2\rangle$  to the excited state  $|e\rangle$  whence it drops back to state  $|1\rangle$  after emitting a spontaneous photon. Using a sequence of pairs of laser pulses of varying frequency and direction, one can concentrate atoms in the region of zero atomic velocity. The width of the velocity distribution of the atoms depends on the width and shape of the Raman transition line which in turn depend on the duration and shape of the laser pulses. At the beginning of the cooling process, the pulses are short enough, which provides for the interaction with a wide velocity group of atoms in the wing of the initial, still wide atomic velocity distribution. In the course of the cooling process, the velocity distribution narrows, and to reduce the resonance width, the duration of the laser pulses is increased.

Raman cooling schemes were developed both for 1D (Kasevich and Chu 1992) and 2D and 3D cooling (Davidson *et al* 1994). Figure 22(a) shows the velocity distribution of sodium atoms in the process of a 1D Raman cooling (Kasevich and Chu 1992). The temperature attained in this experiment amounted to 100 nK, which corresponded to  $\frac{1}{10}$  of the recoil energy. The 2D and 3D Raman cooling schemes are technically difficult to implement. For example, to effect a 3D cooling, one needs to use 18 laser beams. The temperatures reached in the 3D Raman cooling scheme was found to be less than in a 1D scheme, of the order of the recoil energy (Davidson *et al* 1994).

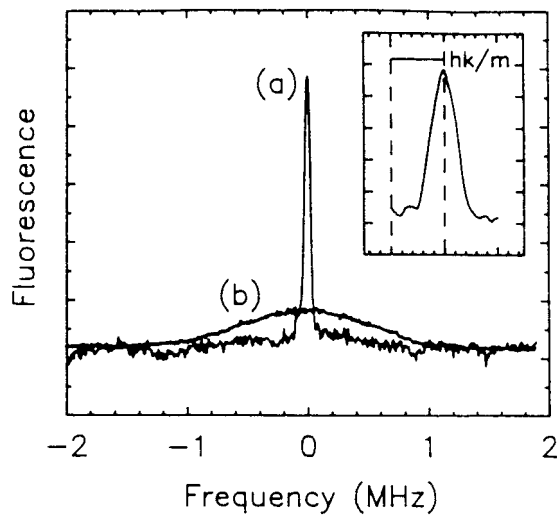


**Figure 22.** Atomic velocity distribution after (a) and before (b) the Raman cooling. Insert shows the central velocity peak and the velocity width relative to the recoil velocity (Kasevich and Chu 1992).

The Raman cooling process can also be used for cooling atoms localized in the optical lattices (section 4.2). Atoms trapped in an optical lattice near the minima of the dipole potential wells execute vibratory motions. If the vibrational structure is well resolved, the atoms can be cooled by the Raman cooling technique known as the sideband cooling technique. This technique was first employed to cool ions localized in deep radio-frequency traps wherein vibrational frequencies exceeded the homogeneous optical linewidth (Diedrich 1989, Monroe *et al* 1990).

For neutral atoms localized in not very deep dipole potential wells, the vibrational spectrum can only be resolved by means of two-photon Raman transitions of extremely narrow width. The Raman cooling of Cs atoms in the dipole potential wells produced by a standing laser wave is illustrated in figure 23. The atoms are first optically pumped to the state  $F = 3$ ,  $m_F = 3$ . Because of the relatively high initial temperature, the atoms occupy high vibrational levels,  $v \gg 1$  (the simplified case illustrated in figure 23 refers to  $v = 1$ ). By applying a weak magnetic field, one can ‘match’ by energy the sublevels  $|F = 3, m_F = 3, v\rangle$  and  $|F = 3, m_F = 2, v - 1\rangle$ . The translational energy of the sublevel  $|F = 3, m_F = 2, v - 1\rangle$  is lower by the magnitude of a vibrational quantum than that of the sublevel  $|F = 3, m_F = 2, v\rangle$ . A two-photon Raman transition (excited by the same lasers as form the optical lattice for the atoms) activates the atom to make a transition from the state  $|F = 3, m_F = 3, v\rangle$  to the state  $|F = 3, m_F = 2, v - 1\rangle$ . To complete one cooling cycle, an additional laser pulse plus spontaneous decay make the atom drop back to the initial internal state  $|F = 3, m_F = 3\rangle$ . When optically pumping a strongly localized atom, there occurs, as a rule, no change in its vibrational state, i.e. at the end of the cooling cycle the state of the atom is  $|F = 3, m_F = 3, v - 1\rangle$ . A many times repeated cooling cycle rapidly transfers the atom to the ground vibrational state  $v = 0$  (the so-called dark state) whence it cannot be excited by any two-photon Raman transition or pump laser. In the first experiment on Raman cooling Cs atoms in a standing laser wave, Hamann *et al* (1998) attained a 95% population in the ground vibrational sublevel. In the subsequent similar experiment, Vuletic *et al* (1998) also demonstrated the possibility of achieving a high atomic density ( $1.4 \times 10^{13}$  atoms  $\text{cm}^{-3}$ ). This opens the door to the further evaporative cooling of atoms and attaining the BEC of atoms.

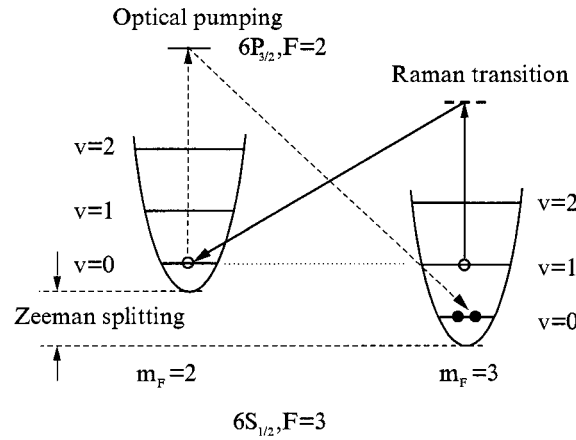


**Figure 23.** Schematic diagram of the Raman cooling of atoms in an optical lattice.

**3.3.2. Velocity-selective coherent population trapping.** The coherent population trapping (CPT) effect is manifest in various domains of physics. Its essence is as follows. Let a quantum mechanical system characterized by the nonperturbed operator  $H_0$  be located in an external field. Its interaction with the field is described by the operator  $V$ . In that case, the temporal evolution of the state of the  $|\Psi\rangle$  system in the interaction representation is described by the Schrödinger equation as

$$i\hbar \frac{\partial}{\partial t} |\Psi\rangle = \exp(i\hbar^{-1} H_0 t) V \exp(i\hbar^{-1} H_0 t) |\Psi\rangle. \quad (3.17)$$

In some special cases, the Schrödinger equation may have a solution  $|\Psi_{nc}\rangle$  satisfying the equation

$$\exp(i\hbar^{-1} H_0 t) V \exp(i\hbar^{-1} H_0 t) |\Psi_{nc}\rangle = 0. \quad (3.18)$$

Equation (3.18) means that the quantum mechanical system in the state  $|\Psi_{nc}\rangle$  does not ‘feel’ the external field. Such a non-coupled (nc) state possesses a series of remarkable properties. Assume that the non-coupled state  $|\Psi_{nc}\rangle = |\Psi_{nc}(t)\rangle$  at the initial instant of time is a superposition of the states of the nonperturbed system described by the Hamiltonian  $H_0$ . At all the subsequent instants of time the state  $|\Psi_{nc}(t)\rangle$  remains a linear superposition of the same nonperturbed states, despite the presence of the external field. The non-coupled state is customarily referred to as a ‘trapped’ state, and the phenomenon itself is called CPT. If the state  $|\Psi_{nc}(t)\rangle$  is a superposition of the ground states of the atom, the accumulation of atoms in the non-coupled state  $|\Psi_{nc}(t)\rangle$  can occur as a result of the spontaneous atomic transitions from the excited atomic states. When the translational atomic motion is considered quantum mechanically the non-coupled can exist at a specific atomic momentum (velocity). In this case the CPT effect is referred to as the VSCPT effect.

The VSCPT was actively discussed in connection with the control of atomic motion (see, for example, the review by Arimondo 1996). The 1D VSCPT scheme for atoms with the total angular momenta  $J$  and  $J'$  of the ground and the excited state, respectively, equal to unity, i.e.  $J = J' = 1$ , in a laser field of configuration  $\sigma^+\sigma^-$  was investigated most fully, both theoretically and experimentally. In the 1D case, the laser beams propagate in the direction of the  $z$ -axis which is taken to be the quantization axis. The atomic states are designated in accordance with the internal and translational states of the atom as  $|i, p\rangle$ , where  $i$  and  $p$  denote the internal state of the atom and its momentum, respectively (figure 24). In the above

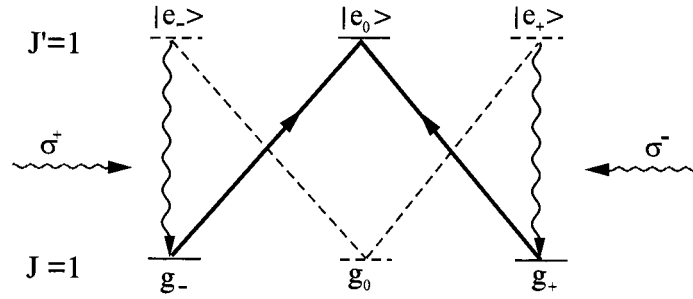


**Figure 24.** Three-level  $\Lambda$ -scheme describing the interaction of  $\sigma^+$ ,  $\sigma^-$  circularly polarized laser waves with atomic transition  $J = 1 - J' = 1$ . Dashed and wavy lines show the ways by which the atoms are pumped into the  $\Lambda$ -system after a few cycles of absorption and spontaneous emission.

laser field configuration the interaction is described in accordance with the so-called  $\Lambda$ -scheme wherein there interact two magnetic sublevels,  $|g_-, p - \hbar k\rangle$  and  $|g_+, p + \hbar k\rangle$ , of the ground state and one sublevel,  $|e_0, p\rangle$ , of the excited state. The coherent trapping of atomic population can conveniently be described in terms of the three states  $|\Psi_{\text{nc}}(t)\rangle$ ,  $|\Psi_{\text{c}}(t)\rangle$  and  $|e, p\rangle$ , where

$$\begin{aligned} |\Psi_{\text{nc}}(p)\rangle &= \frac{1}{\sqrt{2}}(|g_-, p - \hbar k\rangle + |g_+, p + \hbar k\rangle), \\ |\Psi_{\text{c}}(p)\rangle &= \frac{1}{\sqrt{2}}(|g_-, p - \hbar k\rangle - |g_+, p + \hbar k\rangle), \end{aligned} \quad (3.19)$$

are superpositions of the ground states of the atom. It was shown (Arimondo 1996) that the state  $|\Psi_{\text{nc}}(t)\rangle$  is not coupled with light by virtue of the destructive interpretation of the amplitudes of the transitions  $|g_-, p - \hbar k\rangle \rightarrow |e_0, p\rangle$  and  $|g_+, p + \hbar k\rangle \rightarrow |e_0, p\rangle$ .

The state  $|\Psi_{\text{nc}}(t)\rangle$  that is not excited by the laser light is realized in atoms with a momentum of  $p_0 = \pm \hbar k$ . Atoms with a momentum other than  $p_0$  interact with light. Considering its spontaneous decays, the atom executes a Brownian motion in the momentum space. Once it finds itself in the state  $|\Psi_{\text{nc}}(t)\rangle$ , the atom remains therein at all the subsequent instants of time.

In their experiments with the metastable  $^4\text{He}$  atoms, Aspect and co-workers (1988), Law and co-workers (1994), and Doery and co-workers (1995) observed very narrow resonances at atomic velocities of  $v = \pm \hbar k/M$ . The formation of narrow velocity groups of atoms is customarily associated with their cooling. However, spontaneous emission is responsible not only for the accumulation of atoms in the vicinity of the velocities  $v = \pm \hbar k/M$ , but also for the diffusion of a substantial proportion of the atoms from the initial velocity distribution to the region of higher velocities (Fam Le Kien and Balykin 1999). Obviously the diffusion of atoms in the momentum space causes, in contrast to the VSCPT effect, the temperature of the entire atomic ensemble to rise. One of the possible ways to reduce momentum diffusion is to combine the VSCPT effect with the polarization laser cooling techniques (Marte *et al* 1994). Another possibility is to filter atoms in the momentum space: to separate slow atoms in narrow peaks from their fast counterparts in the velocity distribution wings (Fam Le Kien and Balykin 1999). This is achieved by introducing an additional decay channel for the excited level, eventually causing the temperature of the entire atomic ensemble to drop below the recoil temperature.

#### 4. Optical trapping

As was shown in section 2 on an example of a two-level atom, the motion of an atom in a spatially inhomogeneous laser field is generally governed by the dipole gradient force, the radiation pressure force and the momentum diffusion. For an atom slowly moving in a far-detuned laser field the optical excitation is low. As a result, the radiation pressure force originating from the absorption of the laser light and the heating caused by the momentum diffusion are small. Accordingly, the motion of a cold atom in a far-detuned inhomogeneous laser field at not too long interaction time is basically governed by the dipole gradient force. The minima of the potential produced by the dipole gradient force in a far-detuned laser field can thus be used for *optical trapping* of cold atoms at time intervals limited by the heating due to the momentum diffusion.

##### 4.1. Trapping in laser beams

Conceptually, the simplest optical trap for cold atoms can consist of a single focused laser beam formed by a TEM<sub>00</sub> Gaussian laser mode (figure 7). As noted in section 2.2.1, gradient dipole force (2.20*b*) on a two-level atom in a red-detuned Gaussian laser beam forms 3D potential well (2.22) in the vicinity of the laser beam focus. Such an optical trap is customarily referred to as a single-beam dipole trap. The intersection of a number of laser beams in some space region can produce other types of the dipole traps.

The properties of the optical dipole traps largely depend on the magnitude of the detuning. In the *far-off-resonance dipole trap* (FORT), the frequency detuning is assumed to be substantially larger the homogeneous width, but the laser frequency is still close to that of the optical atomic transition. The motion of an atom in the FORT is well described by the RWA. When the detuning is chosen to be comparable with the optical transition frequency, the optical dipole trap is often called the *quasi-electrostatic trap* (QUEST) (Takekoshi *et al* 1995). The properties of QUEST differ greatly from those of the FORT since the RWA can no longer be used to describe the motion of an atom in the QUEST. Both the FORT and the QUEST produce a nearly conservative potential well for atoms, but incorporate inevitable heating due to the momentum diffusion originated from the photon recoil. Although the heating rate due to the momentum diffusion may be very small at a very large detuning, the diffusive heating always introduces an upper limit on the lifetime of atoms in the dipole traps.

*4.1.1. Far-off-resonance dipole traps.* In a single-beam FORT, the detuning is assumed to satisfy the conditions  $|\delta| \gg \gamma, \Omega$ . Under these conditions the effect of radiation pressure force (2.20*a*) can be neglected compared with that of gradient force (2.20*b*). Accordingly, the potential well of the trap at red detuning is defined by equation (2.23),

$$U_{\text{gr}}(\mathbf{r}) = -\hbar \frac{\Omega^2(\mathbf{r})}{|\delta|}. \quad (4.1)$$

The depth of potential well (4.1) is  $U_{\text{gr}}(0) = U_0 = \hbar\Omega^2(0)/|\delta|$ . Due to the conditions on the value of the detuning, the depth of the potential well (4.1) is always small compared with the value of the energy defined by the Rabi frequency,  $U_0 \ll \hbar\Omega(0)$ . In typical experimental conditions the potential well depth  $U_0/K_B$  does not exceed 10 mK.

The lifetime of atoms in a single-beam FORT is typically defined by the heating due to the momentum diffusion and the background gas collisions. The characteristic time of an atom escape from the FORT caused by the diffusive heating,  $\tau_{\text{diff}}$ , can be estimated from the

potential well depth  $U_0$  and momentum diffusion coefficients (2.64) at the focus of the beam,

$$D_{ii} \approx D(0) = \hbar^2 k^2 \gamma \frac{\Omega^2(0)}{\delta^2}. \quad (4.2)$$

Equating the thermal energy of an atom caused by the momentum diffusion,  $E_{\text{th}} \approx (\delta p)^2/2M$ , where  $\delta p \approx \sqrt{D(0)\tau_{\text{diff}}}$ , to the potential well depth, one may obtain the following estimation on the trapping time limited by the momentum diffusion:

$$\tau_{\text{diff}} \approx \frac{2MU_0}{D(0)} \approx \omega_r^{-1} \frac{|\delta|}{\gamma}. \quad (4.3)$$

The characteristic value of the inverse recoil frequency for atoms of medium mass is of the order of  $\tau_r = \omega_r^{-1} \sim 10^{-5}$  s. For a large detuning, the trapping time  $\tau_{\text{diff}}$  can accordingly be much longer than the time  $\tau_r$ . Note that by simultaneously increasing the laser field intensity and detuning one can increase the trapping time  $\tau_{\text{diff}}$  while keeping the potential well depth constant. The characteristic time of an atom escape from the FORT caused by collision with residual gas,  $\tau_{\text{coll}}$ , is defined by the collision cross section  $\sigma_c$ , residual gas density  $n$  and the thermal velocity of the residual gas atoms  $u$ ,

$$\tau_{\text{coll}} \approx 1/\sigma_c n u. \quad (4.4)$$

The first FORT used 220 mW of laser power at detuning 130 GHz for trapping sodium atoms (Chu *et al* 1986). The potential well depth for sodium atoms amounted to 10 mK and the trapping time was limited by a few milliseconds because of fast diffusive heating of the atoms at a relatively small frequency detuning. In the improved trap of this type (Miller *et al* 1994), the lifetime of rubidium atoms in the beam of a titanium–sapphire laser amounted to 0.2 s at detuning  $|\delta| \approx 65$  nm. In the FORT formed by the intersection of two beams of Nd:YAG lasers ( $\lambda = 1.06 \mu\text{m}$ ) the lifetime of sodium atoms in the trap amounted to a few seconds (Adams *et al* 1995). The dependence of the lifetime of atoms in the FORT on the polarization of the laser beam was studied by Corwin *et al* (1999). A cold and dense sample of Cs atoms was obtained in the FORT produced by the Nd:YAG laser (Boiron *et al* 1998). The atomic cloud was produced in a rod shape with a  $6 \mu\text{m}$  transverse waist radius, a temperature of  $2 \mu\text{K}$ , and a density of  $10^{12} \text{cm}^{-3}$ . In contrast to measurements in isotropic samples, no influence of multiple photon scattering or the reabsorption of laser light (Castin *et al* 1998) was recorded.

The main disadvantage of the optical trapping of atoms in the laser beams produced by the TEM<sub>*mm*</sub> optical modes described by Hermitian polynomials is the fast diffusion-associated heating of atoms. This shortcoming is materially reduced when using hollow laser beams produced by the optical modes described by the Laguerre polynomials  $L_0^m$ , where the index  $m = 0, \pm 1, \pm 2, \dots$  defines the azimuthal field distribution in the polar coordinate system. Such hollow laser beams have the intensity minimum on the axis, and atoms trapped in the hollow beams are subject only weakly to the perturbing effect of the laser field (Yang *et al* 1986). The trapping of rubidium atoms in hollow blue-detuned laser beams was reported by Kuga *et al* (1997). A scheme to trap atoms in a blue-detuned FORT formed by a single laser beam and a holographic phase plate was demonstrated by Ozeri *et al* (1999). At a detuning in a region 0.1–30 nm  $10^5$  Rb atoms were trapped for 0.3 s at temperature of  $24 \mu\text{K}$  and a density of  $7 \times 10^{11} \text{cm}^{-3}$ .

**4.1.2. Quasi-electrostatic dipole traps.** In the QUEST, the detuning of the laser beam is comparable with the optical frequencies of an atom. In this case the trapping potential can be found from the general expression for the high-frequency Stark shift in the off-resonance

light field. For a monochromatic linearly polarized light field (2.9) the dipole interaction operator (2.1) is

$$V = -D\mathbf{E} = -D_z E_0(\mathbf{r}) \cos(\mathbf{k}\mathbf{r} - \omega t). \quad (4.5)$$

where  $D_z$  is the matrix element of the dipole moment projection on the field direction. The solution of the Schrödinger equation with the dipole perturbation term (4.5) gives in the second-order perturbation theory the average energy shift  $\Delta E_n$  for the atomic level  $n$  as (Sobelman 1979)

$$\Delta E_n = \frac{E_0^2(\mathbf{r})}{2\hbar} \sum_s |(d_z)_{ns}|^2 \frac{\omega_{ns}}{\omega_{ns}^2 - \omega^2}, \quad (4.6)$$

where  $\omega_{ns} = (E_n - E_s)/\hbar$  is the frequency of the atomic transition between the levels  $n$  and  $s$  and  $(d_z)_{ns}$  is the matrix element of the atomic dipole moment.

For the ground state of an atom representing the basic practical interest, the energy shift is

$$U(\mathbf{r}) = \Delta E_g = -\frac{1}{2}\alpha E_0^2(\mathbf{r}), \quad (4.7)$$

where  $\alpha$  is the polarizability of an atom in the ground state,

$$\alpha = \frac{1}{\hbar} \sum_s |(d_z)_{gs}|^2 \frac{\omega_{sg}}{\omega_{sg}^2 - \omega^2}. \quad (4.8)$$

At the light wave frequency well below the frequency of the lowest atomic dipole transition the polarizability  $\alpha$  is always positive and close to the static polarizability  $\alpha_s = \sum_s |(d_z)_{gs}|^2/\hbar\omega_{sg}$ . In particular, at the wavelength of the CO<sub>2</sub> laser ( $\lambda = 10.6 \mu\text{m}$ ) the confining potential (4.7) can be well approximated by the static potential  $U_s = -\alpha_s E_0^2/2$ .

The potential well in the QUEST is thus defined by the dependence of the laser wave intensity on position,  $I(\mathbf{r}) = (c/8\pi)E_0^2(\mathbf{r})$ . The most important advantage of the QUEST is an extremely low diffusion-associated heating of atoms and accordingly long lifetime of atoms. In the QUEST, the total photon scattering rate is generally defined by the Rayleigh and Raman scattering. The Rayleigh scattering leaves an atom in its original state while the Raman scattering leaves an atom in a different hyperfine-structure sublevel. Typically, the rate of Raman scattering is much smaller than the rate of the Rayleigh scattering as defined by the ordinary Rayleigh formula (Takekoshi *et al* 1995),

$$S_{\text{Rayleigh}} = \frac{8\pi}{3} r_0^2 \left( \frac{\omega}{\omega_0} \right)^4, \quad (4.9)$$

where  $r_0$  is the classical electron radius.

In a most careful experimental investigation of the QUEST an ensemble of Cs atoms was trapped in a 20 W CO<sub>2</sub> laser beam focused into a spot with the waist radius 100  $\mu\text{m}$ . The depth of the potential well (4.7) was estimated to be 115 mK and the Rayleigh scattering rate (4.9) was about  $2.3 \times 10^4 \text{ s}^{-1}$ . The diffusion heating-limited lifetime was accordingly estimated to be about  $\tau_{\text{diff}} \approx 4 \times 10^{10} \text{ s}$ . The actual lifetime of the atoms in the trap,  $\tau \approx 10 \text{ s}$ , was found to be governed by factors other than the diffusion-associated heating, such as collisions with residual gas molecules and three-particle recombination (Takekoshi and Knize 1996). O'Hara *et al* (1999) demonstrated an ultrastable CO<sub>2</sub> laser trap that provided tight confinement of atoms with negligible optical scattering and minimal laser-noise-induced heating (figure 25). By this technique <sup>6</sup>Li atoms were stored in a 0.4 mK deep well with a lifetime of 300 s consistent with a background pressure of  $10^{-11} \text{ Torr}$ . This is the longest storage time ever achieved with an all-optical trap, comparable to the best magnetic traps. A substantial increase of the density of atoms in the QUEST was attained by the Raman cooling of atoms localized in the trap (see

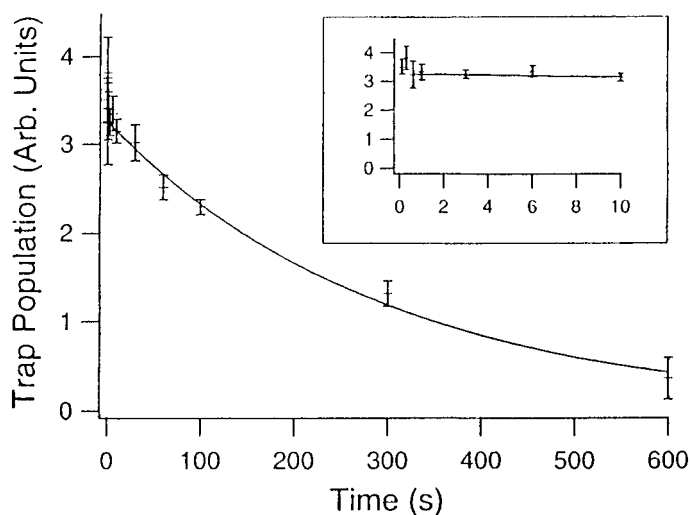


**Figure 25.** Trapped number of atoms versus time for an ultrastable  $\text{CO}_2$  laser trap. The solid curve is a single exponential fit,  $N(t) = A \exp(-t/\tau)$ , and gives  $\tau = 297$  s (O'Hara *et al* 1999).

section 3.3.1). Using this method, an atomic density of  $1.4 \times 10^{13} \text{ cm}^{-3}$  at a temperature of  $2.8 \mu\text{K}$  was achieved in a 1D QUEST (Vuletic *et al* 1998).

The QUEST can also be used for trapping neutral molecules. The main problem here is the production of cold molecules. Nowadays the process of the photoassociation of the laser-cooled atoms is the only known way to produce a sample of cold molecules. Takekoshi *et al* (1998) have reported the first observation of optical trapping of cold neutral molecules in the QUEST. Caesium dimers were produced in the MOT and transferred to the QUEST formed at the focus of a  $\text{CO}_2$  laser beam. The molecules remain in the trap for times of about 0.5 s. The lifetime of trapped molecules was limited mainly by collisions with the thermal background gas.

Finally, note that the basic distinction between the FORT and QUEST consists in the value of the diffusion heating. Since the population of the excited atomic state in the QUEST is extremely small, the diffusion-associated heating of atoms in the QUEST is much smaller than in the FORT.

#### 4.2. Trapping in standing laser waves. Optical lattices

As noted in section 2.2.2, a cold two-level atom placed in a near-resonant standing laser wave (2.25) experiences the action of periodic potential (2.30). From the general physical standpoint, sufficiently cold atoms could be trapped for a long time in the minima of the periodic potential, which would allow one to speak of a stable localization of atoms in regions with dimensions smaller than the laser field wavelength. Actually, no stable trapping of atoms occurs in a standing laser wave, for the momentum fluctuations always cause diffusion-associated heating and escape of the atoms from the potential wells. The only mechanism that could stabilize the energy (temperature) of the atoms at a level substantially lower than the potential well depth is the friction produced by the radiation pressure force. However, in the two-level atom model this mechanism is inoperative because the friction coefficient (2.35) goes to zero in the vicinity of the minima of potential (2.30).

For two-level atoms placed in a standing laser wave, a situation is realized when some atoms stay localized at the potential minima, while others execute infinite motions, the numbers

of the former and the latter being comparable (Letokhov 1968, 1973). This conclusion directly follows from comparison between the average kinetic energy of the atoms and the potential well depth. Taking space-averaged values of friction coefficient (2.35) and the momentum diffusion coefficient  $D_{zz}$  defined by equation (2.65), one can estimate the average kinetic energy of the two-level atoms from the stationary solution of the Fokker–Planck equation (2.63) (Letokhov *et al* 1977):

$$k_B T \approx \frac{\langle D_{zz} \rangle}{M \langle \beta \rangle} = \frac{1 + \alpha_{zz}}{4} \hbar \gamma \left( \frac{|\delta|}{\gamma} + \frac{\gamma}{\delta} \right). \quad (4.10)$$

This energy, as can be seen, coincides, within the order of magnitude, with the depth of the periodic potential (2.30).

The analysis of more complex dipole interaction schemes involving multilevel atoms and counter-propagating laser waves supports the above conclusion that there simultaneously exist localized and non-localized atoms. At the same time, the dynamics of multilevel atoms interacting with counter-propagating laser waves may substantially differ from that of two-level atoms, because an important role for multilevel atoms can be played by the multiphoton optical processes described in sections 2.3 and 2.4.2. However, the deeper cooling provided by the multiphoton processes does not change the physical picture described above (Dalibard and Cohen-Tannoudji 1989). Insofar as deep cooling is effected on small spatial intervals compared with the spatial potential period, its contribution on the average causes no perceptible reduction of the average kinetic energy of the atoms in comparison with potential well depths. At the same time, in the case of multilevel atoms the relative proportion of atoms oscillating in potential wells may be higher than that in the case of two-level atoms.

Thus, the above arguments show that when irradiating atoms with counter-propagating laser waves producing periodic optical potentials, some atoms always find themselves localized at the minima of the periodic potentials. In the case of red detuning, in addition to the periodic potential there also develops a periodic friction force that decelerates the atoms and facilitates their localization. In other words, the periodic potentials produced by counter-propagating laser waves in their turn produce periodic gratings of cold atoms. Such atomic gratings are frequently called *optical lattices*.

A direct experimental proof of the localization of cold atoms in the periodic minima of a standing laser wave potential was obtained by observing the channelling of cold sodium atoms in curved potential wells produced by a spherical standing laser wave (Balykin *et al* 1988b, 1989). In this experiment, a beam of sodium atoms was directed at a grazing angle to the curved potential wells (figure 26). Fast atoms having a high transverse velocity traversed the laser field without changing their direction of motion in any perceptible way. In contrast, cold atoms were constrained in the potential wells of the spherical standing laser wave and deviated as a result through an angle governed by the magnitude of the dipole interaction between the atoms and the laser field. The deflection of slow atoms was observed to occur as a result of their channelling both at the nodes of the standing laser wave in the case of blue detuning and at the loops in the case of red detuning (Ovchinnikov and Letokhov 1992).

Another experimental proof of the localization of cold atoms at the minima of a periodic optical potential was obtained by recording the resonance fluorescence spectra of caesium atoms trapped in the optical potential, either 3D (Westbrook *et al* 1990) or 1D (Jessen *et al* 1992), produced by counter-propagating laser waves of linear and orthogonal polarization (lin $\perp$ lin configuration). The resonance fluorescence spectrum of a motionless two-level atom consists of the well known Mollow triplet that includes a central peak at the laser frequency  $\omega_l$  and two side components displaced to the red and blue side by an amount equal to the Rabi

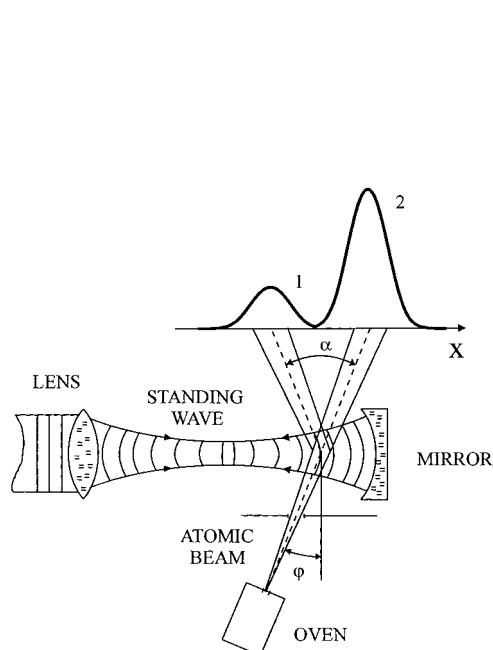


**Figure 26.** Scheme of the experiment on channelling sodium atoms in the standing laser wave. The initial atom beam was directed at a grazing angle to the curved potential wells (Balykin *et al* 1988b).

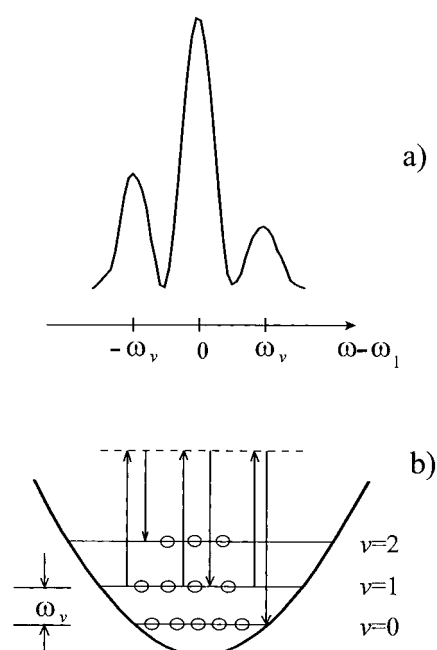


**Figure 27.** (a) Resonance fluorescence of atoms trapped in the periodic potential wells. The spectrum is shown near the central component of the Mollow triplet. (b) The quantum transitions of an atom between the vibrational states responsible for the side components (Jessen *et al* 1992).

frequency (Mollow 1969, 1972). For a two-level atom oscillating in a potential well with a frequency lower than the Rabi frequency, each component of the Mollow triplet is split into the side components corresponding to changes in the vibrational state of the atom. If the ratio between the oscillation amplitude of the atom in the potential well and the radiation wavelength (the Lamb–Dicke factor) is small, each component of the Mollow triplet contains only the first side components (figure 27).

In complete correspondence with figure 27, the recorded resonance fluorescence spectrum excited by a laser field of  $\text{lin}\perp\text{lin}$  configuration also contained, in addition to the central component of the Mollow triplet, clearly distinct side components corresponding to the quantum transitions of the atom between adjacent vibrational levels (2.33) with characteristic frequencies (2.32). The low-frequency side component of the spectrum corresponded to virtual optical transitions accompanied by the vibrational transitions  $\nu \rightarrow \nu + 1$ , i.e. to spontaneous anti-Stokes Raman transitions of the atom. The high-frequency component of the spectrum corresponded to virtual atomic transitions entailing the reduction of the vibrational quantum number,  $\nu \rightarrow \nu - 1$ , i.e. to Stokes Raman transitions. The most intense central component of the Mollow triplet corresponded as usual to optical atom transitions occurring without any change in the vibrational state of the atom, i.e. it had the meaning of the Rayleigh line. The asymmetry observed in the intensities of the side peaks corresponded to the difference between the thermal populations of the adjacent vibrational levels  $\nu$  and  $\nu + 1$ . Inasmuch as the ratio between the populations of the adjacent vibrational levels in an approximation of the Boltzmann distribution is  $\exp(-\hbar\omega_\nu/k_B T)$ , the ratio between intensities of the side peaks was

used to determine the vibrational temperature of the atoms and estimate that the localization region of the atoms was  $\Delta z \approx \lambda/15$  (Jessen *et al* 1992).

One more experimental proof of the localization of cold caesium atoms in the minima of a periodic optical potential produced by a lin⊥lin laser field was obtained by recording the absorption spectrum of a probe laser beam. The absorption of a probe beam depends on the character of the stimulated redistribution of photons between the trapping and the probe fields. The redistribution of photons as a result of stimulated Raman processes proceeds very effectively when the probe laser frequency  $\omega'$  is shifted by an amount equal to the oscillation frequency of the atoms, i.e.  $\omega' = \omega \pm \omega_v$ . Recording the Raman resonances that came to be known as recoil-free Raman resonances made it possible to demonstrate that the specific features of the absorption spectrum fully corresponded to localized atoms (Verkerk *et al* 1992, Courtois *et al* 1994).

A 2D optical lattice was directly observed by recording the spatial distribution of the fluorescence intensity of trapped atoms (Hemmerich and Hänsch 1993).

Various types of 3D optical lattices, both periodic and quasiperiodic, have been realized (Guidoni *et al* 1997, Grynberg *et al* 1993, Petsas *et al* 1994, Jessen and Deutsch 1996). These lattices were used to study the properties of localized cold atoms at temperatures of the order of 10–100  $\mu$ K. The paramagnetic properties of optical lattices in a constant magnetic field were investigated (Meacher *et al* 1995). The Bragg diffraction of laser light by optical lattices was observed, bearing witness to the presence of a long-range order (Birkl *et al* 1995, Weidemüller and Hemmerich 1995). Atom wavepackets were compressed and parametrically deformed by varying modulation of the optical potential depth (Raithel *et al* 1997). The amplification of a probe laser radiation by an optical lattice of rubidium atoms was registered (Guibal *et al* 1997). The amplification effect was explained by the induction of a periodic atom polarization by the trapping field. The energy band structure of the translational motion of atoms in an optical trap was experimentally recorded (Müller-Seyditz *et al* 1997).

The maximum densities of atoms in optical lattices are typically limited to values of the order of  $10^{11}$ – $10^{12}$   $\text{cm}^{-3}$  mainly because of the absorption and scattering of the laser light by the atoms. The increase of atomic density in optical lattices still remains an important problem whose solution would allow one to approach the observation of the quantum statistical effects and possible production of dense atomic crystals. In this connection, attempts to trap atoms in the intensity minima of a laser field seem very promising (Grynberg and Courtois 1994). Such *dark optical lattices* can be produced by the optical pumping of atoms in a magnetic field to the magnetic sublevel that is not excited by the laser light. The first dark optical lattice was realized with  $^{87}\text{Rb}$  atoms placed in a weak magnetic field of the order of 10 G (Hemmerich *et al* 1995).

A promising approach to decreasing the influence of the scattered and absorbed laser light is the use of the far-off-resonance optical lattices (FORL). Friebel *et al* (1998), reported on the trapping of Rb atoms in an extremely far detuned 1D optical lattice produced by the standing wave from a  $\text{CO}_2$  laser. This optical lattice was characterized by a long coherence time because of the low scattering rate. The authors assumed that by fitting such a lattice with one atom per lattice site, a quantum bit (qubit) of information could be stored in each atom (e.g. in two ground-state magnetic sublevels) and individually addressed with a focused laser beam. An average filling factor about one atom per lattice site was recently achieved on the submicron scale (Winoto *et al* 1999, De Pue *et al* 1999). High site occupation was achieved through a compression sequence that included laser cooling in a 3D FORL and adiabatic toggling between the 3D FORL and 1D FORL trap. After the highest filling factor was achieved, laser cooling caused additional loss from lattice sites occupied with more than one atom. Ultimately, 44% of the sites had a single atom cooled to near its vibrational ground state.

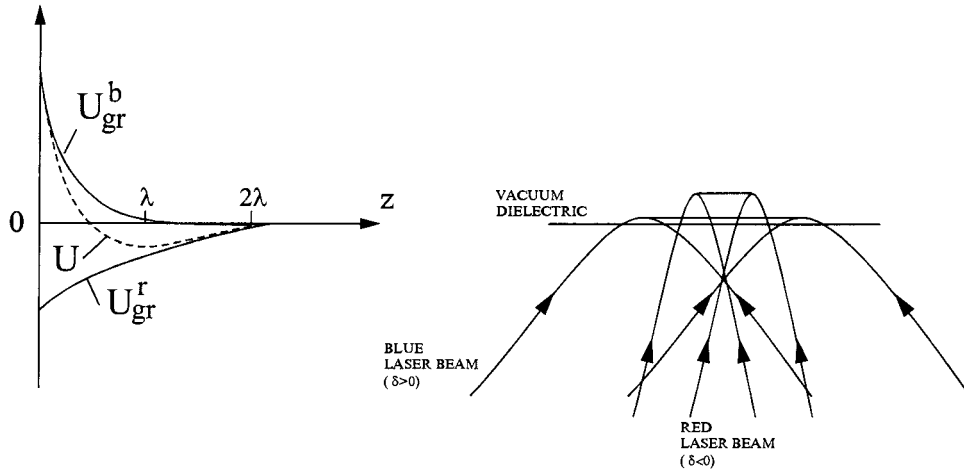


**Figure 28.** Two-frequency atom trap waveguide for two-level atoms (right) and the potentials of an atom in the evanescent waves with blue and red detuning and total potential  $U$ .

#### 4.3. Trapping in optical waveguide modes. Atom waveguides

Any trap for cold atoms, whose one or two linear dimensions are large enough, can be treated and used as a waveguide for de Broglie atom waves. One of the first optical-trap atom waveguide schemes was the scheme of a flat atom waveguide containing two evanescent laser waves with detunings of opposite signs (Ovchinnikov *et al* 1991). A flat two-frequency atom waveguide for two-level atoms is schematically shown in figure 28. In this scheme, the blue-detuned evanescent wave,  $\delta_b > 0$ , produces a repulsive potential, while the red-detuned wave,  $\delta_r < 0$ , produces an attractive potential. As a result, a potential well is produced between the two evanescent waves, which restricts the atomic motion in a direction perpendicular to the interface.

Obviously the red-detuned evanescent wave in this scheme should have a penetration depth into the vacuum exceeding that of the blue-detuned wave,  $\alpha_r^{-1} > \alpha_b^{-1}$  (see equation (2.36)). This condition is satisfied if the incidence angle of the red-detuned laser wave exceeds but little the total internal reflection angle,  $\theta_r > \arcsin(1/n)$ , and that of the blue-detuned wave substantially exceeds the total internal reflection angle,  $\theta_b \gg \arcsin(1/n)$ , where  $n$  is the refractive index of the dielectric (figure 28). Under the above condition and at large detuning, when the effect of the radiation pressure force can be neglected, the total potential for cold atoms in the direction of the  $z$ -axis is a sum of two potentials of form (2.42):

$$U(\mathbf{r}) = U_{\text{gr}}^b - U_{\text{gr}}^r = \hbar \left( \frac{\Omega_{0b}^2}{\delta_b} e^{-2\alpha_b z} - \frac{\Omega_{0r}^2}{|\delta_r|} e^{-2\alpha_r z} \right), \quad (4.11)$$

where  $\Omega_{0b}$  and  $\Omega_{0r}$  are the Rabi frequencies at the dielectric–vacuum interface for the blue- and red-detuned waves, respectively.

The simple atom waveguide considered above provides for the propagation of cold atoms in a plane parallel to the dielectric–vacuum interface. When using laser beams of Gaussian intensity profile, this atom waveguide can be transformed into a 3D trap, for the dominant gradient force produced by the red-detuned Gaussian laser beam can pull the atoms inside the trapping region (Ovchinnikov *et al* 1991). Later, other flat atom waveguide schemes were suggested based on the use of both an optical potential (Desbiolles and Dalibard 1996b, Power *et al* 1997) and a magnetic potential (Hinds *et al* 1998, Li *et al* 1999).

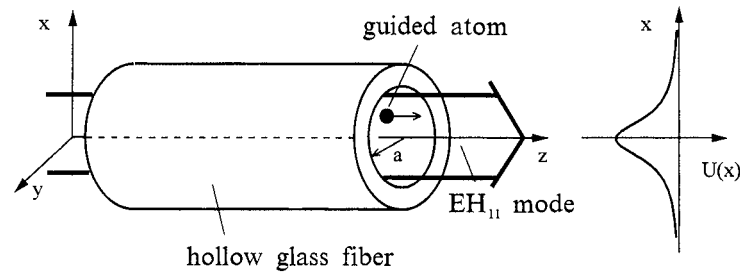


**Figure 29.** Scheme of an atom waveguide based on the optical mode  $\text{EH}_{11}$  propagating in the dielectric waveguide (left) and the optical potential for atoms (right) (Ol'shanii *et al* 1993).

Gauk and co-workers (1998) were the first to demonstrate a flat atom waveguide based on a standing laser wave with a period much longer than the laser wavelength. The waveguide was formed by two interfering laser waves incident upon and reflected from the gold-coated face of a glass prism at small angles. Metastable  $^* \text{Ar}$  atoms were released from a MOT located at some distance from the face of the prism. Two evanescent waves were also produced on the same face of the prism. One of the evanescent waves served to decelerate the atoms released from the trap near the face of the prism and the other, to optically pump the retarded atoms to a sublevel at which the atoms become localized in the loops of the standing wave. In this experiment, about a thousand atoms were localized in a single potential well at a density of  $10^9 \text{ cm}^{-3}$ . The lifetime of the atoms in this flat waveguide amounted to 150 ms and was limited by the momentum diffusion and the tunnelling of the atoms out of the optical potential.

The above-considered flat atom waveguide illustrates the main idea of the atom waveguides on the basis of the dipole gradient force, i.e. an idea of pulling atoms into the intensity maxima of the red-detuned laser field or pushing atoms into the intensity minima of the blue-detuned field. It should be emphasized that it would naturally be sensible to speak of atom waveguides only in the case of sufficiently cold atoms possessing the wave properties. For not very cold atoms moving like classical particles, the above schemes play the role of devices for transporting atoms in the desired direction or serve as 1D or 2D traps.

The first atom waveguide scheme to be practically verified was that shown in figure 29, where the atoms moved inside the intensity maximum of the optical mode  $\text{EH}_{11}$  propagating inside a hollow optical waveguide (Ol'shanii *et al* 1993). Generally speaking, many axially symmetric electromagnetic modes can be excited in a hollow cylindrical dielectric waveguide (Solimeno *et al* 1986). When the internal radius  $a$  of the waveguide is small enough, the principal mode is  $\text{EH}_{11}$ . The radial distribution of the electric field of the mode  $\text{EH}_{11}$  in the cylindrical coordinates  $z, \rho, \varphi$  has the form

$$\mathbf{E} = \frac{1}{2} e E_0 J_0(\chi \rho) e^{i(\beta z - \omega t)} + \text{c.c.}, \quad (4.12)$$

where  $e$  is the unit polarization vector and  $\chi$  and  $\beta$  are the complex propagation constants. In the case of large negative detuning, field (4.12) produces attractive potential (2.42) for atoms:

$$U = -\hbar \frac{\Omega_0^2}{|\delta|} J_0^2(\chi \rho), \quad (4.13)$$

where  $\Omega_0$  is the Rabi frequency for field (4.12).

The above scheme was experimentally implemented for rubidium atoms (Renn *et al* 1995). A glass hollow-core fibre 3 cm long and  $40 \mu\text{m}$  in internal diameter was used in the experiment. The laser light was launched into the hollow region of the glass fibre. A beam of rubidium atoms propagated in the dipole potential whose depth corresponded to an effective atomic

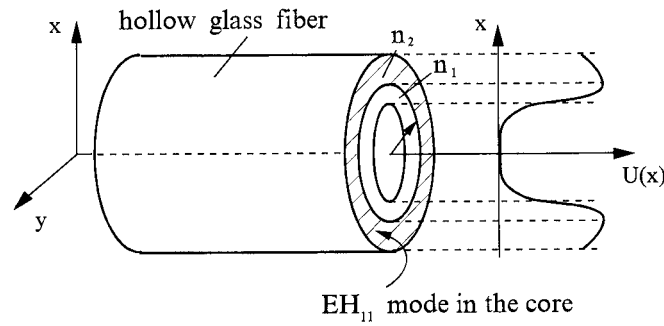


**Figure 30.** Atom waveguide based on hollow dielectric waveguide having two cylindrical dielectric sheaths differing in refractive index (left) and the optical potential (right).

temperature of 70 mK. This magnitude of the potential allowed atoms with transverse velocities of up to  $40 \text{ cm s}^{-1}$  to be transported through the waveguide. A direct experimental proof of the propagation of the atoms in optical potential (4.13) was obtained by measuring the atomic flux at the exit of the waveguide depending on the sign of the detuning.

A considerable disadvantage of the waveguide based on the intensity maximum of an optical waveguide mode is the diffusion-associated heating of the atoms. For this reason, much more attractive are atom waveguides wherein atoms propagate in optical waveguide modes having the minima near the axis (Savage *et al* 1993, Marksteiner *et al* 1994, Ito *et al* 1996, Pillof 1997). At present, there exist various methods to generate such modes. A discussion of these methods can be found in the review on atom waveguides by Balykin (1999). These include the transverse mode selection method (Wang and Littman 1993), the geometrical optical method (Herman and Wiggling 1991), the computer generated method (Paterson and Smith 1996), and the Gaussian beam transformation method (Beijersbergen *et al* 1992).

Especially attractive are the atom waveguides based on hollow dielectric waveguides having two cylindrical dielectric sheaths differing in refractive index (figure 30). When the hole radius  $a \geq \lambda$ , such waveguides can convey with very low losses the optical mode  $\text{HE}_{11}$  mostly localized in the internal cylindrical sheath with the refractive index  $n_1 > n_2$ . The electric field amplitude of the mode  $\text{HE}_{11}$  drops exponentially into the internal hollow region. Accordingly, in the case of blue detuning the mode  $\text{HE}_{11}$  produces a potential well for atoms. At large blue detuning, the shape of the potential for a two-level atom model is defined similar to (4.13) by an expression containing a Bessel function:

$$U = -\hbar \frac{\Omega_0^2}{|\delta|} I_0^2(\chi\rho). \quad (4.14)$$

The atom wave modes existing in potential (4.14) were found by numerical calculation (Al-Awfi and Babiker 1998). Dowling and Gea-Banacloche (1995) analytically found the structure of atom modes for a stepped potential approximating potential (4.14).

The above scheme was also experimentally implemented with rubidium atoms propagating in an optical mode with a wavelength of 780 nm blue-detuned with respect to the  $D_2$  transition (Renn *et al* 1996, Ito *et al* 1996). Figure 31 shows the flux of rubidium atoms passed through the waveguide as a function of the detuning of the laser field producing the surface evanescent wave (Ito *et al* 1996). The curve in figure 31(b) shows the residual atomic flux inside the waveguide in the absence of the laser light. Introducing blue-detuned laser light into the waveguide caused a considerable increase in the flux of atoms passed through the waveguide. The red-detuned laser light almost completely inhibited the propagation of the atoms. In this

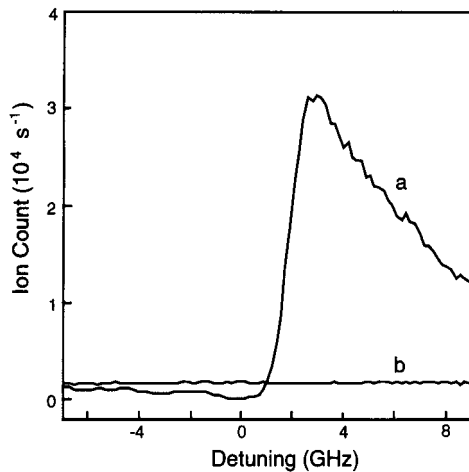


**Figure 31.** The flow of rubidium atoms passing through the atom waveguide as a function of the detuning of the laser field producing the surface evanescent wave (Ito *et al* 1996).

last case, a reduction of atomic flux in comparison with that in the absence of laser light was observed. The effect was explained by the attraction of the atoms in the laser field to the waveguide wall, followed by their condensation on the dielectric surface.

The most important parameter of any atom waveguide is the value of the atomic flux that can be injected into and propagate inside the waveguide. Since the injected atoms have typically a relatively broad velocity distribution, one can easily see that in the case of a single-mode atom waveguide only a very small amount of atoms can be injected into the the atom waveguide. To overcome this difficulty, an atom waveguide named atom hornfibre was proposed (Balykin *et al* 1996, Subbotin *et al* 1997). An atom hornfibre is a hollow tapered curved waveguide 'coated' inside by a blue-detuned evanescent wave. The waveguide has the shape of a curved horn with a large inlet opening, around the size of the atomic cloud released from the MOT, which is a typical pumping source for the atom waveguides. The outlet opening diameter of the horn corresponds to a single-mode atom waveguide. The use of an inelastic reflection of atoms from the evanescent wave (Ovchinnikov *et al* 1995) and the tapered waveguide geometry are considered to be the key steps to reduce the temperature of the propagating atoms and thus substantially increase the flux of atoms through the waveguide (Subbotin *et al* 1997). Ovchinnikov and co-workers (1995) suggested and experimentally investigated a dissipative reflection of atoms from the walls of such a waveguide.

Another laser field configuration with the intensity minimum at the centre of the beam, which is being investigated as a potential atom waveguide, is the  $TEM_{01}^*$  laser mode (the so-called doughnut mode) (Balykin and Letokhov 1987, Kuppens *et al* 1998, Yin *et al* 1998, Matsuura *et al* 1998, Morsch and Meacher 1998, Glas *et al* 1999). Kuppens and co-workers (1988) obtained a  $TEM_{01}^*$  mode from a Gaussian laser beam by a holographic method (Paterson and Smith 1996, Kuppens *et al* 1996). Around 40% of the initial laser beam power was converted to the  $TEM_{01}^*$  mode about 0.4 W in power. When focusing the mode into a spot of 40  $\mu\text{m}$  and at detuning 10 GHz, the laser field produced a potential for the transverse motion of atoms with a vibrational energy of  $\hbar\omega_v = 2.5E_r$ . By using the 2D polarization cooling method, they managed to reduce the temperature of transverse motion down to triple recoil energy, which is comparable with the energy of vibrational motion. This means that atomic motion in such a waveguide must exhibit wave properties. It should be noted at the same time that in most experiments performed to date the motion of atoms have been of classical character. In this connection, these experiments should essentially be considered as merely

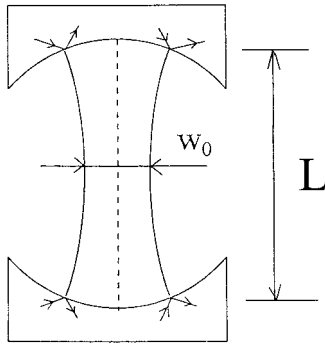


**Figure 32.** Atom cavity formed by two atom mirrors based on evanescent waves.

the first steps toward the development of waveguides for the atomic de Broglie waves.

#### 4.4. Atom cavities

When the energy of atoms is low enough for their motion to have a wave character, any atom trap can be treated as a cavity for the atom de Broglie waves. The restrictions imposed on the spatial propagation of atom wavepackets in the trap by the confining field geometry always set the wavepacket quantization conditions and thus determine the natural atom modes of the trap.

From the general physical standpoint, interest in atom cavities is due to the same reasons as interest in electromagnetic field cavities. Like any electromagnetic cavity, an atom cavity is a selective element allowing one to form individual atomic modes. The selection of individual atom modes must naturally play an important role in the development of atom optics. Another circumstance is the as yet not clearly understood possibility of using atom cavities to develop atom lasers (Mewes *et al* 1997, Anderson and Kasevich 1998, Bloch *et al* 1999). In atom lasers with an active medium in the form of an ensemble of Bose atoms, the pumping of individual atom modes can be effected on account of the BEC of ultracold atoms (Anderson *et al* 1995, Davis *et al* 1995, Bradley *et al* 1995, Guzman *et al* 1996, Wiseman 1997).

The emergence of the atom mirror based on the evanescent wave obviously raised the question as to the possibility of creating an atom analogue of the Fabry–Perot optical cavity. In the first proposal (Balykin and Letokhov 1989), they analysed an atom cavity formed by two atom mirrors based on evanescent waves (figure 32). Simple estimates show that the main specific feature of the atom analogue of the Fabry–Perot cavity is its multimode structure. From the standard quantization condition of atomic motion along the axis of the cavity,

$$k_1 L = M v_1 L / \hbar = n \pi, \quad (4.15)$$

where  $k_1$  is the longitudinal atomic wavevector and  $v_1$ , the longitudinal atomic velocity, one can see that the velocity interval  $\Delta v_1 = h/2ML = (\lambda/2L)v_r$  between the adjacent atomic modes is but a very small fraction of the recoil velocity. This means that even when the velocity of the atoms injected into the cavity is as low as the recoil velocity, i.e. when their effective temperature is of the order of  $100 \mu\text{K}$ , the number of longitudinal modes excited in the cavity is extremely high. Of course, this circumstance does not mean that it is impossible to selectively excite individual longitudinal modes, but points to the necessity of using for the purpose a highly velocity-selective pumping source as the type of BEC mechanism.

The quantization of the transverse atomic motion in the atom analogue of the Fabry–Perot cavity also gives rise to a large number of transverse modes. With the length of the de Broglie waves being  $\lambda_{\text{dB}} = h/Mv$ , the transverse size of the fundamental atom mode may be estimated

as

$$w_0 = \sqrt{\lambda_{dB} L / 4\pi}. \quad (4.16)$$

Accordingly, the geometric divergence of the atom mode, which may be estimated as

$$\delta\varphi \cong w_0/L = \sqrt{\lambda_{dB}/4\pi L}, \quad (4.17)$$

is very small. To illustrate, for sodium atoms moving with velocities of the order of the recoil velocity  $v_r \approx 3 \text{ cm s}^{-1}$  in a cavity with a length of  $L = 5 \text{ cm}$ , the atom mode divergence is  $\delta\varphi \approx 10^{-3}$ . Such a small value of the divergence angle imposes a strong restriction on the geometric divergence of the injected atomic beam. Accordingly, a large divergence of the atomic beam injected into the cavity makes it impossible to achieve a high population in an individual atom mode. The atom cavity can naturally operate with many transverse modes being populated. However, such a multimode operation places a stringent restriction on the total number of cold atoms.

Note that the atom analogue of the Fabry–Perot cavity can also be produced using atom mirrors formed by the potentials of two strongly focused laser beams spaced at a distance of the order of a few laser field wavelengths (Wilkens *et al* 1993).

The atom cavity based on the use of the whispering gallery modes in dielectric spheres or discs of small diameter (Mabushi and Kimble 1994) seems also attractive. An optical whispering gallery mode develops when light propagates in a sphere or disc on account of its total internal reflection from the surface of the sphere or disc. For a sphere of radius  $R \gg \lambda$ , the resonance whispering gallery modes subject to the condition  $\ell\lambda = 2\pi R$ . The fact that such modes propagate by the total internal reflection characterized by a very low loss makes it possible to produce optical modes with a very high  $Q$ -factor,  $Q \approx 10^9$ – $10^{11}$ . In the simplest cavity of this type (Dowling and Gea-Banacloche 1996), the atom is assumed to be localized by two forces: (1) the dipole attractive force of a red-detuned laser whispering gallery mode and (2) the repulsive centrifugal force. In another atom cavity scheme (Mabushi and Kimble 1994) the atom is considered to be kept in circular orbit by two evanescent waves, one repulsive and the other attractive, as in the case of localization of atoms in a flat waveguide considered in section 4.4.

The behaviour of an atom localized about a dielectric sphere must also comply with atomic motion quantization condition (4.15). In the given case, the length  $L$  of the cavity is the circumference of the dielectric microsphere. The results of the numerical modelling of an atom cavity based on whispering gallery modes (Mabushi and Kimble 1994) showed that when using a microsphere  $50 \mu\text{m}$  in diameter and the light field of an evanescent wave with a saturation parameter of  $S < 5 \times 10^{-7}$  (inside the potential well), a caesium atom could be caught and forced to execute a stable orbital motion for approximately 4 s. The potential well depth in that case was  $\Delta U \approx 1 \mu\text{K}$ , and the characteristic size of the localization region, around  $1 \mu\text{m}$  across. The above lifetime of the atom about the microsphere allows it to complete some 450 revolutions.

It should also be noted that the development of atom cavities will require solving many problems, including such important problems as the minimization of the loss due to spontaneous emission in the vicinity of the atom mirrors and allowance for the gravity field effects retarding the vertical motion of atoms and a number of other effects (Deutschmann *et al* 1993, Seifert *et al* 1994, Liston *et al* 1995a, b).

Some other ideas as to the development of atom cavities using various evanescent wave-gravity field combinations are discussed in section 6.

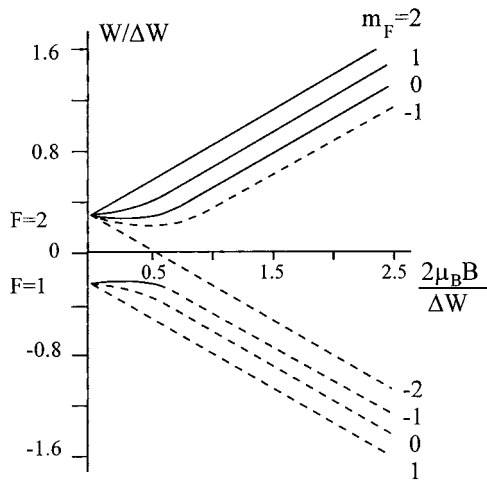


**Figure 33.** Hyperfine-structure magnetic sublevels for  $^{23}\text{Na}$  as functions of magnetic field,  $\Delta W = 1772$  MHz is the ground-state hyperfine splitting. Solid lines correspond to the negative value of the magnetic moment projection onto the direction of the magnetic field,  $\mu_l < 0$ .

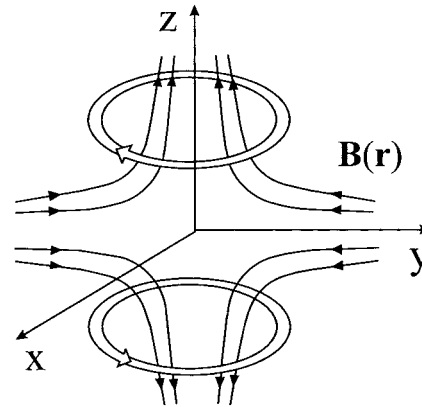


**Figure 34.** Magnetic field  $B(\mathbf{r})$  in a spherical quadrupole magnetic trap generated by two Helmholtz coils.

## 5. Magnetic trapping

### 5.1. Static magnetic traps

All static magnetic traps use nonuniform stationary magnetic fields for trapping atoms. In a nonuniform magnetic field  $\mathbf{B} = \mathbf{B}(\mathbf{r})$ , an atom with a permanent magnetic moment  $\vec{\mu}$  has the magnetic dipole interaction energy

$$U = -\vec{\mu}\mathbf{B} = -\mu_l B, \quad (5.1)$$

where  $\mu_l$  is the projection of the magnetic moment  $\vec{\mu}$  onto the field direction. Accordingly, an atom in the field  $\mathbf{B}(\mathbf{r})$  is acted on by the magnetic dipole force

$$\mathbf{F} = \nabla(\vec{\mu}\mathbf{B}) = \mu_l \nabla B. \quad (5.2)$$

Inasmuch as the Maxwell equations allow for no static magnetic field maximum in free space, force (5.2) can be used to trap atoms only in the minimum of the static magnetic field (Wing 1984). Force (5.2) can hold an atom near the minimum of a static magnetic field if the direction of the magnetic moment  $\vec{\mu}$  is opposite to that of the magnetic field,  $\mu_l < 0$ . As an example, the solid lines in figure 33 show the lower magnetic sublevels for  $^{23}\text{Na}$  atom, at which it can be trapped in the minimum of a static magnetic field.

The static magnetic traps can naturally be classed by the magnitude of the magnetic field minimum,  $B_{\min}$ . In the magnetic traps of the first kind  $B_{\min} = 0$ . These traps have a simple geometric structure and use comparatively simple, highly symmetric magnetic fields. In such fields, however, an important negative role is played by the non-adiabatic Majorana transitions in the zero-field region, which cause changes in the mutual orientation of the magnetic moment of the atom and the magnetic field and thus allow the atoms to leave the trap. Magnetic traps of the second kind having  $B_{\min} \neq 0$  are devoid of this shortcoming, but have a complex geometric structure and use very complex asymmetric fields (Bergeman *et al* 1987).

The most important static magnetic trap of the first kind is the so-called spherical quadrupole trap proposed by W Paul (Niehues 1976). In this trap, two opposite circular

currents produce a static magnetic field in the form of a spherical quadrupole (figure 34). The radii of the circular currents are taken to be approximately  $\frac{4}{5}$  of the distance between the planes of the currents in order that the trap can have the same potential well depth along and across the symmetry axis. If the  $z$ -axis is the symmetry axis of the circular currents and the currents are symmetrical with respect to the  $xy$ -plane, the magnetic field near the centre of the quadrupole trap has the form

$$\mathbf{B} = -\frac{1}{2}ax - \frac{1}{2}ay + az, \quad (5.3)$$

where  $a$  is the magnetic field gradient at the central point  $x = y = z = 0$  (Bergeman *et al* 1989). The magnitude of magnetic field (5.3) increases at the displacement away from the centre of the trap. Accordingly, magnetic field (5.3) produces a potential well for atoms having a negative magnetic moment projection on the field direction,  $\mu_l = -\mu$  ( $\mu > 0$ ):

$$U = -\mu_l B = \frac{1}{2}\mu a \sqrt{\rho^2 + 4z^2}, \quad (5.4)$$

where  $\rho = (x^2 + y^2)^{1/2}$  is the polar coordinate in the  $xy$ -plane. The gradient of the magnitude of magnetic field (5.3) varies with direction. For this reason, the magnetic dipole force in field (5.3) is neither central, nor harmonic.

At typical magnitude of the magnetic moment about the Bohr magneton,  $\mu \approx \mu_B$ , and a moderate magnetic field strength at the edges of the trap,  $B = 100$  G, a quadrupole magnetic trap can hold atoms with a temperature of the order of 10 mK.

The principal shortcoming of magnetic traps having a zero magnetic field minimum is the presence of a channel for the atoms to leave the zero-field region. When the moving atom traverses the zero-field region sufficiently fast, its magnetic moment cannot adiabatically follow the rapidly changing magnetic field direction. As a result, the change of the mutual orientation of the atom magnetic moment and the magnetic field causes an atom to leave the trap. Atom transitions from trapped to untrapped states (non-adiabatic Majorana transitions or spin flips) have a noticeable probability even for very cold atoms (Bergeman *et al* 1989, Petrich 1995). In the quadrupole magnetic trap, this escape mechanism usually limits the lifetime of cold atoms in the central region to a few seconds. At the same time, it should be borne in mind that when the volume of this central region is but a small fraction of the total trap volume, the fraction of atoms pushed out of the trap may be small.

The first experiment on trapping of cold atoms in a static magnetic field was done with a quadrupole magnetic trap (Migdal *et al* 1985). The trap was loaded with  $^{23}\text{Na}$  atoms preliminarily cooled to a temperature of 17 mK by a counter-propagating laser beam. The trapping time was no longer than a minute because of collisions between the trapped atoms and the residual gas particles. Among the latest experiments can be mentioned the following ones. Weinstein *et al* (1998a, b), reported on magnetic trapping chromium atoms via buffer-gas loading. The large chromium magnetic moment of  $6\mu_B$  allowed for trapping at elevated buffer-gas temperatures, opening up the possibility of trapping the chromium sample inside a simple cryostat. A microscopic quadrupole magnetic trap for atoms was realized with a combination of permanent magnets, coils, and ferromagnetic pole pieces (Vuletic *et al* 1998). The attainable magnetic field gradients of  $3 \times 10^5$  G cm $^{-1}$  infer a spatial extension of the ground state of the trapped atom much smaller than the wavelength of the optical transitions. The field gradient could be varied over a wide range allowing for an efficient loading of  $4 \times 10^5$  lithium atoms from a shallow potential by adiabatic transport and compression. During the compression a 275-fold density increase was observed.

In recent years, quadrupole magnetic fields have found wide application in the MOTs considered in section 6.

A most important example of a static magnetic trap of the second kind is the Ioffe trap first developed for use in plasma confinement schemes (Gott *et al* 1962, Artsimovich 1964,

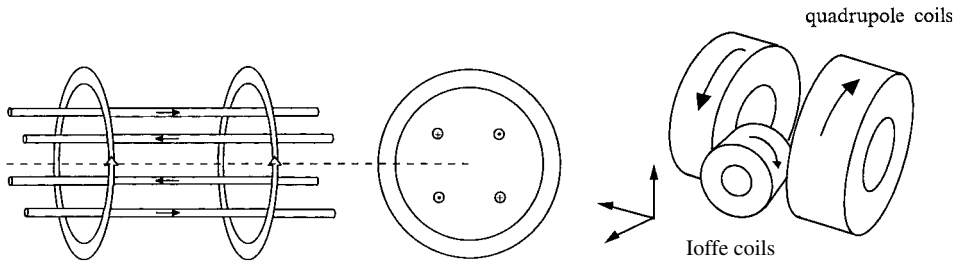


**Figure 35.** Geometry of currents in the Ioffe trap.

**Figure 36.** Magnetic trap combined of the Ioffe coil and quadrupole coils (Esslinger *et al* 1998).

Krall and Trivelpiece 1973, Bergeman *et al* 1987). In this trap, the magnetic field of two equal circular currents provides for the axial confinement of atoms, and four rectilinear currents serve for their transverse confinement (figure 35). The Ioffe trap has recently been used for trapping atoms at ultralow temperatures of the order of 100–10 nK attained by the evaporative cooling technique (Ketterle and Van Druten 1996).

An experimentally attractive variety of the Ioffe trap is the trap proposed by Hänsch and co-workers. It consists of two circular currents, as in the case of quadrupole trap, and a third circular current normal to the first two and located at a certain distance from the quadrupole configuration (figure 36). A smooth activation of the third circular current transforms the magnetic trap of the first kind into one of the second kind (Esslinger *et al* 1998, Bloch *et al* 1999). Atoms in such a trap are initially caught in the quadrupole field and then transferred to the trap of the second kind by activating the third circular current.

Along with static magnetic traps based on the magnetic fields produced by electric currents, there have been developed a number of traps built of permanent magnets (Frerichs *et al* 1992, Höpe 1993, Ricci *et al* 1994, Tollet *et al* 1995). Such traps are very easy to manufacture, but not always convenient in experiments, for they permit no manipulation of the magnetic field.

## 5.2. Quadrupole magnetic trap with time-orbiting potential

One of the direct ways to close the channel whereby atoms escape from the central region of the quadrupole magnetic trap is to displace potential (5.4) in the symmetry plane of the trap and effect its rapid circling in this plane, i.e. to convert the static potential into an orbiting potential. Thanks to the fact that the minimum of the orbiting potential moves about the central point of the quadrupole trap, the time-averaged orbiting potential (TOP) proves other than zero at the centre of the trap, which closes the channel whereby atoms are lost on account of the Majorana transitions (Petrich *et al* 1995).

In the TOP quadrupole magnetic trap, the total magnetic field  $B_t$  consists of the quadrupole magnetic field (5.3) and the homogeneous rotating field  $b$ ,

$$B_t = B + b. \quad (5.5)$$

The homogeneous magnetic field  $b$  rotates with angular frequency  $\Omega$  in a plane normal to the symmetry axis of the trap:

$$b = b_0(e_x \cos \Omega t + e_y \sin \Omega t), \quad (5.6)$$

where  $e_x$  and  $e_y$  are the unit vectors along the  $x$ - and  $y$ -axis, respectively. The rotation frequency  $\Omega$  is assumed to be higher than the characteristic oscillation frequencies  $\omega_{\text{osc}}$  of an atom in potential (5.4), but naturally lower than the Larmor precession frequency  $\omega_L$  in order

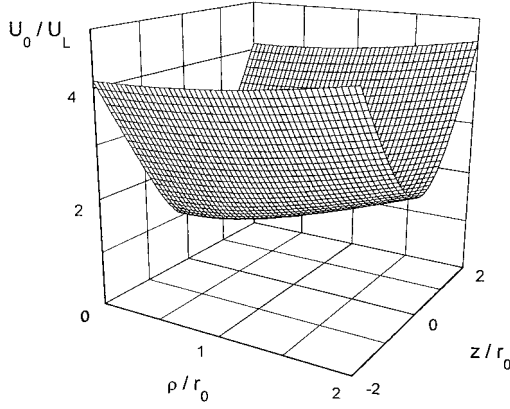


**Figure 37.** The time-averaged value  $U_0$  of the time-orbiting potential (5.7) as function of the cylindrical coordinates  $\rho$  and  $z$ .  $U_L = \mu b_0$  is the magnetic interaction energy in the centre of the trap,  $r_0$  is the radius of a circular orbit for rotating potential.

that the rotating and hence oscillating field cannot destroy the coupling between an atom and the trapping field.

The addition of the rotating field transforms potential (5.4) into an orbiting potential which for atoms having a negative projection  $\mu_l$  of the magnetic moment  $\mu$  on the field direction,  $\mu_l = -\mu$  ( $\mu > 0$ ), has the form

$$U = -\mu B_t = \mu \sqrt{(b_0 \cos \Omega t - \frac{1}{2}ax)^2 + (b_0 \sin \Omega t - \frac{1}{2}ay)^2 + a^2 z^2}. \quad (5.7)$$

As follows from expression (5.7), the time-dependent magnetic dipole interaction potential  $U$  rotates around the  $z$ -axis so that its minimum moves in the  $xy$ -plane in a circle with a radius  $r_0 = 2b_0/a$ .

The motion of an atom in periodic potential (5.7) can conveniently be analysed on expanding the potential into a Fourier series and going over to the cylindrical coordinates  $x = \rho \cos \varphi$ ,  $y = \rho \sin \varphi$ ,  $z$ :

$$U = U_0 - U_1 \cos(\Omega t - \varphi) - U_2 \cos 2(\Omega t - \varphi) - \dots \quad (5.8)$$

In expansion (5.8), different parts play different roles. The time-independent potential  $U_0$  causes slow atomic motion on characteristic timescale  $\tau_{\text{slow}} \cong 1/\omega$ , where the quantities  $\omega$  define the characteristic eigenfrequencies of atomic oscillations in the potential  $U_0$ . We stress that the time-constant potential  $U_0$  is other than zero at the centre of the trap. The oscillating parts of the potential,  $U_1, U_2, \dots$ , cause fast oscillations of the atomic momentum and coordinate on a characteristic timescale  $\tau_{\text{fast}} \cong 1/\Omega$ .

When an atom is at a short distance from the centre of the trap, the amplitudes of the orbiting potential harmonics  $U_0, U_1, U_2, \dots$  can be expanded into the powers of the small coordinates  $\rho, z$ . When expanding up to the second order in  $\rho$  and  $z$ , the amplitudes of the first three harmonics are as follows:

$$U_0 = U_L + \frac{1}{2}k(\rho^2 + 8z^2), \quad U_1 = 2kr_0\rho, \quad U_2 = \frac{1}{2}k\rho^2, \quad (5.9)$$

where  $U_L = \mu b_0 = \hbar\omega_L$  is the magnetic interaction energy at the trap centre  $r = 0$ ,  $\omega_L$  is the Larmor frequency, and  $k = \mu b_0/2r_0^2$  is the spring constant of the harmonic part of the potential  $U$ . According to expression (5.9), the harmonic potential  $U_0$  causes an atom to oscillate along the  $x$ -,  $y$ -, and  $z$ -axes with the frequencies (figure 37)

$$\omega_x = \omega_y = \omega_\rho = \sqrt{k/M}, \quad \omega_z = 2\sqrt{2}\omega_\rho. \quad (5.10)$$

In accordance with the idea of a magnetic trap with a time-orbiting potential, the three fundamental frequencies  $\omega_\rho, \Omega$  and  $\omega_L$  are assumed to be related by the inequalities

$$\omega_\rho \ll \Omega \ll \omega_L. \quad (5.11)$$

The left-hand inequality in expression (5.11) is necessary in order that the effect of the time-averaged potential  $U_0$  can exceed that of the potential harmonics  $U_1, U_2 \dots$ . The right-hand inequality in expression (5.11) excludes the non-adiabatic Majorana transitions on account of the rotation of the magnetic field  $\mathbf{b}$ . In typical experimental conditions,  $\omega_\rho/2\pi \sim 10\text{--}100$  Hz,  $\Omega/2\pi \sim 10^4$  Hz, and  $\omega_L/2\pi \sim 10^7$  Hz, so that  $\omega_\rho/\Omega \sim 10^{-2}\text{--}10^{-3}$  and  $\Omega/\Omega_L \sim 10^{-3}$ .

Quantum mechanical analysis shows that the motion of the atom in the TOP trap is a sum of two basic motions: a slow oscillatory motion in the time-averaged potential and fast oscillations with a frequency governed by the rotation frequency of the magnetic field. At the typical experimental values of the three fundamental frequencies  $\omega_\rho$ ,  $\Omega$  and  $\omega_L$  the fast oscillation amplitude of the atomic coordinates is negligibly small compared with the amplitude of slow atomic oscillations in the time-averaged potential. By contrast, the amplitude of the high-frequency oscillations of the atomic momentum is, generally speaking, commensurable with the momentum distribution width for the vibrational ground state of the atom in the potential of the trap. Such a deep modulation of the momenta of atoms becomes substantial at low atomic temperatures, when the average thermal atomic energy becomes comparable with the energy of atomic oscillations in the time-averaged potential. Accordingly, at low temperatures the momentum distribution of atoms acquires a ring-shaped structure in the symmetry plane of the trap (Minogin *et al* 1998a, b).

### 5.3. Magnetic trap with an optical plug

One more way to ‘close’ the central, zero magnetic field region in the quadrupole magnetic trap is to irradiate this region by a blue-detuned laser beam. With this method, the atom is acted on by the gradient force which pushes atoms out of the central part of the trap. Davis *et al* (1995) used as an ‘optical plug’ an argon laser beam focused into a spot  $30 \mu\text{m}$  across at the centre of the quadrupole magnetic trap. The potential barrier produced by the laser beam amounted to  $350 \mu\text{K}$ , which was sufficient to ‘close’ the region where the Majorana transitions were possible. Figure 38 shows the shape of the potential produced by the quadrupole magnetic trap with an optical plug. As one can see, the potential has two minima displaced from the centre of the trap by  $50 \mu\text{m}$ . Near its bottom the potential can be approximated by a 3D anisotropic harmonic potential defined by the frequencies  $\omega_x = \omega_y \sqrt{4x_0^2/w_0^2 - 1}$ ,  $\omega_y = \sqrt{\mu B'/2Mx_0}$ ,  $\omega_z = \sqrt{3}\omega_y$ , where  $x_0$  is the distance from the centre of the quadrupole trap to the potential minimum,  $\mu$  is the atom’s magnetic moment,  $M$  is the atom’s mass,  $B'$  is the axial magnetic field gradient and  $w_0$  is the laser beam waist. The magnetic trap with an optical plug was successfully used for the experimental observation of the BEC in a gas of sodium atoms (Davis *et al* 1995).

### 5.4. Magnetic mirrors and cavities

Magnetic dipole force (5.2) acting on an atom with a magnetic moment  $\mu$  in an inhomogeneous magnetic field  $\mathbf{B} = \mathbf{B}(\mathbf{r})$  can be used not only for trapping cold atoms, but also to produce magnetic mirrors for slow atoms, similar to the atom mirrors based on evanescent laser waves (see section 2.2.3). One type of magnetic mirror can be formed by exponentially decaying magnetic fields produced by either arrays of permanent magnets (Opat *et al* 1992, Sidorov *et al* 1996) or magnetic surfaces such as audio (video) tapes or flexible computer disks (Roach *et al* 1995, Hughes *et al* 1997, Hinds and Hughes 1999). The other type of magnetic mirrors for atoms can be realized with arrays of current-carrying wires (Drndic *et al* 1998, Lau *et al* 1999). A magnetic mirror of this second type was earlier used for the reflection of cold neutrons (Vladimirskii 1960).

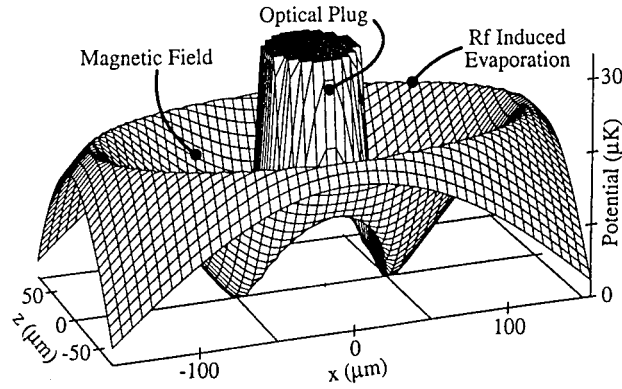


**Figure 38.** Adiabatic potential due to the magnetic quadrupole field, the optical plug, and the rf field. This cut of the 3D potential is orthogonal to the propagation direction ( $y$ ) of the blue-detuned laser. The symmetry axis of the quadrupole field is the  $z$ -axis (Davis et al 1995).

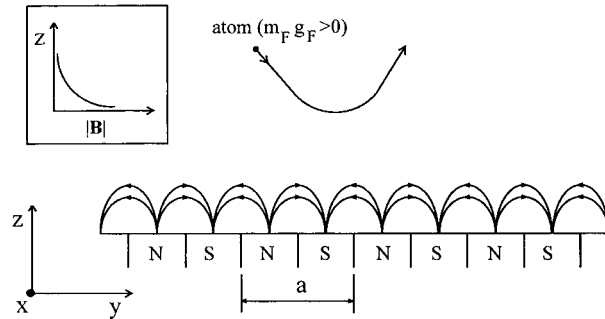


**Figure 39.** Scheme of magnetic mirror for atoms formed by an array of permanent magnets. The insert shows the magnitude of the magnetic field as function of coordinate  $z$  (Sidorov et al 1996).

Figure 39 shows a schematic of a magnetostatic mirror for cold atoms. The magnetic field of the mirror is produced by an array of permanent magnets having their length along the  $x$ -axis much greater than the period  $a$  and a varying magnetization  $M(y, z) = \pm M_0$ . Away from the surface of the magnets,  $z \gg a/2\pi$ , the magnetic field is

$$B(y, z) = B_0 e^{-kz} (1 + \frac{1}{3} e^{-2kz} \cos 2ky + \dots), \tag{5.12}$$

where  $B_0 = 2\mu_0 M_0 / \pi$  and  $k = 2\pi/a$ . For an atom occupying the hyperfine-structure magnetic sublevel  $F, m_F$  the magnetic energy of atom in field (5.12) is

$$U(y, z) = m_F g_F \mu_B B(y, z), \tag{5.13}$$

where  $g_F$  is the Landé  $g$ -factor and  $\mu_B$  is the Bohr magneton. When the atom is in a ‘positive’ magnetic state where  $m_F g_F > 0$ , its energy decreases as it moves away from the surface of the magnets. This means that when the kinetic energy of the atom is lower than the barrier height, potential (5.13) reflects the atoms incident thereon.

For slow atoms whose magnetic moment adiabatically follows the varying magnetic field, the quality of the magnetic mirror based on potential (5.13) depends mainly on the ratio between the first terms in relation (5.12). The second term in equation (5.12), which depends on the  $y$ -coordinate, distorts the atomic wave front and thus causes the diffuse scattering of the reflected atomic wave. At the same time, this term decays much faster than the first. In this connection,

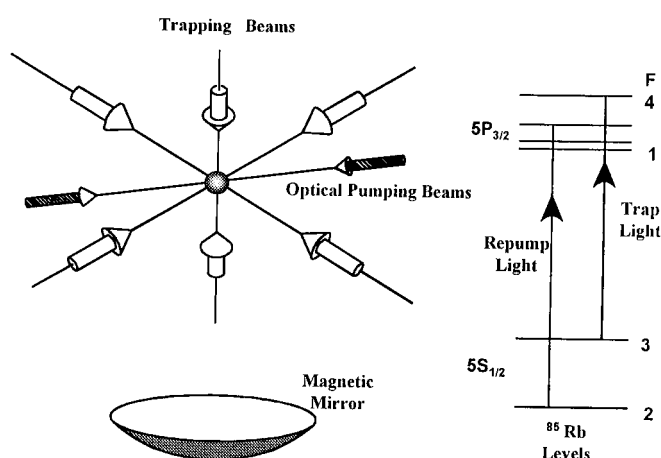


**Figure 40.** Magneto-gravity trap. The energy diagram on the right shows the  $^{85}\text{Rb}$  D2 line used for trapping atoms in the  $F = 3$  ground state and the transition used for repumping atoms from  $F = 2$  state into  $F = 3$  state. On the left are shown six MOT beams directed along Cartesian axes. The cloud of  $5 \times 10^6$  cold atoms formed in the trap has a 1 mm diameter. After release from the MOT the atoms are cooled by optical molasses to a temperature of  $20 \mu\text{K}$  and optically pumped by a pair of circularly polarized laser beams. Atomic cloud falls a few cm onto the magnetic mirror below, whose diameter is typically 1 or 2 cm. (Adapted from Hughes *et al* 1997.)

its contribution is substantial for relatively fast atoms that penetrate deep into the field and is less important for cold atoms.

A practical implementation example is the magnetostatic mirror assembled of rare-earth neodymium–iron–boron permanent dipole magnets 1.04 mm wide, 20 mm long, and 12 mm thick. A set of 18 such magnets produced a magnetic field of form (5.12) having an initial strength  $B_0 = 4200 \text{ G}$  and a characteristic decay length  $a/2\pi = 0.33 \text{ mm}$  (Sidorov *et al* 1996). This magnetic mirror was used to reflect cold caesium atoms occupying the magnetic sublevel  $F = 4, m = 4$  of the ground state  $6^2\text{S}_{1/2}$ . At an effective atom temperature 20 mK the experimentally measured mirror reflection coefficient proved close to 100%.

Another very similar approach to the development of atom mirrors for cold atoms is the use of a periodically magnetized ferromagnetic surface which reflects atoms like a mirror on account of the magnetic potential produced by this surface. The experimental testing of this approach showed that the ferromagnetic mirror is also capable of reflecting practically 100% of the incident atoms (Roach *et al* 1995).

The successful implementation of these two types of magnetic mirror made it possible to develop gravito-magnetic traps and cavities for cold atoms on the basis of a combination of reflecting magnetic mirrors and the gravity field (Hughes *et al* 1997, Saba *et al* 1999).

A schematic diagram of one such cavity is shown in figure 40 (Hughes *et al* 1997). It consists of a horizontally arranged concave magnetic mirror made of a piece of a computer floppy disk magnetized in a sinusoidal fashion. The radius of curvature of the mirror is  $R = 54 \text{ mm}$ . The source of rubidium atoms used in the experiment was a MOT located at a distance of  $R/4$  from the surface of the mirror. When the laser and magnetic fields of the trap were switched off, the trapped Rb atoms started falling onto the mirror in the gravity field. During their fall the atoms were pumped by an additional laser radiation to a ‘positive’ magnetic sublevel ( $F = 3, m_F > 0$ ). The number of reflected atoms was measured by catching them again in the trap a certain time after their release.

To study the dynamics of reflection and focusing of atoms by the concave mirror of the magneto-gravitational cavity, the atoms were irradiated with a probe laser beam, and the scattered photons were recorded with a video camera. It was shown that as the atomic cloud propagates, it expands as a result of thermal spreading and then gets focused again to its initial size following the reflection of the atoms. In the experiment (Saba *et al* 1999), they observed a clear image of the atoms following their 14-fold reflection. The main factor responsible for the diffuse spreading of the atomic cloud is the imperfection of the magnetic mirror.

### 5.5. Magnetic trapping of molecules

Similar to paramagnetic atoms having a permanent magnetic moment in a specific magnetic state, paramagnetic molecules can be trapped in different kinds of magnetic traps. The key problem in the magnetic trapping of molecules is the preliminary cooling of a molecular sample to low temperature where the thermal energy is of the order the depth of the trap. This key problem has been recently solved by the buffer-gas loading technique, relying on the cooling of molecules by thermalization with a buffer gas (Weinstein *et al* 1998a). Because the technique is based on the elastic collisions it can be applied practically to any molecule independently of the internal energy-level structure. Applying this technique Weinstein *et al* (1998a, b) have reported on cooling CaH molecules down to 400 mK and confining the cold molecular sample in a magnetic trap.

## 6. Magneto-optical trapping

### 6.1. Simplified scheme and basic configuration

The idea of magneto-optical trapping of atoms can be understood by considering the idealized 1D scheme shown in figure 41(a) (Dalibard 1987). In this scheme, the atoms are placed in a weak magnetic field  $\mathbf{B} = B\mathbf{e}_z$  which increases linearly in the positive direction of the  $z$ -axis,  $B(z) = az$ , being equal to zero at the central point  $z = 0$ . For simplicity, the atoms are assumed to have two electronic states: the ground state with the energy  $E_g^0$  and the total angular momentum equal to zero,  $F_g = 0$ , and the excited electronic state with the energy  $E_e^0$  and the total angular momentum  $F_e = 1$ . The excited electronic state is split in the magnetic field into three Zeeman magnetic sublevels,  $m_e = 0, \pm 1$ . The energies  $E_e^{\pm 1} = \hbar\omega_0 \pm \mu B(z)$  of two extreme magnetic sublevels,  $m_e = \pm 1$ , depend on the atomic coordinate  $z$ , where  $\omega_0$  is the atomic transition frequency in a zero magnetic field, i.e. at the point  $z = 0$ , and  $\mu$  is the projection of the magnetic moment  $\vec{\mu}$  onto the field direction. The atoms are irradiated by two circularly polarized  $\sigma^+$ ,  $\sigma^-$  laser beams propagating in the directions  $\pm z$ . The frequency  $\omega$  of the laser beams is assumed to be red-shifted with respect to the frequency of the unperturbed atomic transition,  $\omega < \omega_0$ .

In the above scheme, the atom is acted on by the radiation pressure force  $\mathbf{F} = F\mathbf{e}_z$  caused by the one-photon transitions between the ground state and two upper-state magnetic sublevels  $m_e = \pm 1$ . For a motionless atom, the rate of atom excitation to the upper-state sublevels depends on the atom's coordinate. When the coordinate  $z$  is positive, the atom is excited with a higher probability to the magnetic sublevel  $m_e = -1$  and with a lower probability to the sublevel  $m_e = 1$ , and when the coordinate  $z$  is negative, it is excited with a higher probability to the sublevel  $m_e = 1$  and with a lower probability to the sublevel  $m_e = -1$ . As a result, the direction of the radiation pressure force on a motionless atom depends on the sign of the coordinate  $z$ . When the atom coordinate is negative,  $z < 0$ , it mainly interacts with the  $\sigma^+$ -polarized radiation, and experiences a force in the positive direction of the  $z$ -axis. In contrast,

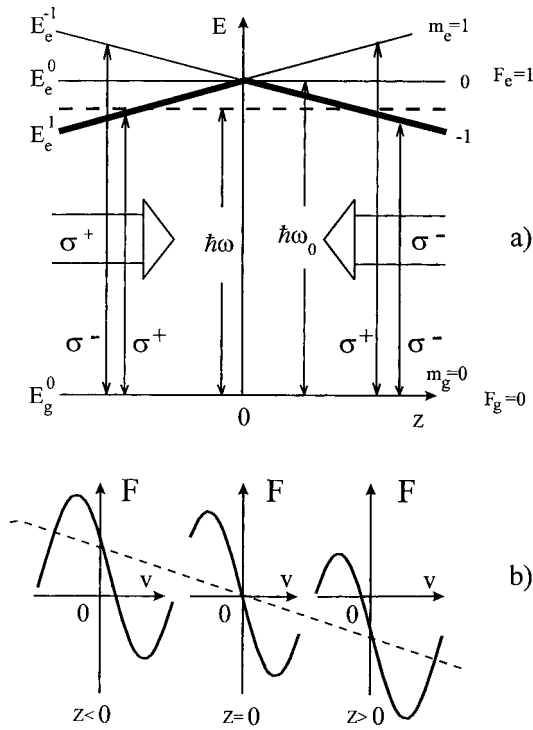


**Figure 41.** (a) Scheme of a 1D magneto-optical trapping of atoms. (b) The radiation pressure force as a function of atom velocity for three values of atomic coordinate,  $z < 0$ ,  $z = 0$  and  $z > 0$ . Atoms are assumed to have a nondegenerate ground-state magnetic sublevel  $|g\rangle = |F_g = 0, m_g = 0\rangle$  and three excited-state magnetic sublevels  $|e_{\pm 1}\rangle = |F_e = 1, m_e = \pm 1\rangle$ ,  $|e_0\rangle = |F_e = 1, m_e = 0\rangle$ . Two counter-propagating  $\sigma^+$ ,  $\sigma^-$  laser waves are red-detuned with respect to the optical transition  $|0, 0\rangle \rightarrow |1, 0\rangle$ .

with a positive atom coordinate,  $z > 0$ , the atom mainly interacts with the  $\sigma^-$ -polarized laser light and is subject to a force in the negative direction of the  $z$ -axis. The radiation pressure force in the scheme of figure 41(a) is thus always directed opposite to the displacement of the atom. Accordingly, the radiation pressure force produces a potential well for atoms located at the central point  $z = 0$ .

For an atom moving near the centre of the trap, the efficiency of atom excitation by a red-detuned laser light depends strongly on the direction of the atom velocity. When the atom moves in the positive direction of the  $Oz$  axis it is more effectively excited by the  $\sigma^-$ -polarized laser light. In contrast, the atom moving in the negative direction is mostly excited by the  $\sigma^+$ -polarized laser light. For these reasons, the radiation pressure force is directed opposite to the atomic velocity and thus produces the cooling of atoms. The qualitative dependence of the radiation pressure force on velocity for three different atom coordinates is shown in figure 41(b).

Thus, in the above scheme the radiation pressure force simultaneously displaces atoms to the centre of the trap and cools atoms near the central region.

The 1D magneto-optical trapping scheme considered above can easily be generalized to three dimensions. The most frequently used 3D scheme of MOT includes a magnetic field in the form of spherical quadrupole (5.2) and a laser field produced by three orthogonal pairs of counter-propagating laser beams with polarizations  $\sigma^{\pm}$  (figure 42). In this basic configuration of the MOT, the radiation pressure force is responsible both for the formation of a 3D potential well for atoms and for a 3D cooling of atoms near the centre of the trap. Some other configurations of MOT can be found in the literature cited in section 6.6.

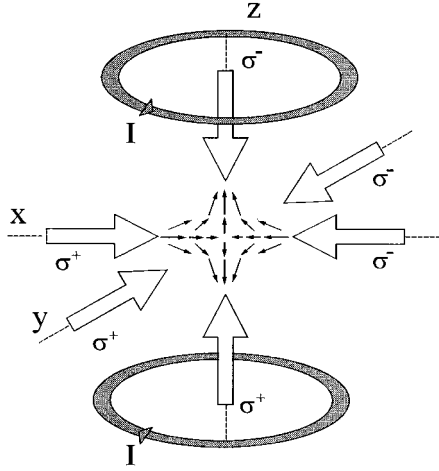


**Figure 42.** Scheme of a 3D MOT. Two circular currents produce a magnetic field in the form of spherical quadrupole. The laser field is produced by three pairs of counter-propagating laser beams with circular polarizations  $\sigma^\pm$ .

### 6.2. (1 + 3)-level atom model

For the above-considered (1 + 3)-level atom model, the interaction of the atom with the 1D  $\sigma^\pm$  laser field configuration defined by equation (2.58) is described by a three-level V-scheme. The lower energy level  $E_g^0$  retains its magnitude at any value of the coordinate  $z$ , and the energies of the upper levels  $E_e^{\pm 1}(z)$  are the linear functions of the displacement of the atom from the central point  $z = 0$ .

In the case of weak optical saturation, the radiation pressure force in the above interaction scheme may be written in the form of a sum of two forces (2.20a) taken in a linear approximation in the saturation parameter  $G$ :

$$F = \hbar k \gamma G \left\{ \frac{1}{1 + (\delta - kv - \omega_L(z))^2 / \gamma^2} - \frac{1}{1 + (\delta + kv + \omega_L(z))^2 / \gamma^2} \right\}, \quad (6.1)$$

where  $\omega_L(z) = \mu B(z) / \hbar = \mu_B g_e a z / \hbar$  is the position-dependent Larmor frequency,  $g_e$  is the  $g$ -factor and the detuning  $\delta = \omega - \omega_0$  may have any sign. In a linear approximation in velocity and coordinate, i.e. for atoms slowly moving in the vicinity of the centre of the trap, radiation pressure force (6.1) in the case of red detuning is reduced to a sum of two forces, a friction force and a harmonic restoring force:

$$F = -M\beta v - M\omega_v^2 z, \quad (6.2)$$

where the friction coefficient  $\beta$  and oscillation frequency  $\omega_v$  are defined by the relations

$$\beta = 8G\omega_r (|\delta|/\gamma) / (1 + \delta^2/\gamma^2)^2, \quad \omega_v = \sqrt{\beta(\mu_B g_e a / \hbar k)}, \quad (6.3)$$

and  $\omega_r = \hbar k^2 / 2M$  is the recoil frequency.

In the same linear approximation in the saturation parameter, the longitudinal momentum diffusion coefficient for a three-level V-scheme is reduced to the sum of the two diffusion coefficients  $D_{zz}$  (2.64) for the two counter-propagating laser waves. For small atomic velocity and displacement, the longitudinal diffusion coefficient according to equation (2.64) is

$$D = D_{zz} = \hbar^2 k^2 \gamma \frac{G}{1 + \delta^2/\gamma^2} (1 + \alpha_{zz}). \quad (6.4)$$

The cooling and restoring force (6.2) jointly with the diffusion coefficient (6.4) fully define the steady-state atomic velocity and coordinate distribution in the 1D MOT. According to

the steady-state solution of a 1D Fokker–Planck equation with force (6.2) and diffusion coefficient (6.4) the steady-state atomic distribution is a Gaussian one,

$$w(v, z) = \frac{1}{\sqrt{\pi}u} \exp\left(-\frac{v^2}{u^2}\right) \cdot \frac{1}{\sqrt{\pi}s} \exp\left(-\frac{z^2}{s^2}\right), \quad (6.5)$$

where the velocity distribution half-width is

$$u = \sqrt{2k_B T/M}, \quad (6.6)$$

the coordinate distribution half-width is

$$s = \sqrt{2k_B T/M\omega_v^2}, \quad (6.7)$$

and the temperature is defined as

$$T = \frac{D}{M\beta k_B} = \frac{1 + \alpha_{zz}}{4} \frac{\hbar\gamma}{k_B} \left( \frac{|\delta|}{\gamma} + \frac{\gamma}{|\delta|} \right). \quad (6.8)$$

The minimum temperature attained at detuning  $\delta = -\gamma$  is defined by the natural linewidth:

$$T_{\min} = \frac{1 + \alpha_{zz}}{2} \frac{\hbar\gamma}{k_B}. \quad (6.9)$$

The above-considered model of the MOT thus describes the trapping and cooling of atoms by the radiation pressure force coming from the one-photon processes. Accordingly, the model describes only the so-called Doppler cooling of atoms inside the MOT. In this model, the minimum temperature is of the order of the Doppler limit temperature,  $T_{\min} \approx T_D = \hbar\gamma/k_B$ . This minimum temperature accordingly defines both the minimum velocity width (6.6) and the minimum spatial size (6.7) of the trapped atomic cloud.

### 6.3. (3 + 5)-level atom model

The theory of the magneto-optical trapping of atoms in the case of an interaction scheme featuring two-photon or higher-order multiphoton processes substantially differs from the one considered above, for multiphoton processes sharply change the friction force and momentum diffusion tensor.

Steane and Foot (1991) were the first to suggest that the Doppler theory is not always adequate to describe the behaviour of atoms in the MOT. Their measurements of such MOT parameters as the friction coefficient, elastic constant, and the size of the atomic cloud showed that the multilevel structure of atomic levels might play an important role. In their experiment, the temperature of Cs atoms in the MOT proved substantially lower than the Doppler limit and amounted to some  $30 \mu\text{K}$ . In later experiments (Townsend *et al* 1992, Drewsen *et al* 1994) it was found that at a low atomic density in the MOT the temperature of atoms is identical to that in an optical molasses free from an external magnetic field.

The main differences occurring between two-level and multilevel atoms in the MOT can be illustrated using as an example a model of a (3 + 5)-level atom interacting with a 1D red-detuned  $\sigma^\pm$  laser field configuration (2.58) in the presence of a nonuniform magnetic field  $B(z) = az$  (figure 43). In such a scheme, the radiation pressure force on an atom slowly moving in the central region of the trap contains the friction force and a harmonic force due to the two-photon processes (Jun *et al* 1999a, b). As a result, along with a deeper, sub-Doppler cooling of the atoms, there takes place their localization in a region whose size is much smaller than that defined by equation (6.7). The spatial behaviour of the radiation pressure force on a (3 + 5)-level atom in the laser field (2.58), which illustrates the contributions from the two-photon processes, is shown in figure 44.

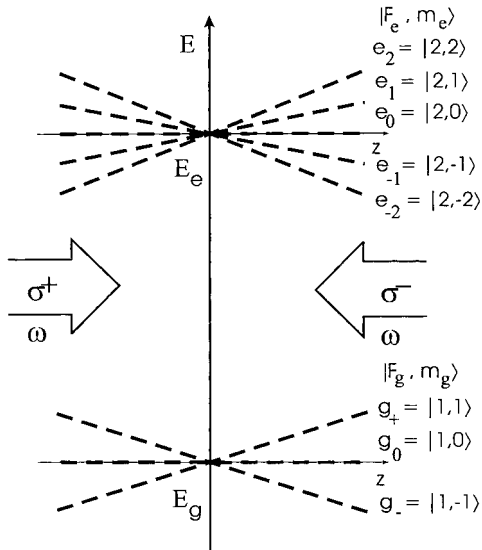


**Figure 43.** The Zeeman-shifted energy levels for a (3 + 5)-level atom interacting with counter-propagating laser beams with circular polarizations  $\sigma^\pm$ .

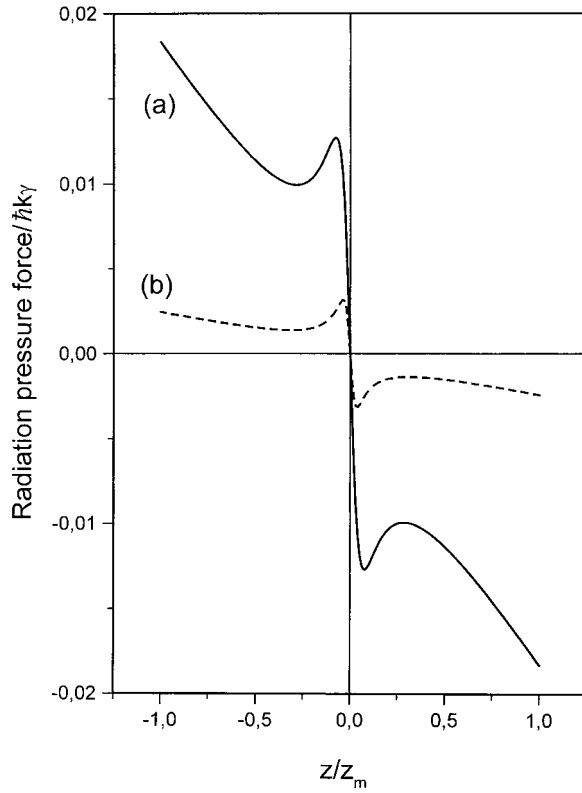


**Figure 44.** The radiation pressure force for a motionless (3+5)-level atom as a function of the atom's coordinate at saturation parameter  $G = 4$  and for detuning (a)  $\delta = -10\gamma$  and (b)  $\delta = -20\gamma$ . The central structure is due to the two-photon process related with the ground-state coherence.

For a motionless atom the radiation pressure force on a (3 + 5)-level atom includes an ordinary one-photon restoring force and a two-photon restoring force,

$$F(z) = -\frac{25 G\gamma^3}{11 |\delta|^3} \hbar k \varpi - \frac{60 G\gamma}{17 |\delta|} \frac{\mu^2}{\mu^2 + \varpi^2} \hbar k \varpi, \tag{6.10}$$

where  $\varpi = \mu_B g a z / \hbar$  is the Zeeman frequency shift assumed to be the same for the upper and lower magnetic sublevels. Force (6.10) creates the double-structure potential well where the first and second terms come from the one-photon and two-photon processes,

$$U(z) = \frac{25}{22} \frac{G\gamma^3}{|\delta|^3} \hbar\gamma \frac{kz^2}{z_m} + \frac{5}{88} \hbar\gamma \frac{G^2\gamma^3}{|\delta|^3} kz_m, \quad (6.11)$$

where  $z_m = \hbar\gamma / \mu_B g a$  is the characteristic distance from the centre of the trap at which the Zeeman frequency shift equals one-half of the natural linewidth.

#### 6.4. 3D MOT

The dynamics of atoms in any real 3D MOT is much more involved than that described in section 6.1. Two factors substantially complicate the motion of atoms in the 3D trap. First, in actually used atoms the lower and upper states are hyperfine-structure levels including several magnetic sublevels. For this reason, the atom–laser field interaction always proceeds by a complex multilevel scheme. Secondly, the polarization direction and intensity of the laser field in the scheme of figure 42 vary on the scale of the optical wavelength. This circumstance, as in the case of optical lattices (section 4.2), causes a small-scale modulation of the magnetic sublevel populations and coherences between the magnetic sublevels. These effects may give rise to additional friction forces due to the non-adiabatical time evolution of the magnetic sublevel populations and atomic coherences for moving atoms (Ungar *et al* 1989, Weiss *et al* 1989, Dalibard and Cohen-Tannoudji 1989).

It should be noted that the hyperfine structure in the ground and excited states is no obstacle for magneto-optical trapping. If there are a number of hyperfine-structure levels in the excited state, any of them can be chosen to serve as the upper working level. If the ground state of the atom is split into several hyperfine-structure levels, a multi-frequency laser light then can be used to excite the atoms from the hyperfine-structure levels.

#### 6.5. Density effects

The above estimations for atomic temperature defined by equation (6.8) and (3.15) are valid for a low-density atomic cloud in the MOT. At a high density and (or) for large number of trapped atoms the absorption of the laser light and subsequent reabsorption of the spontaneous emission may strongly effect both the temperature of atoms and the spatial distribution of atoms in the MOT (Drewsen *et al* 1994, Walker *et al* 1990, Cooper *et al* 1994, Castin *et al* 1998). Simple estimates show that the increase in the temperature of atoms caused by rescattering of absorbed laser light is proportional to the cube root of the number of trapped atoms (Cooper *et al* 1994).

The absorption of a photon from the laser light and subsequent emission of a photon increases the momentum diffusion coefficient in equation (6.8) and accordingly increases the temperature of atoms as

$$T_d = T(1 + \xi f), \quad (6.12)$$

where  $T$  is the temperature in a low-density atomic cloud,  $T_d$  is the temperature in a dense cloud,  $f = \sigma n l$  is the fraction of the spontaneous emission reabsorbed by atoms before leaving the trapped atomic cloud,  $\sigma$  is the absorption cross section,  $n$  is the number density,  $l$  is the dimension of the cloud and  $\xi$  is a factor of order unity. The temperature of trapped atoms can thus be expressed as a sum of the temperature for non-interacting atoms and an additional term including the fraction of photons that are reabsorbed after emission by the atoms. Introducing the total number of atoms,  $N = n l^3$ , gives the fraction of reabsorbed atoms as  $f = \sigma n^{2/3} N^{1/3}$ .

Accordingly, the temperature for a dense atomic cloud includes a term proportional to the cube root of the total number of atoms,

$$T_d = T(1 + \xi \sigma n^{2/3} N^{1/3}). \quad (6.13)$$

This estimate has been verified experimentally.

In the MOT, the restrictions on the maximum density and minimum temperature of atoms stem from the very nature of the trap: the scattered laser photons are absorbed again by the atoms, which gives rise to effective forces that push the atoms apart and thus limit their density and temperature. The effect of the radiation trapping in a dense atomic sample localized in the MOT was directly observed for Cs atoms as the lengthening of the natural radiative lifetime (Fioretti *et al* 1998b).

### 6.6. Experimental results

The first magneto-optical trapping scheme was experimentally tested with sodium atoms (Raab *et al* 1987). Since the ground state  $3S_{1/2}$  of sodium atom is split to two hyperfine-structure levels with the total angular momenta  $F = 1, 2$ , the atoms were excited on the dipole transition  $3S_{1/2} \rightarrow 3P_{3/2}$  by a two-frequency laser light. The two-frequency excitation avoided the optical pumping of atoms to one of the two lower hyperfine-structure levels and thus provided for a long-term atom–laser light interaction. In the first experiment, about  $10^7$  atoms were confined in the MOT for about 2 min at a temperature below 1 mK. The trapping time of the atoms was mainly limited by the collisions with the residual gas particles.

The principal features of the MOT are its ability to simultaneously cool and trap atoms, a fairly large potential well depth, the relatively large capture velocity, and a weak sensitivity to disturbances in the directions of the laser beams and their polarization imperfection. The MOT is capable of effective operation not only in the standard geometry shown in figure 42, but also with the use of only four laser beams in a tetrahedral geometry (Shimizu *et al* 1991). The trap parameters also vary but insignificantly when replacing one or several beam pairs of  $\sigma^+ - \sigma^-$  configuration by linearly polarized beam configurations (Walker *et al* 1991).

An important advantage of the MOT over purely magnetic traps is that it uses very weak magnetic fields, approximately 100 times weaker. In the MOT, the magnetic field is used only to produce a small Zeeman shift of the magnetic sublevels, whereas pure magnetic traps require a substantial magnetic field strength to produce magnetic dipole force (5.1). A no less important advantage of the MOT is also the possibility of injecting atoms into it both from an atomic beam and from an atomic gas (Monroe *et al* 1990).

Over the years, the MOT has become the most popular trap for cold atoms. To date, there is a very impressive list of atom isotopes that have been successfully localized in MOTs. This includes atom isotopes of such alkali metals as lithium (Lin *et al* 1991), sodium (Raab *et al* 1987, Lu *et al* 1994), potassium (Williamson III *et al* 1995, Santos *et al* 1995, Wang *et al* 1996, Behr *et al* 1997, Catoliotti *et al* 1998, Prevedelli *et al* 1999), rubidium (Fox *et al* 1993, Gwinner *et al* 1994), caesium (Monroe *et al* 1990, Sagna *et al* 1995, Dudle *et al* 1996, Jun *et al* 1999a, b) and francium (Simsarian *et al* 1996, Lu *et al* 1997, Grossman *et al* 1999); atom isotopes of alkali earth metals, such as calcium and strontium (Kurosu and Shimizu 1990) and atom isotopes of inert gases, such as helium (Bardou *et al* 1992, Kumakura *et al* 1992, Rooijackers *et al* 1997), neon (Shimizu *et al* 1989), argon and krypton (Katori and Shimizu 1990), and xenon (Walhout *et al* 1993). Recently, the MOT was loaded with chromium atoms (Bell *et al* 1999) and a magneto-optical trapping of Yb atoms was successively carried out using both the singlet  $^1S_0 - ^1P_1$  transition (Honda *et al* 1999) and the intercombination  $^1S_0 - ^3P_1$  transition (Kuwamoto *et al* 1999).

In typical MOTs, the temperature of the atomic cloud ranges between 1 mK and 10  $\mu$ K, and the density of atoms, between  $10^8$  and  $10^{11}$   $\text{cm}^{-3}$ . Attaining high atomic densities in MOTs is mainly limited by collisions between the trapped atoms and residual gas particles, the trapping of radiation, collisions between atoms in the lower states with the optically excited atoms, and the above-barrier momentum diffusion-associated escape of atoms from the trapping region (Sesko *et al* 1989, Townsend *et al* 1992, Metcalf and van der Straten 1994, Anderson *et al* 1994, Willems *et al* 1997).

A material increase in the atomic density has been attained in what is known as the dark MOT wherein the localized atoms are optically pumped to a hyperfine-structure sublevel at which they are off resonance with the main localizing laser field. This method was successfully used to localize sodium atoms (Ketterle *et al* 1993). They demonstrated a substantial improvement of the trap parameters in comparison with the standard MOT: the atomic density amounted to  $10^{12}$   $\text{atoms cm}^{-3}$  at a large total number of localized atoms (over  $10^{10}$ ). The application of the dark MOT technique to other elements comes up against considerable problems (Townsend *et al* 1996). As a rule, an increase in the density of atoms is achieved at the cost of their increased temperature.

Balykin (1997) suggested a method to increase the density of atoms in the MOT, based on the irradiation of the atomic cloud with a pulsed laser radiation. The method is essentially as follows. At a certain instant of time, the laser field localizing the atoms is switched off, and the atoms freely fly away from the centre of the trap during a time long enough for their density to decrease. Thereafter the atoms are irradiated with a short pulse of the laser light used initially to form the trap. If the atom–laser pulse interaction time is commensurable with the inverse of the decay coefficient of the atoms in the trap, the velocity of the atoms is reversed and damped to a value governed only by the magnitude of the magnetic field and the atomic coordinate at the instant the laser pulse is switched on. The time it takes for the atom to return to the centre of the trap is the same for all the atoms, and this leads to a substantial ( $\sim 10^2$ ) increase of the density. Arlt *et al* (1998) suggested the use of the pyramidal MOT with a small hole at its vertex as a source of slow atoms. Atoms are first captured in the trap and then pushed through the hole by a laser beam. The flux of cold atoms was about  $10^9$   $\text{s}^{-1}$  and found to be readily scalable to obtain higher fluxes. Note also the proposal on a booster for ultrafast loading of the trap (Vredenberg *et al* 1998).

## 7. Gravito-optical traps and cavities

In recent years, another effective method of trapping cold atoms has been developed: the gravito-optical method based on a combined use of electromagnetic and gravitational forces. The key element in this method is the atom mirror (Cook and Hill 1982), which was experimentally implemented for a beam of sodium atoms (Balykin *et al* 1987, 1988a, Kasevich *et al* 1990), caesium atoms (Aminoff *et al* 1993), and a variety of other atoms (Dowling and Gea-Banacloche 1996).

Conceptually, the simplest gravito-optical atom trap cavity can consist of a single concave atomic mirror arranged horizontally (figure 45). In this geometry, the role of the second mirror is played by the gravitational field (Liston *et al* 1995a, b, Wallis *et al* 1992, Wallis 1997). A cavity of this geometry is the simplest version of the two-mirror vertical cavity proposed by Balykin and Letokhov (1989). In this cavity, the curvature of the mirror is small, and the vertical atomic motion spectrum at not very small quantum numbers (quasiclassical approximation) is determined by the well known quantum mechanical problem of the bouncing of a particle on an absolutely elastic plane in the gravity field (see, for example, Flugge (1971)). The

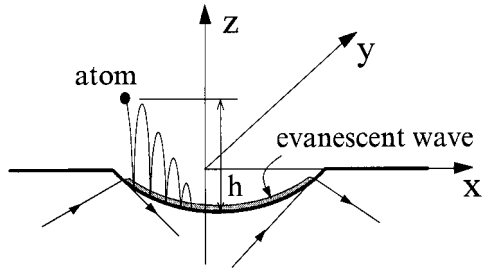


**Figure 45.** Gravito-optical atom trap cavity based on a single concave atom mirror arranged horizontally.

corresponding spectrum is defined by the eigenvalues of the Airy functions:

$$\varepsilon_n = Mgl_g \left[ \frac{3\pi}{2} \left( n - \frac{1}{4} \right) \right]^{2/3}, \quad (7.1)$$

where  $l_g = (\hbar^2/2gM^2)^{1/3}$  is the characteristic gravitational length governed by the mass of the particle. For atoms of medium mass, the characteristic gravitational length is of the order of a micron, and the characteristic values of energy (7.1) correspond to the effective temperatures of the order of 10 nK.

In this cavity, the transverse (horizontal) size of the atomic mode can be expressed in terms of the distance  $L$  from the surface of the mirror to the classical turning point, which determines the length of the cavity. For estimation purposes, the gradient force potential can be taken to be stepped near the surface of the mirror. The surface shape of the mirror in the simplest approximation can be treated as a paraboloid of revolution,

$$z = \frac{x^2 + y^2}{2R}, \quad (7.2)$$

where  $R$  is the radius of curvature of the mirror at its centre.

Assuming that the atom mirror has a parabolic shape, the transverse size of the atomic mode in the vicinity of the mirror is estimated as

$$\delta x_M \cong \left( \frac{2l_g^3 R^2}{R - 2L} \right)^{1/4}, \quad (7.3)$$

and at the upper point of the classical trajectory at a distance  $L$  from the mirror as

$$\delta x_S \cong (2l^3(R - 2L))^{1/4}. \quad (7.4)$$

The distance to the upper point of the classical trajectory is determined by the atomic velocity in the neighbourhood of the mirror,  $L = v^2/2g$ , and can be associated with the energy of longitudinal motion given by (7.1). With the typical gravitational length being, as indicated above, of the order of a micron, the size of the atom mode comes to a few tens of microns.

The gravito-optical trapping scheme was experimentally investigated for caesium atoms (Aminoff *et al* 1993). The atoms were preliminarily localized and cooled in a MOT. When the MOT was switched off, the atoms fell freely onto the atom mirror from a height of 3 mm. The atoms were observed to execute about ten bounces. In each reflection event, around 40% of the atoms were lost as a result of (a) photon scattering during the reflection, (b) background gas collisions and (c) residual misalignment of the mirror with respect to the vertical axis.

Note that the intensity of the evanescent wave in the atomic mirror can be increased by two or three orders of magnitude on account of the excitation of the surface plasmons produced by introducing a thin metal layer in the dielectric–vacuum interface (Esslinger *et al*

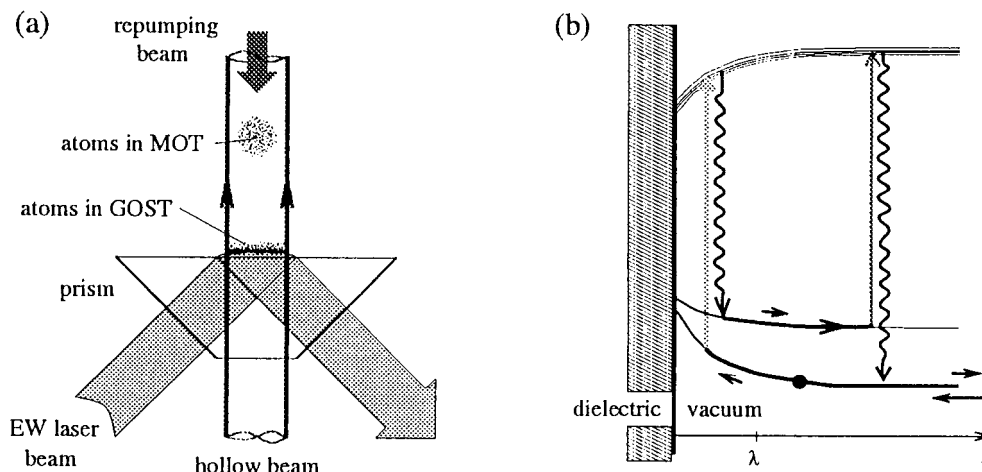


**Figure 46.** (a) Scheme of a gravito-optical trap based on the inelastic reflection of atoms from an evanescent laser wave. (b) The atom transitions between hyperfine-structure states responsible for cooling atoms in the trap (Ovchinnikov *et al* 1995, Soding *et al* 1995).

1993, Feron *et al* 1993, Seifert *et al* 1994). Another method to intensify the evanescent wave is to introduce a dielectric film of high refractive index, which produces a dielectric optical fibre for laser radiation. The repeated reflection of the laser light from the dielectric–vacuum and dielectric–dielectric interfaces substantially increases the intensity of the evanescent wave (Kaiser *et al* 1994).

The reflecting surface formed by the evanescent wave is a very rich structural component for creating atomic traps and waveguides of varying geometry (figure 48). In the past few years, such light surfaces have formed the basis for several types of half-open traps and waveguides. Further development of the simplest gravito-optical trapping scheme resulted in the vertically arranged pyramidal and conical traps (Dowling and Gea-Banacloche 1995, 1996, Ovchinnikov *et al* 1995) and also atom gravitational cavities based on hollow optical fibres (Harris and Savage 1995).

Figure 46(a) presents a schematic diagram of a gravito-optical trap where atoms are cooled as a result of their inelastic reflection from an evanescent wave (Ovchinnikov *et al* 1995, Soding *et al* 1995). With this scheme, Cs atoms were trapped in a horizontal plane by the gradient force produced by a hollow blue-detuned laser beam (Ovchinnikov *et al* 1997). The trap implemented for caesium atoms embedded a cooling mechanism associated with the optical pumping of the atoms between the hyperfine-structure states (figure 46(b)). An inelastic reflection takes place when the atom enters the evanescent wave in a lower ground state and, by scattering a photon during the reflection process, it is pumped into the less repulsive state. The dot in figure 46(b) shows a Cs atom that approaches the dielectric surface at the lower hf state, then scatters a photon, leaves the evanescent wave at the upper ground state, and is finally pumped back into the lower state. The experimental dependence of the temperature of the trapped atoms as a function of the time storage is shown in figure 47. Open circles describe the vertical temperature of atoms in the trap and closed circles, the horizontal temperature. The solid lines are the theoretical fits. As is seen from figure 47, the vertical temperature follows an exponential decay caused by the cooling mechanism. The horizontal motion is not cooled directly: its temperature decreases due to the motional coupling of the horizontal and vertical degrees of freedom of the atom.

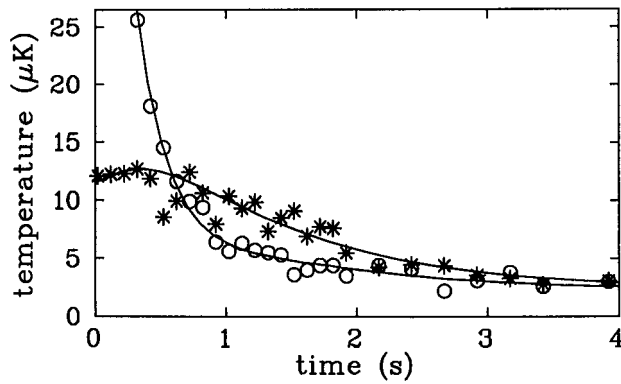


**Figure 47.** Temperature of Cs atoms localized in the gravito-optical trap based on an inelastic reflection as a function of the trapping time (Ovchinnikov *et al* 1997).

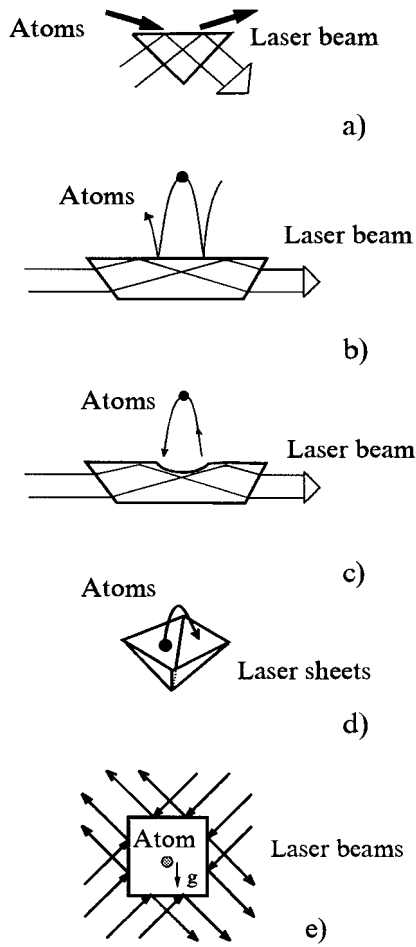


**Figure 48.** Schemes of dipole traps based on evanescent waves: (a), (b) traps based on atom mirrors; (c) gravito-optical trap based on a single concave mirror; (d) gravito-optical trap with laser sheets as atom reflectors; (e) box-type trap with evanescent side waves.

The use of light surfaces formed by evanescent waves makes it in principle possible to create atom traps as well (figure 48). One possible version is the enclosed trap in the form

of a cube having all its sides coated with evanescent waves (figure 48(e)) (Cook and Hill 1982, Dowling and Gea-Banacloche 1995, 1996). Yin and Zhu (1998) proposed a novel gravito-optical trap composed of a blue-detuned plug beam and blue-detuned dark hollow beam generated from the output beam of a LP<sub>01</sub> mode in a micrometre-sized hollow fibre.

## 8. Applications

The methods developed during the past decades for the electromagnetic trapping of neutral atoms are of interest in applications in many domains of physics. Among them one may note briefly the following.

### 8.1. Laser trapping spectroscopy

The idea of Doppler-free ultrasensitive laser spectroscopy was first discussed in 1975 (Letokhov 1975). At that time the method seemed a distant goal. Nowadays, the method is commonly employed in many spectroscopic experiments. Two impressive applications are listed below.

First, one may note the use of cold trapped atoms in ultrahigh-resolution spectroscopy. A striking example is the observation of a two-photon transition  $1S \rightarrow 2S$  in cold hydrogen atoms localized in a magnetic trap (Cesar *et al* 1996). Two-photon Doppler-free spectroscopy of trapped atoms was reported by Cesar *et al* (1999). A cold trapped atomic sample may provide a unique source for improved measurements of the fine-structure constant (Zhao *et al* 1989).

Second, we should mention the first experiments with rare atoms. Rowe *et al* (1999), have measured the ground-state hyperfine structure of the laser-trapped radioactive  $^{21}\text{Na}$  ( $t_{1/2} = 22$  s) collected in a MOT on-line at the cyclotron at Lawrence Berkeley National Laboratory. Lu *et al* (1997) realized efficient collection of  $^{221}\text{Fr}$  ( $t_{1/2} = 4.9$  min) in a vapour cell MOT. They measured energies and the hyperfine structure of the  $7^2P_{3/2}$  and  $7^2P_{1/2}$  states with 900 trapped atoms with a signal-to-noise ratio of about 60 in 1 s. These experiments show the good prospects for the laser trapping spectroscopy of very rare atomic samples.

### 8.2. Bose–Einstein condensation

The most impressive application of the methods for cooling and trapping neutral atoms is the observation of BEC in dilute atomic samples (Anderson *et al* 1985, Bradley *et al* 1995, Davis *et al* 1995). The first attempts to observe a BEC of atomic hydrogen started 20 years ago (Silvera and Walraven 1980, Greytak and Kleppner 1984). However, only after the development of laser cooling techniques, MOTs and the evaporative cooling technique has it become possible to produce cold dense atomic samples satisfying the BEC condition (1.6) for the critical phase density for Rb atoms (Anderson *et al* 1995), Li atoms (Bradley *et al* 1995), and Na atoms (Davis *et al* 1995). Recently, the critical phase density has been achieved for atomic hydrogen (Fried *et al* 1998). Nowadays, the study of BEC in atomic samples is one of the fastest-developing areas in atomic physics. The latest experimental and theoretical progress in the field can be found in recent reviews (Dolforo *et al* 1998, Burnett 1996, Parkins and Walls 1997).

### 8.3. Atom laser

The progress of BEC research has recently resulted in the development of an atom laser, i.e. a device which emits a coherent atomic beam. In a BEC a macroscopic number of bosonic atoms occupy the ground state of the system, which can be described by a single wavefunction.

A pulsed output coupler which coherently extracts atoms from a condensate was demonstrated by Mewes *et al* (1997) and Andrews *et al* (1997). Producing BEC in a novel magnetic trap (Esslinger *et al* 1998) T Hänsch and co-workers realized an atom laser with a CW output coupler (Bloch *et al* 1999). Obviously, this very promising application of atom trapping is likely to see speedy development in the near future.

#### 8.4. Intense atomic beams

Cold atoms localized in the electromagnetic traps can be used as sources of slow incoherent atomic beams with high phase density. Lu *et al* (1996) used the MOT to produce a slow CW atomic beam with intensity  $5 \times 10^9$  atoms  $s^{-1}$  and brightness  $5 \times 10^{12}$  atoms  $sr s^{-1}$ . Atomic beams with much higher brightness can be obtained under the pulse extraction of atoms from the MOT. Fukuyama *et al* (2000) have used the pulse release of atoms from the MOT to produce an atomic beam with brightness  $1.1 \times 10^{15}$  atoms  $sr s^{-1}$ . The incoherent but very intense atomic beams may have various important applications in atomic spectroscopy and atomic physics.

#### 8.5. Nuclear physics

Cold and trapped radioactive atoms open new experimental opportunities in nuclear physics. Trapped radioactive atoms can be used in the fundamental symmetry experiments, including the experiments on nuclear  $\beta$ -decay, atomic parity nonconservation, and the search for parity and time-reversal violating electric dipole moments. The first successful experiments on the trapping of radioactive atoms were realized for isotopes  $^{21}\text{Na}$  (Lu *et al* 1994),  $^{79}\text{Rb}$  (Gwinner *et al* 1994),  $^{210}\text{Fr}$  (Simsarian *et al* 1996),  $^{38m}\text{K}$ ,  $^{37}\text{K}$  (Behr *et al* 1997),  $^{221}\text{Fr}$  (Lu *et al* 1997). It is expected that further activity in this direction will be concentrated on efforts to undertake meaningful measurements with trapped radioactive species.

Recently, experiments on nuclear decay have started to use the MOT as a source of cold well localized atoms. The low-energy recoiling nuclei can freely escape the MOT and be detected in coincidence with  $\beta$ -decays to reconstruct the information on the properties of the particles coming from the nuclear reactions. An example of such an experiment is the beta-neutrino correlation measurement on laser trapped  $^{38m}\text{K}$  and  $^{37}\text{K}$  (Behr *et al* 1999). In the experiment ions  $^{38m}\text{K}$  and  $^{37}\text{K}$  produced at the on-line isotope separators TISOL and ISAC at TRIUMF (Canada) were converted to neutral potassium atoms by stopping in a Zn foil. Next, the rethermalized low-energy atoms were captured by the first MOT and finally transferred by a laser push beam and magneto-optical funnels into the second MOT free of a large number of the non-localized atoms. The overall capture efficiency into the second MOT was  $7 \times 10^{-4}$ . The experiment has detected several hundred thousand recoil- $\beta^+$  coincidences, sufficient for further use with a goal to test the standard model.

Many new nuclear experiments are now in progress which explore the MOT as a convenient target for the measurements. Typically, the mass-separated ion beam is first converted to neutral atomic beam and after that the neutral atoms are captured initially by the first MOT and finally transferred to the second MOT used as a target. This principal scheme developed by the Los Alamos National Laboratory was used for trapping radioactive isotopes  $^{82}\text{Rb}$  (Gückert *et al* 1998) and  $^{82-84}\text{Rb}$ ,  $^{135,137}\text{Cs}$  (Vierra *et al* 1999). It is expected that the target MOT can be used for the following measurements: (1) the high-precision parity violation measurement of beta-decay asymmetry on polarized  $^{82}\text{Rb}$ ; (2) measurements of the properties of ultracold  $^{84}\text{Rb}$  fermionic atoms sympathetically cooled by  $^{87}\text{Rb}$  atoms in the state of the BEC; (3) ultrasensitive measurements with the use of trapped atoms.

Electromagnetic trapping of atoms is also considered to be the most likely scheme for the production of atomic antihydrogen and its spectroscopic investigation. The crucial point here is the laser cooling of the hydrogen atoms. The only possible optical transition for the effective laser cooling of hydrogen is the 1S–2P transition with the vacuum ultraviolet wavelength 121.6 nm. Pahl *et al* (1999) reported on the development of the first CW source of coherent Lyman- $\alpha$  radiation. The source is based on four-wave mixing in mercury vapour. Ultrahigh-resolution laser spectroscopy of a few trapped antihydrogen atoms opens a unique opportunity to compare the spectra of hydrogen and antihydrogen and thus realize a stringent test of the fundamental CPT symmetry (Bluhm *et al* 1999), and to compare the gravitational forces on matter and antimatter.

Particularly suitable for the spectroscopic investigation of trapped atomic antihydrogen is the use of resonance-enhanced two-photon spectroscopy (RETS) (Hijmans, 1999). This technique is based on the stimulated absorption of photons at two different wavelengths, one nearly resonant with the 1S–2P transition, the other with the 2P–3S(D) transition. The sensitivity of RETS is much higher than the two-photon spectroscopy method that uses resonant two-photon excitation at the 1S–2P transition. RETS had previously been tested for temperature and density measurements in atomic hydrogen localized in a magnetic trap (Mosk *et al* 1998).

#### 8.6. Ultrasensitive isotope trace analysis

An important property of the MOT consists in the ability to catch the atoms whose optical frequencies are shifted from the laser frequency by only a few natural linewidths. This property has been applied for ultrasensitive isotope trace analysis. Chen *et al* (1999) developed the technique for the detection of a counted number of radioactive isotopes  $^{85}\text{Kr}$  and  $^{81}\text{Kr}$  with abundances  $10^{-11}$  and  $10^{-13}$  against the stable isotope  $^{83}\text{Kr}$ . The technique was called atom trap trace analysis (ATTA). At present, only the technique of the accelerator mass spectrometry (AMS) (Collon *et al* 1997) has a detection sensitivity comparable with that of ATTA. Unlike the AMS technique based on the high-power cyclotron, the ATTA technique is much simpler and does not require a special operation environment. In the experiments by Chen *et al* (1999) krypton gas was injected into a DC discharge volume where the atoms were excited to the metastable level. 2D transverse laser cooling was used to collimate the atomic beam and the Zeeman slowing technique was used to load the atoms in the MOT. Under the specific laser frequency chosen for trapping  $^{81}\text{Kr}$  or  $^{85}\text{Kr}$  isotopes, only the chosen isotope could be trapped by the MOT. The experiment was able to detect a single trapped isotope which remained in the MOT for about a second. Figure 49 shows the fluorescence produced by an individual  $^{81}\text{Kr}$  isotope stored in the MOT in the experiment. Note that the fluorescence signal coming from a single isotope atom considerably exceeds the noise due to the scattered laser light.

#### 8.7. Ultracold atom collisions

The trapping of ultracold atoms gives an opportunity to study the collisional processes in cold atomic samples. Süptitz *et al* (1994) reported on the simultaneous cooling and trapping of two different Rb isotopes and measurement of a cross-isotope collisional rate. A similar experiment was done by Santos *et al* (1995) with two different atomic species, Na and K. This experiment gave an estimation on the elastic collisions cross section of the Na–K system as  $3.8 \times 10^{-13} \text{ cm}^2$ . Houbiers *et al* (1998) studied the elastic and inelastic collisions of  $^6\text{Li}$  atoms in magnetic and optical traps. This research was important for estimation of the possibility to achieve quantum degeneracy in a fermionic gas. In the case of fermionic  $^6\text{Li}$ , it has been shown

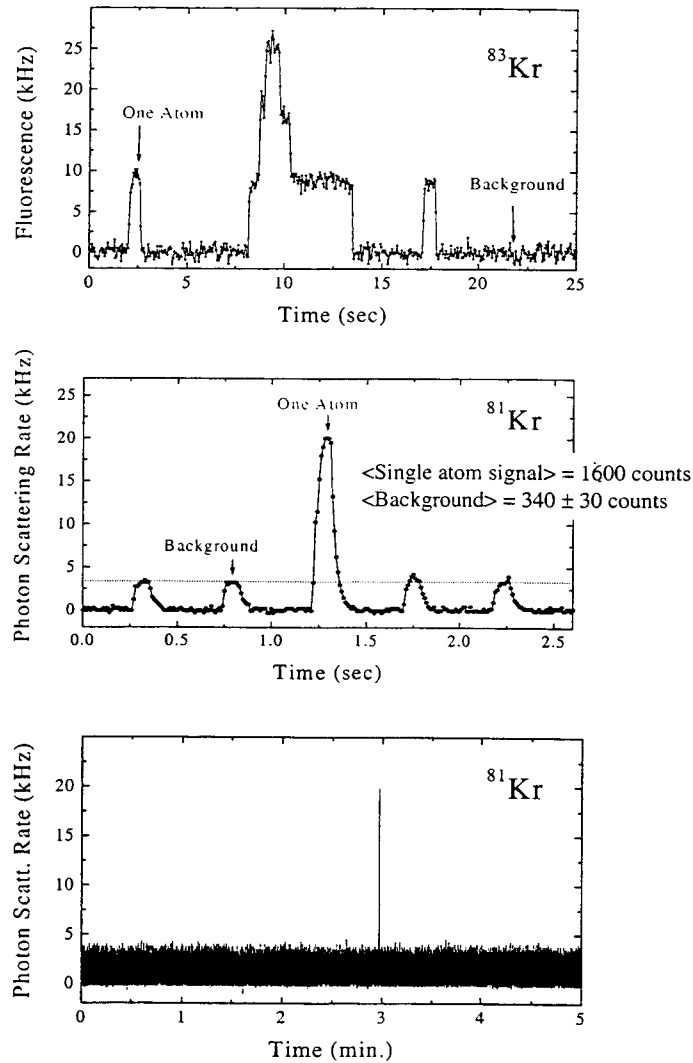


**Figure 49.** Fluorescent single-atom detection of the rare long-lived radioactive isotope  $^{81}\text{Kr}$  using the MOT (Chen *et al* 1999).

theoretically that a transition to a superfluid state could be realized at a critical temperature of the order of temperatures obtained in BEC experiments (Stoof *et al* 1996, Houbiers *et al* 1997): see also the theoretical study of interacting Fermi gas in a harmonic trap (Bruun and Burnett 1998).

Anderson *et al* (1998) studied the resonant dipole–dipole energy transfer in nearly frozen Rb Rydberg gas in a MOT. In a room temperature vapour of Rb Rydberg atoms, resonant dipole–dipole energy transfer occurs via binary collisions. In contrast, in the  $300\ \mu\text{K}$  vapour in the MOT many atoms interact simultaneously, as in an amorphous solid. As a result of simultaneous multiple atom interactions, the energy transfer resonances are broadened substantially in frequency. In the laser-induced collisions between ultracold atoms, the combination of low velocities and long-range interactions results in collision times which

can exceed the excited-state lifetime. Using pulsed excitation, Gensemer and Gould (1998) found this collisional process for Rb to take place on a  $10^{-6}$  s timescale.

Many collisional processes have been investigated on cold atoms localized in a MOT. Among numerous important experiments one may note the following: observation of a Feshbach resonance in cold atom (Rb) scattering (Courtelle *et al* 1998); study of Penning and associative ionization of two metastable cold (1 mK) helium atoms (Mastwijk *et al* 1998); study of elastic and inelastic collisions of cold spin-polarized  $^{133}\text{Cs}$  atoms (Arndt *et al* 1997, Söding *et al* 1998, Leo *et al* 1998); observation of cold collision frequency shift of 1S–2S transition in hydrogen (Kilian *et al* 1998); measurement of long-range forces between cold Cs atoms (Fioretti *et al* 1999); measurements of ionizing collisional rate of metastable rare-gas atoms (Kr, Ar) in an optical lattice (Kunugita *et al* 1997). By confining  $^3\text{He}$  and  $^4\text{He}$  in their respective MOTs, ionization rate coefficients for Penning collisions between the cold He ( $2s^3S_1$ ) atoms have been measured (Kumakura *et al* 1999). At a temperature of 0.5 mK, the rate coefficients obtained are  $3.8 \times 10^{-10} \text{ cm}^3 \text{ s}^{-1}$  for  $^4\text{He}$ – $^4\text{He}$  collisions and  $1.1 \times 10^{-9} \text{ cm}^3 \text{ s}^{-1}$  for  $^3\text{He}$ – $^3\text{He}$ , a difference of a factor of 3. Similar results were reported by Tol *et al* (1999) who achieved the large number ( $1.5 \times 10^9$ ) of cold metastable helium atoms in a MOT. Measurements of the collisional rates in a Na/Rb mixture in a MOT were done by Telles *et al* (1999).

Finally, note the collisional experiments with different atoms captured in a MOT. Shaffer *et al* (1999a, b) described a comprehensive investigation of a trap loss in a two-species Na–Cs MOT. Observed losses, due to the interspecies interactions, are attributed to collisions in which a change in the fine-structure state of the Na partner causes the escape of atoms from the trap. Results are described in terms of the heteronuclear pair potentials and the interaction of the colliding pairs with the radiatively active environment.

### 8.8. Formation of cold molecules

The application of well established laser cooling techniques to molecules does not seem to be possible because of the absence the cyclic interaction schemes which could keep molecules from being optically pumped into inaccessible states. The most successful technique to produce translationally cold molecules is the combination of the techniques of trapping atoms with the photoassociation technique (Thorsheim 1987). Photoassociation of cold atoms can be realized by both a single-colour excitation (figure 50) (Nikolov *et al* 1999) and two-colour excitation (figure 51) (Band and Julienne 1995).

The first experiment on the formation of cold molecules ( $\text{Cs}_2$ ) by the technique of photoassociation of cold Cs atoms in a MOT was done by Fioretti *et al* (1998). A pair of ground state cold Cs atoms is resonantly excited to a  $O_g^-$  rovibrational state of  $\text{Cs}_2$  using a CW laser. A significant fraction of these molecules decay to bound levels of the  $^3\Sigma_n^+$  ground state, yielding long-lived translationally cold molecules. The latter are detected by pulsed laser ionization into  $\text{Cs}_2^+$  ions, thorough a time-of-flight mass selection. Takekoshi *et al* (1998) realized the first observation of optically trapped cold neutral molecules  $\text{Cs}_2$ . Caesium dimers in the electronic ground state were produced directly in a MOT and transferred to a dipole trap formed at the focus of a  $\text{CO}_2$  laser beam. A cold molecule's trap lifetime was on the order of one-half a second. Takekoshi *et al* (1999) also observed translationally cold dimers  $\text{Cs}_2$  produced directly in a MOT and the photoassociation of cold Cs atoms in the trap. The measured translational temperature of the neutral caesium dimers was about  $100 \mu\text{K}$ .

In another pioneering work (Nikolov *et al* 1999) ultracold potassium molecules were produced in the  $X^1\Sigma_g^+$  electronic ground state by photoassociation in a MOT. The authors observed deeply bound molecules with vibrational quantum numbers about  $v \approx 36$  and translational temperature of about  $300 \mu\text{K}$ . About  $10^3$  molecules  $\text{s}^{-1}$  were produced, and much

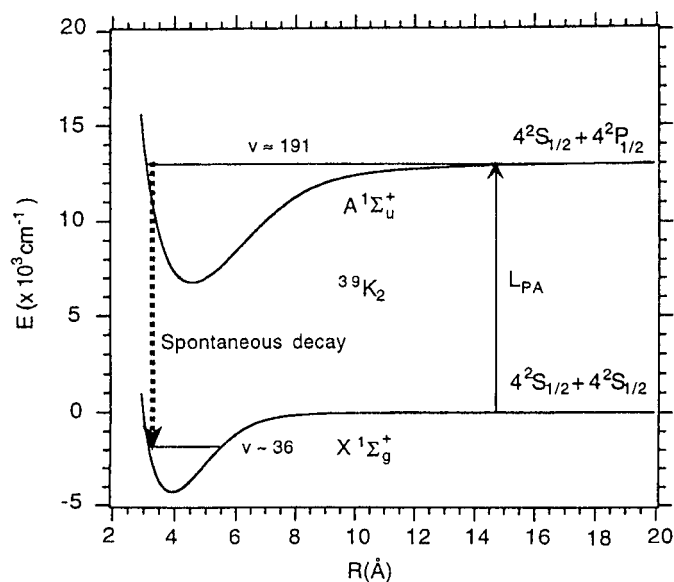


**Figure 50.** Single-photon photoassociation of cold  $^{39}\text{K}$  atoms to the  $v = 191$  level of the  $A\Sigma_v^+$  state  $^{39}\text{K}_2$  yields the formation of translationally cold  $^{39}\text{K}_2$  molecules in vibrationally excited levels (e.g.,  $v = 36$ ) of the  $X^1\Sigma_g^+$  ground electronic state (Nikolov *et al* 1999).

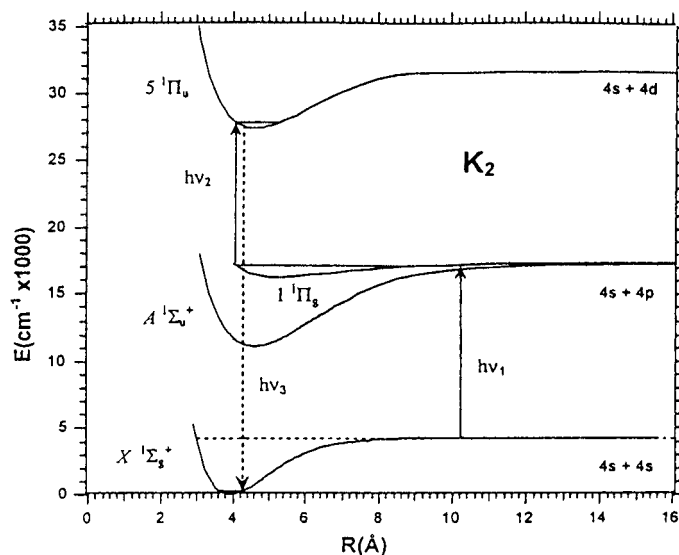


**Figure 51.** Scheme for the formation of translationally ultracold molecules by two-colour excitation of  $^{39}\text{K}_2$  (Band and Julienne 1995).

higher production rates should be attainable in the future. Ultracold heteronuclear molecules NaCs were produced by Shaffer *et al* (1999) in a novel two-species MOT. Individual trap atom densities were about  $10^{10} \text{ cm}^{-3}$  with around  $10^6$  Na atoms and  $10^7$  Cs atoms. The formation of ultracold heteronuclear molecules opens up new and exciting avenues of research in molecular spectroscopy.

### 8.9. Cavity QED, single atoms etc

New and interesting applications of the MOT were recently demonstrated by Kimble and co-workers. His group realized the trapping of single cold atoms in a cavity (Ye *et al* 1999). This opened an opportunity for the deterministic control of atom–photon interactions quantum by quantum. Cavity QED has led to many new effects, including the realization of a quantum phase gate (Turchette *et al* 1995), the creation of Fock states of the radiation field (Walther *et al* 1999) and the demonstration of quantum nondemolition detection for single photons (Nogues *et al* 1999) etc. Ye *et al* (1999) note that ‘all serious schemes for quantum computation and communication via cavity QED rely on developing techniques for atom *confinement*’. This explains the importance of the experiments on trapping of single atoms under conditions of cavity QED. Kimble’s group used in the experiments the FORT, providing a confining potential to trap atoms within the cavity mode.

Among other interesting applications of the MOT one may note the quantum nondemolition (QND) measurements with the use of cold trapped Rb atoms (Roch *et al* 1997, Sinatra *et al* 1998) and observation of the superfluorescence from optically trapped Ca atoms (Kumarakrishnan and Han 1998).

Atom interferometers built around atomic waveguides and quantum mechanical atomic gravitational cavities seem very promising for high-precision measurements (Harris and Savage 1995). The Saniac effect for atoms is larger than for photons (Scully and Dowling 1993). Atom interferometers have already demonstrated the potential for precision measurement of gravity and inertial effects (Adams *et al* 1994).

An interesting technological application of optical lattices can be the deposition of atomic structures with a resolution better than the optical wavelength. In one such experimental attempt, sodium atoms, after being channelled in periodic potential wells, were deposited on a surface, forming lines a few tens of nanometres wide (Timp *et al* 1992, Gupta *et al* 1996, Drodofsky *et al* 1997). In another example of nanolithography using optical lattices, chromium atoms were deposited on the surface of 1D and 2D gratings (McClelland *et al* 1993).

The list of applications of the methods of electromagnetic trapping of cold atoms and molecules will certainly grow fast and expand into different fields of science. As one remarkable example one may note the measurements of Earth’s gravity gradient (Snadden *et al* 1998) and gravitational acceleration by dropping cold atoms from the trap (Peters *et al* 1999). In the coming years we should see many productive ‘marriages’ of trapping techniques with many advanced fields of science and technology.

### Acknowledgment

This work was supported in part by the Russian Foundation for Basic Research (Grant No 99-02-16215).

### References

- Adams C S, Carnal O and Mlynek J 1994 *Adv. Atom. Mol. Opt. Phys.* **34** 1
- Adams C S, Lee H J, Davidson N, Kasevich M and Chu S 1995 *Phys. Rev. Lett.* **74** 3577
- Adams C S and Riis E 1997 *Prog. Quantum Electron.* **21** 1
- Al-Awfi S and Babiker M 1998 *Phys. Rev. A* **58** 4768
- Aminoff C G, Steane A M, Bouyer P, Desbiolles P, Dalibard J and Cohen-Tannoudji C 1993 *Phys. Rev. Lett.* **71** 3083
- Anderson B P and Kasevich M A 1998 *Science* **282** 1886
- Anderson M H, Ensher J R, Matthews M R, Wieman C E and Cornell E A 1995 *Science* **269** 198
- Anderson M H, Petrich W, Ensher J R and Cornell E A 1994 *Phys. Rev. A* **50** R3597

- Anderson W R, Veale J R and Gallagher T F 1998 *Phys. Rev. Lett.* **80** 249
- Andreev S V, Balykin V I, Letokhov V S and Minogin V G 1981 *Pis. Zh. Eksp. Teor. Fiz.* **34** 463 (Engl. Transl. 1981 *JETP Lett* **34** 442)
- 1982 *Pis. Zh. Eksp. Teor. Fiz.* **82** 1429 (Engl. transl. 1982 *Sov. Phys.–JETP* **55** 828)
- Andrews M R, Townsend C G, Miesner H-J, Durfee D S, Kurn D M and Ketterle W 1997 *Science* **275** 637
- Arimondo E 1996 *Progress in Optics* vol 35, ed E Wolf (Amsterdam: Elsevier) p 257
- Arlt J J, Marago O, Webster S, Hopkins S and Foot C J 1998 *Opt. Commun.* **157** 303
- Arndt M, Ben Dahan M, Guery-Odelin D, Reynolds M W and Dalibard J 1997 *Phys. Rev. Lett.* **79** 625
- Artsimovich L A 1964 *Controlled Thermonuclear Reactions* (New York: Gordon and Breach)
- Ashkin A 1970 *Phys. Rev. Lett.* **24** 156
- 1978 *Phys. Rev. Lett.* **40** 729
- 1980 *Science* **210** 1081
- 1988 *Laser in Life Sciences* Berichte der Bunsen-Gesellschaft für Physikalische Chemie Band 93 N3 pp 255–60
- Ashkin A and Gordon J P 1983 *Opt. Lett.* **8** 511
- Askarian G A 1962 *Zh. Eksp. Teor. Fiz.* **42** 1567
- Aspect A, Arimondo E, Kaiser R, Vansteenkiste N and Cohen-Tannoudji C 1988 *Phys. Rev. Lett.* **61** 826
- Aspect A, Dalibard J, Heidmann A, Salomon C and Cohen-Tannoudji C 1986 *Phys. Rev. Lett.* **57** 1688
- Balykin V I 1997 *JETP Lett.* **66** 349
- 1999 *Adv. At. Mol. Opt. Phys.* **41** 181
- Balykin V I, Laryushin D V, Subbotin M V and Letokhov V S 1996 *JETP Lett.* **63** 808
- Balykin V I and Letokhov V S 1987 *Opt. Commun.* **64** 151
- 1989 *Appl. Phys. B* **48** 517
- Balykin V I, Letokhov V S and Minogin V G 1985a *Usp. Fiz. Nauk* **147** 117 (Engl. transl. 1985a *Sov. Phys.–Usp* **28** 803)
- Balykin V I, Letokhov V S, Minogin V G, Rozhdestvensky Yu V and Sidorov A I 1985b *J. Opt. Soc. Am. B* **2** 1776
- Balykin V I, Letokhov V S, Minogin V G and Zueva T V 1984a *Appl. Phys. B* **35** 149
- Balykin V I, Letokhov V S and Mishin V I 1979 *Pis. Zh. Eksp. Teor. Fiz.* **29** 614 (Engl. transl. 1979 *JETP Lett.* **29** 560)
- 1980 *Zh. Eksp. Teor. Fiz.* **78** 1376 (Engl. transl. *Sov. Phys.–JETP* **51** 692)
- Balykin V I, Letokhov V S, Ovchinnikov Yu B and Sidorov A I 1987 *Pis. Zh. Eksp. Teor. Fiz.* **45** 282 (Engl. transl. 1987 *JETP Lett.* **45** 353)
- 1988a *Phys. Rev. Lett.* **60** 2137
- Balykin V I, Letokhov V S, Ovchinnikov Yu B, Sidorov A I and Shulga S V 1988b *Opt. Lett.* **13** 958
- Balykin V I, Letokhov V S and Sidorov A I 1984b *Zh. Eksp. Teor. Fiz.* **86** 2019 (Engl. transl. 1984b *Sov. Phys.–JETP* **59** 1174)
- 1984c *Pis. Zh. Eksp. Teor. Fiz.* **40** 251 (Engl. transl. 1984c *JETP Lett.* **40** 1026)
- Balykin V I, Lozovik Yu E, Ovchinnikov Yu B, Sidorov A I, Shulga S V and Letokhov V S 1989 *J. Opt. Soc. Am. B* **6** 2178
- Band Y B and Jullienne P S 1995 *Phys. Rev. A* **51** R4317
- Bardou F, Emile O, Courty J M, Westbrook C I and Aspect A 1992 *Europhys. Lett.* **20** 681
- Barger R L and Hall J L 1969 *Phys. Rev. Lett.* **22** 4
- Behr J A et al 1997 *Phys. Rev. Lett.* **79** 375
- 1999 *1st Euroconf. on Atomic Physics at Accelerators: Laser Spectroscopy and Applications (Mainz, 1999)*
- Beijersbergen M J, Allen L, vander Ween H E L O and Woerdman J P 1992 *Opt. Commun.* **96** 132
- Bell A S, Stuhler J, Locher S, Hensler, Mlynek J and Pfau T 1999 *Europhys. Lett.* **45** 156
- Bergeman T, Frez G and Metcalf H J 1987 *Phys. Rev. A* **35** 1535
- Bergeman T H, McNicholl P, Kycia J, Metcalf H and Balazs N L 1989 *J. Opt. Soc. Am. B* **6** 2249
- Birkel G, Gatzke M, Deutsch I H, Rolston S L and Phillips W D 1995 *Phys. Rev. Lett.* **75** 4583
- Bloch I, Hänsch T W and Esslinger T 1999 *Phys. Rev. Lett.* **82** 3008
- Bluhm R, Kostelecky V A and Russell N 1999 *Phys. Rev. Lett.* **82** 2254
- Boiron D, Michaud A, Fournier J M, Simard L, Sprenger M, Grynberg G and Salomon C 1998 *Phys. Rev. A* **57** R4106
- Botin A P, Kazantsev A P and Smirnov V S 1976 *Zh. Eksp. Teor. Fiz.* **71** 122
- Bradley C C, Sackett C A and Hulet R G 1997 *Phys. Rev. Lett.* **78** 985
- Bradley C C, Sackett C A, Tollett J J and Hulet R G 1995 *Phys. Rev. Lett.* **75** 687
- Brezger B, Shulze Th, Schmidt P O, Merteus R, Pfau T and Mlynek J 1999 *Europhys. Lett.* **46** 148
- Bruun G M and Burnett K 1998 *Phys. Rev. A* **58** 2477
- Burnett K 1996 *Contemp. Phys.* **37** 1
- Castin Y and Dalibard J 1991 *Europhys. Lett.* **14** 761

- Castin Y, Girac J I and Lewenstein M 1998 *Phys. Rev. Lett.* **80** 5305
- Cataliotti F S, Cornell E A, Fort C, Inguscio M, Marin F, Prevedelli M, Ricci L and Tino G M 1998 *Phys. Rev. A* **57** 1136
- Cesar C L, Fried D G, Killian T C, Polcyn A D, Sanberg J C, Yu I A, Greytak T J, Kleppner D and Doyle J M 1996 *Phys. Rev. Lett.* **77** 255
- Cesar C L and Kleppner D 1999 *Phys. Rev. A* **59** 4564
- Chang S, Garraway B M and Minogin V G 1990a *Opt. Commun.* **77** 19
- 1990b *J. Phys. Soc. Japan* **59** 3155
- Chang S, Kwon T Y, Lee H S and Minogin V G 1999a *Phys. Rev. A* **60** 2308
- 1999b *Phys. Rev. A* **60** 3148
- Chen C Y, Li Y M, Bailey K, O'Connor T P, Young L and Lu Z-T 1999 *Science* **286** 1139
- Chu S 1991 *Science* **253** 861
- 1997 *Rev. Mod. Phys.* **70** 685
- Chu S, Bjorkholm J E, Ashkin A and Cable A 1986 *Phys. Rev. Lett.* **57** 314
- Chu S, Hollberg L, Bjorkholm J E, Cable A and Ashkin A 1985 *Phys. Rev. Lett.* **55** 48
- Cohen-Tannoudji C 1997 *Rev. Mod. Phys.* **70** 707
- Cohen-Tannoudji C, Dupont-Roc J and Grynberg G 1992 *Atom-Photon Interactions* (New York: Wiley)
- Collon P *et al* 1997 *Nucl. Instrum. Methods B* **123** 122
- Cook R J 1980a *Phys. Rev. Lett.* **44** 976
- 1980b *Phys. Rev. A* **22** 1078
- Cook R J and Hill R K 1982 *Opt. Commun.* **43** 258
- Cooper C J, Hillenbrand G, Rink J, Townsend C G, Zetie K and Foot C J 1994 *Europhys. Lett.* **28** 397
- Cornell E A, Monroe C and Wieman C E 1991 *Phys. Rev. Lett.* **67** 2439
- Corwin K L, Kuppens S J M, Cho D and Wieman C E 1999 *Phys. Rev. Lett.* **83** 1311
- Courtelle Ph, Freeland P S, Heinzen D J, van Abeelen F A and Verhaar B J 1998 *Phys. Rev. Lett.* **81** 69
- Courtois J-Y, Grynberg G, Lounis B and Verkerk P 1994 *Phys. Rev. Lett.* **72** 3017
- Dalibard J 1987 Personal communication
- Dalibard J and Cohen-Tannoudji C 1989 *J. Opt. Soc. Am. B* **6** 2023
- Dalibard J, Reynaud S and Cohen-Tannoudji C 1983 *Opt. Commun.* **47** 395
- 1984 *J. Phys. B: At. Mol. Phys.* **17** 4577
- Davidson N, Lee H J, Kasevich M and Chu S 1994 *Phys. Rev. Lett.* **72** 3158
- Davidson N, Lee H J, Adams C S, Kasevich M and Chu S 1995 *Phys. Rev. Lett.* **74** 1311
- Davis K B, Mewes M-O, Andrews M R, van Druten N J, Durfee D S, Kurn D M and Ketterle W 1995 *Phys. Rev. Lett.* **75** 3969
- Dehmelt H G 1967 *Advances in Atomic and Molecular Physics* vol 3, ed D R Bates and I Esterman (Orlando: Academic) p 53
- 1969 *Advances in Atomic and Molecular Physics* vol 5, ed D R Bates and I Esterman (Orlando: Academic) p 109
- DePue M T, McCormick C, Winoto S L, Oliver S and Weiss D S 1999 *Phys. Rev. Lett.* **82** 2262
- Desbiolles P, Arndt M, Szrfigiser P and Dalibard J 1996a *Phys. Rev. A* **54** 4292
- Desbiolles P and Dalibard J 1996b *Opt. Commun.* **132** 540
- Deutschmann R, Ertmer W and Wallis H 1993 *Phys. Rev. A* **47** 2169
- Dicke R 1953 *Phys. Rev.* **82** 472
- Diedrich F, Bergquist J C, Itano W J and Wineland D J 1989 *Phys. Rev. Lett.* **62** 403
- Dolforo Fr, Giorgini S, Pitaevskii L P and Stringari S 1998 *Rev. Mod. Phys.*
- Dowling J P and Gea-Banacloche J 1995 *Phys. Rev. A* **52** 3997
- 1996 *Adv. At. Mol. Opt. Phys.* **37** 1
- Drewsen M, Laurent P, Nadir A, Santerelli G, Clairon A, Castin Y, Grison D and Salomon C 1994 *Appl. Phys. B* **59** 283
- Drndic M, Johnson K S, Thywissen J H, Prentiss M and Westervelt R M 1998 *Appl. Phys. Lett.* **72** 2906
- Drodofsky U, Stuhler J, Schulze Th, Drewsen M, Brezger B, Pfau T and Mlynek J 1997 *Appl. Phys. B* **65** 755
- Dudle G, Sagna N, Berthoud P and Thomann P 1996 *J. Phys. B: At. Mol. Opt. Phys.* **29** 4659
- Emile O, Bardou F, Salomon C, Laurent Ph, Nadir A and Clairon A 1992 *Europhys. Lett.* **20** 687
- Ertmer W, Blatt R, Hall J L and Zhu M 1985 *Phys. Rev. Lett.* **54** 996
- Esslinger T, Bloch I and Hänsch T W 1998 *Phys. Rev. A* **58** R2664
- Esslinger T, Weidemüller M, Hemmerich A and Hansch T W 1993 *Opt. Lett.* **18** 450
- Fam Le Kien and Balykin V I 1999 *JETP* **88** 246
- Feron S *et al* 1993 *Opt. Commun.* **102** 83
- Fioretti A, Comparat D, Crubillier A, Dulie O, Manson-Sceeuws F and Pillet P 1998a *Phys. Rev. Lett.* **80** 4402

- Fioretti A, Comparat D, Drag C, Gallagher T F and Pillet P 1999 *Phys. Rev. Lett.* **82** 1839
- Fioretti A, Molisch A F, Müller J H, Verkerk P and Allegrini M 1998b *Opt. Commun.* **149** 415
- Flugge S 1971 *Practical Quantum Mechanics* vol 1 (Berlin: Springer)
- Fortagh J, Grossmann A and Zimmermann C 1998 *Phys. Rev. Lett.* **81** 5310
- Fox R W, Gilbert S L, Hollberg L and Marquardt J H 1993 *Opt. Lett.* **18** 1456
- Frerichs V, Kaenders W and Meschede D 1992 *Appl. Phys. B* **55** 242
- Friebel S, D'Andrea C, Walz J, Weitz M and Hänsch T W 1998 *Phys. Rev. A* **57** R20
- Fried D G, Killian T C, Willmann L, Landhuis D, Moss S C, Kleppner D and Greytak T J 1998 *Phys. Rev. Lett.* **81** 3811
- Friedburg H and Paul W 1951 *Naturwiss.* **38** 159
- Fukuyama Y, Kanon H, Balykin V I and Shimizu K 2000 *Appl. Phys. B* at press
- Gaponov A V and Miller M A 1958 *Zh. Eksp. Teor. Fiz.* **34** 242
- 1958 *Zh. Eksp. Teor. Fiz.* **34** 751
- Gauck H, Hartl M, Sehneble D, Schnitzker, Pfau T and Mlynek J 1998 *Phys. Rev. Lett.* **81** 5298
- Gensemer S D and Gould P L 1998 *Phys. Rev. Lett.* **80** 936
- Glas P, Naumann M, Schirmacher A and Petrash Th 1999 *Opt. Commun.* **166** 71
- Goldenberg H M, Kleppner D and Ramsey N F 1960 *Phys. Rev. Lett.* **5** 361
- Golub R and Pendlebury J M 1979 *Rep. Prog. Phys.* **42** 439
- Gordon J P and Ashkin A 1980 *Phys. Rev. A* **21** 1606
- Gott Y V, Ioffe M S and Tel'kovskii V G 1962 *Nucl. Fusion (Suppl.)* **3** 1045
- Greytak T J and Kleppner 1984 *New Trends in Atomic Physics* ed G Grynberg and R Stora (Amsterdam: North-Holland)
- Grossman J S, Orozco L A, Pearson M R, Simsarian J E, Sprouse G D and Zhao W Z 1999 *Phys. Rev. Lett.* **83** 3522
- Grynberg G and Courtois J 1994 *Europhys. Lett.* **27** 41
- Grynberg G, Lounis B, Verkerk P, Courtois J-Y and Salomon C 1993 *Phys. Rev. Lett.* **70** 2249
- Gückert R, Zhao X, Crane S G, Hime A, Taylor W A, Tupa D, Vierra D J and Wollnik H 1998 *Phys. Rev. A* **58** R1637
- Guibal S, Mennerat-Robilliard C, Larousserie D, Triche C, Courtois J-Y and Grynberg G 1997 *Phys. Rev. Lett.* **78** 4703
- Guidoni L, Triche C, Verkerk P and Grynberg G 1997 *Phys. Rev. Lett.* **79** 3363
- Gupta R, McClelland J J, Marte P and Cellotta R J 1996 *Phys. Rev. Lett.* **76** 4689
- Guzman A M, Moore M and Meystre P 1996 *Phys. Rev. A* **53** 977
- Gwinner G, Behr J A, Cahn S B, Ghosh A, Orozco L A, Sprouse G D and Xu F 1994 *Phys. Rev. Lett.* **72** 3795
- Hamann S E, Haycock D L, Klose G, Pax P H, Deutsch I H and Jessen P S 1998 *Phys. Rev. Lett.* **80** 4149
- Hänsch T W and Shallow A L 1975 *Opt. Commun.* **13** 68
- Harris D J and Savage C M 1995 *Phys. Rev. A* **51** 3967
- Heer C V 1963 *Rev. Sci. Instrum.* **34** 532
- Hemmerich A and Hänsch T W 1993 *Phys. Rev. Lett.* **70** 410
- Hemmerich A, Weidemüller M, Esslinger T, Zimmermann C and Hänsch T 1995 *Phys. Rev. Lett.* **75** 37
- Herman R M and Wigginton T A 1991 *J. Opt. Soc. Am. A* **8** 932
- Hess H 1986 *Phys. Rev. B* **34** 3476
- Hijmans T W 1999 *1st Euroconf. on Atomic Physics at Accelerators: Laser Spectroscopy and Applications (Mainz, 1999)*
- Hinds E A, Boshier M G and Hughes I G 1998 *Phys. Rev. Lett.* **80** 645
- Hinds E A and Hughes I G 1999 *J. Phys. D: Appl. Phys.* **32** R119
- Honda K, Takahashi Y, Kuwamoto T, Fujimoto M, Toyoda K, Ishikawa K and Yabuzaki T 1999 *Phys. Rev. A* **59** R934
- Höpe A, Haubrich D, Müller G, Kaenders W G and Meschede D 1993 *Europhys. Lett.* **22** 669
- Houbiers M, Ferwerda R, Stoof H T C, Alexander W I, Sackett C A and Hulet R G 1997 *Phys. Rev. A* **56** 4864
- Houbiers M, Stoof H T C, McAlexander W I and Hulet R G 1998 *Phys. Rev. A* **57** R1497
- Hughes I G, Barton P A, Roach T M, Boshier M G and Hinds E A 1997 *J. Phys. B: At. Mol. Opt. Phys.* **30** 2119
- Ito H, Nakata T, Sakaki K, Ohtsu M, Lee K I and Jhe W 1996 *Phys. Rev. Lett.* **76** 4500
- Javanainen J 1992 *Phys. Rev. A* **46** 5819
- Jessen P S and Deutsch I H 1996 *Adv. At. Mol. Opt. Phys.* **37** 95
- Jessen P S, Gerz C, Lett P D, Phillips W D, Rolston S L, Spreuw R J C and Wesrbrook C I 1992 *Phys. Rev. Lett.* **69** 49
- Joffe M A, Ketterle W, Martin A and Pritchard D E 1993 *J. Opt. Soc. Am. B* **10** 2257
- Jun J W, Chang S, Kwon T Y, Lee H S and Minogin V G 1999a *Phys. Rev. A* **60** 3960
- Jun J W, Chang S, Lee H S, Minogin V G and Jhe W 1999b *Phys. Rev. A* **60** 4738
- Kaiser R, Levy Y, Vansteenkiste N, Aspect A, Seifert W, Leipold D and Mlynek J 1994 *Opt. Commun.* **104** 234
- Kasevich M and Chu S 1992 *Phys. Rev. Lett.* **69** 1741

- Kasevich M A, Weiss D S and Chu S 1990 *Opt. Lett.* **15** 607
- Katori H, Ido T, Isoya Y and Kuwata-Gonokami M 1999 *Phys. Rev. Lett.* **82** 1116
- Katori H and Shimizu F 1990 *Japan. J. Appl. Phys.* **29** L2124
- Kazantsev A P 1972 *Zh. Eksp. Teor. Fiz.* **63** 1628  
—1974 *Zh. Eksp. Teor. Fiz.* **66** 1599
- Kazantsev A P, Surdutovich G I and Yakovlev V P 1990 *Mechanical Action of Light on Atoms* (Singapore: World Scientific)
- Ketterle W, Kendall B D, Joffe M A, Martin A and Pritchard D 1993 *Phys. Rev. Lett.* **70** 2253
- Ketterle W and Pritchard D E 1992 *Appl. Phys. B* **54** 403
- Ketterle W and Van Druten N J 1996 *Adv. At. Mol. Opt. Phys.* **37** 181
- Kilian T C, Fried D G, Willman L, Landhurs D, Moss S C, Greytak T J and Kleppner D 1998 *Phys. Rev. Lett.* **81** 3807
- Klimov V V and Letokhov V S 1995a *Pis. Zh. Eksp. Teor. Fiz.* (Engl. Transl. 1995a *JETP Lett.* **61**)  
—1995b *Opt. Commun.* **121** 130
- Krall N A and Trivelpiece A W 1973 *Principles of Plasma Physics* (New York: McGraw-Hill)
- Kuga T, Torii Y, Shiokawa N, Hirano T, Shimizu Y and Sasada H 1997 *Phys. Rev. Lett.* **78** 4713
- Kugler K-J, Moritz K, Paul W and Trinks U 1985 *Nucl. Instrum. Methods A* **228** 240
- Kugler K-J, Paul W and Trinks U 1978 *Phys. Lett. B* **72** 422
- Kumakura M and Morita N 1992 *Japan. J. Appl. Phys.* **31** L276  
—1999 *Phys. Rev. Lett.* **82** 2848
- Kumarakrishnan A and Han X L 1998 *Phys. Rev. A* **58** 4153
- Kunugita H, Ido T and Shimizu F 1997 *Phys. Rev. Lett.* **79** 621
- Kuppens S, Rauner M, Schiffer M, Sengstock K and Ertmer W 1998 *Phys. Rev. A* **58** 3068
- Kurosu T and Shimizu F 1990 *Japan. J. Appl. Phys.* **29** L2127
- Kuwamoto T, Honda K, Takahashi Y and Yabuzaki T 1999 *Phys. Rev. A* **60** R745
- Lamb W Jr 1964 *Phys. Rev. A* **134** 1429
- Lau D C, Sidorov A I, Opat G I, McLean R J, Rowlands W J and Hannaford P 1999 *Eur. Phys. J. D* **5** 193
- Lawall J, Kulin S, Bardou F, Saubamea B, Bigelow N, Leduc M and Cohen-Tannoudji C 1995 *Phys. Rev. Lett.* **75** 4194
- Lee H J, Adams C S, Kasevich M and Chu S 1996 *Phys. Rev. Lett.* **76** 2658
- Lee P H and Skolnick M L 1967 *Appl. Phys. Lett.* **10** 303
- Lemonick A, Pipkin F and Hamilton D R 1955 *Rev. Sci. Instrum.* **26** 1112
- Leo P J, Tiesinga E, Julianne P S, Walter D K, Kadlecsek S and Walker T G 1998 *Phys. Rev. Lett.* **81** 1389
- Letokhov V S 1967 *Pis. Zh. Eksp. Teor. Fiz.* **6** 597  
—1968 *Pis. Zh. Eksp. Teor. Fiz.* **7** 348 (Engl. Transl. 1968 *JETP Lett.* **7** 272)  
—1973 *Proc. Colloquium Int. du CNRS (Aussais May 1973)* pp 127–37  
—1975 *Science* **190** 344  
—1992 *Dye Lasers: 25 Years* ed M Stuke (*Topics in Applied Physics*) vol 70 (Berlin: Springer) pp 153–68
- Letokhov V S and Minogin V G 1978 *Appl. Phys.* **17** 99  
—1980 *Opt. Commun.* **35** 199  
—1981 *Phys. Rep.* **73** 3
- Letokhov V S, Minogin V G and Pavlik B D 1976 *Opt. Commun.* **19** 72  
—1977 *Zh. Eksp. Teor. Fiz.* **72** 1328 (Engl. Transl. *Sov. Phys.–JETP* **45** 698)
- Letokhov V S and Pavlik B D 1976 *Appl. Phys.* **9** 229
- Lett P D, Watts R N, Westbrook C I, Phillips W D, Gould P L and Metcalf H J 1988 *Phys. Rev. Lett.* **61** 169
- Lin Z, Shimizu K, Zhan M, Takuma H and Shimizu F 1991 *Japan. J. Appl. Phys.* **30** 795
- Lisitsyn V N and Chebotayev V P 1968 *Zh. Eksp. Teor. Fiz.* **54** 419
- Liston G J, Tan S M and Walls D F 1995a *Phys. Rev. A* **52** 3057  
—1995b *Appl. Phys. B* **60** 211
- Lovelace R V E, Mehanian G, Tommila T J and Lee D M 1985 *Nature* **318** 30
- Lu Z T, Bowers C J, Freedman S J, Fujikawa B K, Mortara J L and Shang S-Q 1994 *Phys. Rev. Lett.* **72** 3791
- Lu Z-T, Corwin K L, Renn M J, Anderson M H, Cornell E A and Wieman C E 1996 *Phys. Rev. Lett.* **77** 3331
- Lu Z T, Corwin K L, Vogel K R, Wieman C E, Dinneen T P, Maddi J and Gould H 1997 *Phys. Rev. Lett.* **79** 994
- Mabushi H and Kimble H J 1994 *Opt. Lett.* **19** 749
- Manek I, Ovchinnikov Yu B and Grimm R 1998 *Opt. Commun.* **147** 67
- Marksteiner S, Savage C M, Zoller P and Rolston S L 1994 *Phys. Rev. A* **50** 2680
- Marte P, Dum R, Taieb, Zoller P, Shahriar S and Prentiss M 1994 *Phys. Rev. A* **49** 4886
- Mastwijk H C, Thomson J W, van der Straten P and Niehaus A 1998 *Phys. Rev. Lett.* **80** 5516
- Matsuura Y, Hanamoto K, Sato S and Miyagi M 1998 *Opt. Lett.* **23** 1858

- McClelland J J, Scholten R E, Palm E C and Cellota R J 1993 *Science* **262** 887
- Meacher D R, Guibal S, Mennerat C, Courtois J-Y, Petsas K I and Grynberg G 1995 *Phys. Rev. Lett.* **74** 1958
- Metcalf H J 1984 *Prog. Quantum Electron.* **8** 169
- Metcalf H and van der Straten P 1994 *Phys. Rep.* **244** 203
- Mewes M-O, Andrews M R, Kurn D M, Durfee D S, Townsend C G and Ketterle W 1997 *Phys. Rev. Lett.* **78** 582
- Migdall A L, Prodan J V, Phillips W D, Bergeman T H and Metcalf H J 1985 *Phys. Rev. Lett.* **54** 2596
- Miller J D, Cline R A and Heinzen D J 1994 *Phys. Rev. A* **47** R4567
- Minogin V G 1980 *Zh. Eksp. Teor. Fiz.* **79** 2044
- Minogin V G and Javanainen J 1982 *Opt. Commun.* **43** 119
- Minogin V G and Letokhov V S 1987 *Laser Light Pressure on Atoms* (New York: Gordon and Breach)
- Minogin V G and Serimaa O T 1979 *Opt. Commun.* **30** 373
- Minogin V G, Subbotin M V and Melentiev P N 1998a *Zh. Eksp. Teor. Fiz.* **114** 23
- 1998b *J. Exp. Theor. Phys.* **87** 12
- Minogin V G, Richmond J A and Opat G I 1998b *Phys. Rev. A* **58** 3138
- Mollow B R 1969 *Phys. Rev.* **188** 1969
- 1972 *Phys. Rev. A* **5** 2217
- Molmer K 1991 *Phys. Rev. A* **44** 5820
- Monroe C, Swann W, Robinson H and Wieman C E 1990 *Phys. Rev. Lett.* **65** 1571
- Morinaga M and Shimizu F 1994 *Laser Phys.* **4** 412
- Morsch O and Meacher D R 1998 *Opt. Commun.* **148** 49
- Mosk A P, Reynolds H W, Hijmans T W and Walraven J T M 1998 *Phys. Rev. Lett.* **81** 4440
- Müller-Seydlitz T, Hartl M, Brezger B, Hänsel H, Keller C, Schnetz A, Spreuw R J C, Pfau T and Mlynek J 1997 *Phys. Rev. Lett.* **78** 1038
- Neihues R 1976 *Thesis* Physics Institute, University of Bonn unpublished
- Nikolov A N, Eyler E E, Wang X T, Li J, Wang H, Stwalley W L and Gould P L 1999 *Phys. Rev. Lett.* **82** 703
- Nogues G, Rauschenbeutel A, Osnaghi S, Brune M, Raimond J M and Haroche S 1999 *Nature* **400** 239
- O'Hara K M, Granado S R, Gehm M E, Savard T A, Bali I, Freed C and Thomas J E 1999 *Phys. Rev. Lett.* **82** 4204
- Ol'shanii M A, Ovchinnikov Yu B and Letokhov V S 1993 *Opt. Commun.* **98** 77
- Opat G I, Wark S J and Cimmino A 1992 *Appl. Phys. B* **54** 396
- Oraevskii A N 1997 *Quantum Electron.* **24** 1127
- Ovchinnikov Yu B and Letokhov V S 1992 *Comm. At. Mol. Phys.* **27** 185
- Ovchinnikov Yu B, Manek I and Grimm R 1997 *Phys. Rev. Lett.* **79** 2225
- Ovchinnikov Yu B, Shul'ga S V and Balykin V I 1991 *J. Phys. B: At. Mol. Opt. Phys.* **24** 3173
- Ovchinnikov Yu B, Soding J and Grimm R 1995 *Pis. Zh. Eksp. Teor. Fiz.* **61** 23 (Engl. transl. 1995 *JETP Lett.* **61** 21)
- Ozeri R, Knaykovich L and Davidson N 1999 *Phys. Rev. A* **59** R1750
- Pahl A, Eikema K S E, Walz J and Hänsch T W 1999 *Laser Spectroscopy and Applications: 1st Euroconf. on Atomic Physics at Accelerators (Sept. 1999)*
- Parkins A S and Walls D F 1998 *Phys. Rep.* **303** 1
- Paterson C and Smith R 1996 *Opt. Commun.* **124** 121
- Paul W 1990 *Rev. Mod. Phys.* **62** 531
- Peik E 1999 *Europhys. J. D* **6** 179
- Peters A, Chung K Y and Chu S 1999 *Nature* **400** 849
- Petrich W, Anderson M H, Ensher J R and Cornell E A 1995 *Phys. Rev. Lett.* **74** 352
- Petsas K I, Coates A B and Grynberg G 1994 *Phys. Rev. A* **50** 5173
- Phillips W D 1998 *Rev. Mod. Phys.* **70** 721
- Phillips W D, Gould P L and Lett P B 1988 *Science* **239** 877
- Phillips W D and Metcalf H 1982 *Phys. Rev. Lett.* **48** 596
- Pillof H C 1997 *Opt. Commun.* **143** 25
- Power W L, Pfau T and Wilkins M 1997 *Opt. Commun.* **143** 25
- Prevedelli M, Cataliotti F S, Cornell E A, Ensher J R, Fort C, Ricci L, Tino G M and Inguscio M 1999 *Phys. Rev. A* **59** 886
- Pritchard D E 1983 *Phys. Rev. Lett.* **51** 1336
- Pritchard D, Helmerson K, Bagnato V S, Lafyatis G P and Martin A G 1987 *Laser Spectroscopy* vol 8, ed W Person and S Svanberg *Opt. Sciences Series, vol 55* (Berlin: Springer) pp 68–72
- Pritchard D E, Raab E L, Bagnato V S, Wieman C E and Watts R N 1986 *Phys. Rev. Lett.* **57** 310
- Prodan J V, Migdall A, Phillips W D, So J, Metcalf H and Dalibard J 1985 *Phys. Rev. Lett.* **54** 992
- Prodan J V, Phillips W D and Metcalf H 1982 *Phys. Rev. Lett.* **49** 1149
- Raab E L, Prentiss M, Cable A, Chu S and Pritchard D E 1987 *Phys. Rev. Lett.* **23** 2631

- Raithel G, Birkel G, Phillips W D and Rolston S L 1997 *Phys. Rev. Lett.* **78** 2928
- Reichel J, Hansel W and Hänsch T W 1999 *Phys. Rev. Lett.* **83** 3398
- Renn M J, Montgomery D, Vdovin O, Anderson D Z, Wieman C E and Cornell E A 1995 *Phys. Rev. Lett.* **75** 3253
- Renn M J, Donley E A, Cornell E A, Wieman C E and Anderson D Z 1996 *Phys. Rev. A* **53** R648
- Ricci L, Zimmermann C, Vuletic V and Hänsch T W 1994 *Appl. Phys. B* **59** 195
- Roach T M, Abele H, Boshier M G, Grossman H L, Zetie K P and Hinds E 1995 *Phys. Rev. Lett.* **75** 629
- Roch J-F, Vignerou K, Grelu P, Sinatra A, Poizat J-P and Grangier P 1997 *Phys. Rev. Lett.* **78** 634
- Rooijackers W, Hogervorst W and Vassen W 1997 *Opt. Commun.* **135** 149
- Rowe M A, Freedman S J, Fujikawa B K, Gwinner G, Shang S-Q and Vetter P A 1999 *Phys. Rev. A* **59** 1869
- Saba C V, Barton P A, Boshier M G, Hughes I G, Rosenbusch P, Sauer B E and Hinds E A 1999 *Phys. Rev. Lett.* **82** 468
- Sagna N, Dudle G and Thomann P 1995 *J. Phys. B: At. Mol. Opt. Phys.* **29** 4659
- Salomon C, Dalibard J, Phillips W D, Clairon A and Guellati S 1990 *Europhys. Lett.* **12** 683
- Santos M S, Nussenzeig P, Marcassa L G, Helmerson K, Flemming J, Zilio S C and Bagnato V S 1995 *Phys. Rev. A* **52** R4340
- Savage C M, Marksteiner S and Zoller P 1993 *Fundamentals of Quantum Optics* vol 3, ed F Ehlötzky (Berlin: Springer)
- Scully M O and Dowling J P 1993 *Phys. Rev. A* **48** 3186
- Seifert W, Adams C S, Balykin V I, Heine C, Ovchinnikov Yu and Mlynek J 1994 *Phys. Rev. A* **49** 3814
- Seifert W, Kaiser R, Aspect A and Mlynek J 1994 *Opt. Commun.* **111** 566
- Sesko D, Walker T, Monroe C, Gallagher A and Wieman C E 1989 *Phys. Rev. Lett.* **63** 961
- Shaffer J P, Chalupczak W and Bigelow N P 1999a *Phys. Rev. Lett.* **82** 1124
- 1999b *Phys. Rev. A* **60** R3365
- Shimizu F, Shimizu K and Takuma H 1989 *Phys. Rev. A* **39** 2758
- 1991 *Opt. Lett.* **16** 339
- Sidorov A I, McLean R J, Rowlands W J, Lau D C, Murphy J E, Walciewicz M, Opat G I and Hannaford P 1996 *Quantum Semiclass. Opt.* **8** 713
- Silvera I F and Walraven J T H 1980 *Phys. Rev. Lett.* **44** 164
- Simsarian J E, Ghosh A, Gwinner G, Orozco L A, Sprouse G D and Voytas P A 1996 *Phys. Rev. Lett.* **76** 3522
- Sinatra A, Roch J F, Vignerou K, Grelu Ph, Poizat J-P, Wang K and Grangier P 1998 *Phys. Rev. A* **57** 2980
- Snadden M J, McGuirk J M, Bouyer P, Haritos K G and Kasevich M A 1998 *Phys. Rev. Lett.* **81** 971
- Sobelman I I 1979 *Atomic Spectra and Radiative Transitions* (Berlin: Springer)
- Söding J, Grimm R and Ovchinnikov Yu B 1995 *Opt. Commun.* **119** 652
- Söding J, Guery-Odelin D, Desbiolles, Ferrari G and Dalibard J 1998 *Phys. Rev. Lett.* **80** 1869
- Solimeno S, Grosignani B B and Diponto P 1986 *Guiding, Diffraction and Confinement of Optical Radiation* (New York: Academic)
- Steane A M and Foot C J 1991 *Europhys. Lett.* **14** 231
- Stenholm S 1986 *Rev. Mod. Phys.* **58** 699
- Stenholm S, Minogin V G and Letokhov V S 1978 *Opt. Commun.* **25** 107
- Stern W and Gerlach O 1921 *Z. Phys.* **8** 110
- Stoof H T C, Houbiers M, Sackett C A and Hulet R G 1996 *Phys. Rev. Lett.* **76** 10
- Subbotin M V, Balykin V I, Laryushin D V and Letokhov V S 1997 *Opt. Commun.* **139** 107
- Takekoshi T and Knize R J 1996 *Opt. Lett.* **21** 77
- Takekoshi T, Patterson B M and Knize R J 1998 *Phys. Rev. Lett.* **81** 5105
- 1999 *Phys. Rev. A* **59** R5
- Takekoshi T, Yeh J R and Knize R J 1995 *Opt. Commun.* **114** 421
- Telles G D, Marcassa L G, Muniz S R, Miranda S G, Antunes A, Westbrook C and Bagnato V S 1999 *Phys. Rev. A* **59** R23
- Thorsheim H R, Weiner J and Julienne P S 1987 *Phys. Rev. Lett.* **59** 2420
- Timp G, Behringer R E, Tennant D M, Cunningham J E, Prentiss M and Berggren K K 1992 *Phys. Rev. Lett.* **69** 1636
- Tol P J T, Herschbach N, Hessels E A, Hogervorst W and Vassen W 1999 *Phys. Rev. A* **60** R761
- Tollet J J, Bradley C C, Sackett C A and Hulet R G 1995 *Phys. Rev. A* **51** R22
- Townsend C J, Edwards N, Cooper C J, Zetie K P, Foot J, Steane A M, Szriftgiser P, Perrin H and Dalibard J 1992 *Phys. Rev. A* **52** 1423
- Townsend G G, Edwards N H, Zetie K P, Cooper C J, Rink J and Foot C J 1996 *Phys. Rev. A* **54** 1702
- Turchette Q A, Hood C J, Lange W, Mabuchi H and Kimble H J 1995 *Phys. Rev. Lett.* **75** 4710
- Ungar P J, Weiss D S, Riis E and Chu S 1989 *J. Opt. Soc. Am. B* **6** 2058
- Vasilenko L S, Chebotayev V P and Shishaev A V 1970 *Pis. Zh. Eksp. Teor. Fiz.* **12** 113
- Verkerk P, Lounis B, Salomon C, Cohen-Tannoudji C, Courtois J-Y, Guibal S and Grynberg G 1992 *Phys. Rev. Lett.*

68 3861

- Vierra D J, Brice S J, Grane S G, Gückert R, Hime A and Zhao X 1999 *Laser Spectroscopy and Applications: 1st Euroconf. on Atomic Physics at Accelerators (Sept. 1999)*
- Viletic V, Fischer T, Praeger M, Hänsch T W and Zimmermann 1998 *Phys. Rev. Lett.* **80** 1634
- Vladimirskii V V 1960 *Zh. Eksp. Teor. Fiz.* **39** 1062 (Engl. transl. 1961 *Sov. Phys.-JETP* **12** 740)
- Vredenburg E J D, van Leeuwen K A H and Beijerinck H C W 1998 *Opt. Commun.* **147** 375
- Vuletic V, Chin C, Kerman A J and Chu S 1998 *Phys. Rev. Lett.* **81** 5768
- Walhout M, Megens H J L, Witte A and Rolston S L 1993 *Phys. Rev. A* **48** R879
- Walker T, Hoffman D, Feng P and Williamson R S III 1991 *Phys. Lett. A* **163** 309
- Walker T, Sesko D and Wieman C 1990 *Phys. Rev. Lett.* **64** 408
- Wallis H 1997 *Phys. Rev. A* **56** 2060
- Wallis H, Dalibard J and Cohen-Tannoudji C 1992 *Appl. Phys. B* **54** 407
- Walther H et al 1999 *ICOLS 99: Proc. 14th Int. Conf. on Laser Spectroscopy (Innsbruck)* ed R Blatt et al at press
- Wang X and Littman M G 1993 *Opt. Lett.* **18** 767
- Wang H, Gould P L and Stwalley W C 1996 *Phys. Rev. A* **53** R1216
- Weidemüller M and Hemmerich A G 1995 *Phys. Rev. Lett.* **75** 4583
- Weinstein J D, deCarvalho R, Guillet B, Friedrich B and Doyle M 1998a *Nature* **395** 148
- Weinstein J D, deCarvalho R, Kim J, Patterson D, Friedrich B and Doyle M 1998b *Phys. Rev. A* **57** R3173
- Weiss D S, Riis E, Shevy Y, Ungar P J and Chu S 1989 *J. Opt. Soc. Am. B* **6** 2072
- Westbrook C I, Watts R N, Tanner C E, Rolston S L, Phillips W D, Lett P D and Gould P L 1990 *Phys. Rev. Lett.* **65** 33
- Wilkens M, Goldstein E, Taylor B and Meystre P 1993 *Phys. Rev. A* **47** 2366
- Willems P A, Boyd R A, Bliss J L and Libbrecht K G 1997 *Phys. Rev. Lett.* **78** 1660
- Williamson R S III and Walker J 1995 *J. Opt. Soc. Am. B* **12** 1393
- Wing W 1980 *Phys. Rev. Lett.* **45** 631
- Wing W H 1984 *Prog. Quantum Electron.* **8** 181
- Winoto S L, Depue M T, Bramall N E and Weiss D S 1999 *Phys. Rev. A* **59** R19
- Wiseman H M 1997 *Phys. Rev. A* **56** 2068
- Yang K-H, Stwalley W C, Heneghan S P, Bahns J T, Wang K-K and Hess T R 1986 *Phys. Rev. A* **34** 2962
- Ye J, Vernooy D W and Kimble H J 1999 *Phys. Rev. Lett.* **83** 4987
- Yin J and Zhu Y 1998 *Opt. Commun.* **152** 421
- Yin J, Zhu Y, Jhe W and Wang Z 1998 *Phys. Rev. A* **58** 509
- Zel'dovich Ya B 1973 *Usp. Fiz. Nauk* **110** 139 (Engl. transl. *Sov. Phys.-Usp.* **16** 427)
- Zhao P, Lawall J R, Kam A W, Lindsay M D, Pipkin F M and Lichten W 1989 *Phys. Rev. Lett.* **63** 1593
- Zueva T V, Letokhov V S and Minogin V G 1981 *Zh. Eksp. Teor. Fiz.* **81** 84 (Engl. transl. *Sov. Phys.-JETP* **54** 38)